UNDERWATER SYSTEMS INC.

(1)

8121 GEORGIA AVENUE • SILVER SPRING, MD. 20910 • TELEPHONE: 301-589-1188

(1)

SUS SOURCE LEVEL ERROR ANALYSIS

By:

Curtis I. Holmer

With Contributions From:

Les Pitts
Richard Hecht
Marvin Weinstein

January 20, 1978

UNDERWATER SYSTEMS, Inc.
World Building • 8121 Georgia Ave. • Silver Spring, Md. 20910 • (301) 589-1188

UNCLASSIFIED

SECURITY CLASSIFICATION OF THIS PAGE (When Data Entered)

REPORT DOCUMENTATION PAGE

READ INSTRUCTIONS BEFORE COMPLETING FORM

1. REPORT NUMBER: N/A
2. GOVT ACCESSION NO.:
3. RECIPIENT'S CATALOG NUMBER:

4. TITLE (and Subtitle): SUS SOURCE LEVEL ERROR ANALYSIS.
5. TYPE OF REPORT & PERIOD COVERED: Final Report.
6. PERFORMING ORG. REPORT NUMBER: N/A

7. AUTHOR(s): Curtis I. Holmer
8. CONTRACT OR GRANT NUMBER(s): N00014-76-C-0109

9. PERFORMING ORGANIZATION NAME AND ADDRESS:
Underwater Systems, Inc.
8121 Georgia Ave.
Silver Spring, MD 20910

10. PROGRAM ELEMENT, PROJECT, TASK AREA & WORK UNIT NUMBERS:

11. CONTROLLING OFFICE NAME AND ADDRESS:
Long Range Acoustic Propagation Project
Naval Ocean Research & Development Activity
NSTL Station, MI 39529

12. REPORT DATE: January 20, 1978
13. NUMBER OF PAGES: 147

14. MONITORING AGENCY NAME & ADDRESS (if different from Controlling Office):

15. SECURITY CLASS. (of this report): Unclassified
15a. DECLASSIFICATION/DOWNGRADING SCHEDULE:

16. DISTRIBUTION STATEMENT (of this Report)

Unlimited Distribution

DISTRIBUTION STATEMENT A
Approved for public release;
Distribution Unlimited

17. DISTRIBUTION STATEMENT (of the abstract entered in Block 20, if different from Report)

18. SUPPLEMENTARY NOTES

N/A

19. KEY WORDS (Continue on reverse side if necessary and identify by block number)

SUS
Digital Signal Analysis
Transient Signals
Error Analysis
SUS Signal Model
Signal Clipping
Transducer Calibration
Fast Fourier Transform (FFT)

20. ABSTRACT (Continue on reverse side if necessary and identify by block number)

The report provides an analysis of major terms which contribute to signal analysis error in a proposed experiment to calibrate source levels of SUS (Signal Underwater Sound). A unique model of the digital signal analysis process was used to verify and empirically extend the results of analytic studies. The analytic findings indicate that the discrete Fourier transform, without windowing, is error free when the signal is adequately anti-alias filtered, and wholly contained in the analysis time window. The model was used to generate

DD FORM 1 JAN 73 1473 EDITION OF 1 NOV 65 IS OBSOLETE

UNCLASSIFIED

SECURITY CLASSIFICATION OF THIS PAGE (When Data Entered)

exact spectra for comparison with digitally analyzed spectra. Errors due to FFT roundoff, aliasing, quantization and registration were studied to verify error expressions and to identify empirical error bounds. Discrete amplitude representation (quantization) was found to introduce systematic error at low frequencies, for the particular time series that were studied, when insufficient resolution was provided. Analytic expressions for FFT roundoff and anti-aliasing error were found and confirmed. Registration (signal positioning in the time window) was not found to be a factor. An overall calibration error of +1 dB for 1/3 octave band analysis of source level is achievable, subject to resolution of other problems for which knowledge of the process is incomplete. These problems include yield variability, non-linear surface reflection and shock vs acoustic propagation of the lead pulse. Mini-experiments to study the latter problems are described.

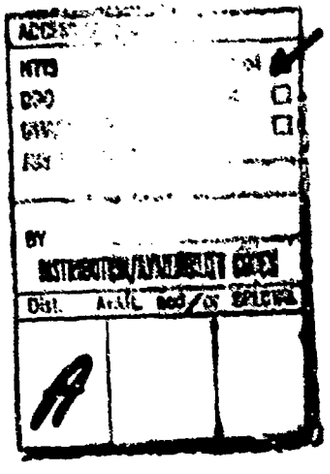

Table of Contents

Table of Contents Con't.

List of Figures

List of Figures Con't.

List of Figures Con't.

List of Tables

SUMMARY

A computer simulation of the signal generated by SUS has been performed for the purpose of determining the accuracy that could be achieved in the performance of a source level experiment. It is postulated that for 1/3 octave bands, current source level estimates are correct to within ±2 dB and a new experiment would be warranted only if an accuracy of ±1 dB could be achieved. With the exception of a few problems that either cannot be simulated, or for which our knowledge of the physics is inadequate, it is concluded that an accuracy within ±1 dB is achievable. The difficulities arise in regard to the yield variability of SUS, the form of non-linearity that can be introduced on surface reflection, and the transition between shock and acoustic propagation for the shock wave portion of the signal. Although the latter two problems have been included in the simulation studies on the basis of existing knowledge, a set of mini-experiments to investigate these three factors is recommended.

1. INTRODUCTION

SUS shots are commonly used for long range acoustic propagation loss measurements. The equivalent acoustic source level of explosives has been known approximately for well over a decade[1]. As acoustic measurement and prediction accuracies have improved, additional measurements and analyses have been performed by many scientists to more accurately determine these levels. An advanced prediction model in common usage was proposed by Gaspin and Schuler[2] in 1971. Following the CHURCH ANCHOR and SQUARE DEAL Experiments it became apparent that different segments of the acoustic community were still using significantly different values for the equivalent acoustic source level. The Manager, LRAPP, appointed a committee to study this problem. The committee reported[3] that they were unable to resolve these differences, which were as large as six decibels in some frequency bands, and recommended the performance of a new, carefully controlled experiment.

---

[1] D. E. Weston, "Underwater Explosions as Acoustic Sources", Proceedings of the Physical Society, 76, p 233-249, 1960.

[2] J. B. Gaspin and V. K. Schuler, "Source Levels of Shallow Underwater Explosions", Naval Ordnance Laboratory Report, NOLTR 71-160, October 1961.

[3] "SUS Source Level Committee Report", MC Report 112, prepared for LRAPP by Underwater Systems, Inc., November 1975.

These recommendations were the subject of a SUS Source Level Workshop held in July 1976, and reported in Ref 4. The range of differences in SUS source levels was reduced by about 3 dB as a result of newly reported information. The general consensus of the workshop was that SUS source levels were known to about $\pm$ 2 dB for most cases of interest and somewhat less well known in other cases. Further, it was felt that by performing a new experiment accuracies within $\pm$ 1 dB could be achieved.

Subsequent to the Workshop, the Manager, LRAPP, established a working group to recommend a new experiment design consistent with the Workshop conclusions. Dr. A. F. Wittenborn served as chairman of this working group and Underwater Systems, Inc. provided technical support. Dr. Wittenborn has requested that Underwater Systems, Inc. perform a supportive investigation of a number of technical problems that arise in the performance of measurements and the processing of the data. In essence, the investigation is directed toward more accurately determining the accuracy that could be achieved in a new experiment. If SUS source levels are now known to within $\pm$ 2 dB, a new experiment would be of value only if the potential accuracy of $\pm$ 1 dB estimated by the Workshop could be achieved. Additionally, to the extent that there is not sufficient current knowledge to resolve the matter for all factors known to contribute to inaccuracy,

---

[4] Report of SUS Source Level Workshop, Airlie Conference Center, 7-8 July 1976, prepared for LRAPP by Underwater Systems, Inc. and Tracor, Inc., July 1976.

Underwater Systems, Inc. was requested to recommend a set of mini-experiments, each of which would be designed to investigate a single phenomenon. Finally, in the event that the studies and mini-experiments demonstrate the feasibility of achieving an accuracy of $\pm$ 1 dB, the additional knowledge obtained would permit a reduction in the size of the experiment that would have to be performed to determine source levels within that accuracy.

In Chapter 2 of this report, issues that had previously been raised relative to the sensor and electronic systems are addressed. It is shown that a standard steady-state acoustic calibration of the system of the type normally performed at Orlando is satisfactory. Integration of the signal over the sensor extent is automatically accounted for in such a calibration, provided that the entire system is linear.

Chapter 3 is concerned with signal processing and data interpretation. An analytic representation of an explosive signal has been developed that closely replicates the description given in Ref 2 in both the time and frequency domain. A closed form Fourier Transform of this analytic signal is obtained that represents "truth" for all subsequent operations. The effect of the measurement range on equivalent acoustic source level is investigated as a guide toward determining whether it is possible to perform an experiment that defines the range beyond which the shock wave can be treated as an acoustic signal within tolerable error. Digital processing is examined from the standpoint of the digitization rate, quantization level, registration, and system

bandwidth, to identify the errors that can be introduced during signal processing. Finally, the practical case in which the received signal is the sum of the directly-propagated signal and the time-delayed surface reflection is simulated for both linear and non-linear reflection processes to investigate procedures for deconvolving the reflected signal and determining the errors associated with this process.

Chapter 4 describes a set of mini-experiments to investigate the factors for which our basic physical knowledge is insufficient to permit a confident estimate of the errors that might be introduced.

Chapter 5 presents the conclusions and recommendations reached.

2. SYSTEM RESPONSE

The two major factors of an experimental determination of source level that affect the overall accuracy of the experiment are the measurement system calibration and the subsequent data processing. In this section we explore three factors which impact on measurement system accuracy. These factors are:

- Steady-State and Transient System Characteristics: as they affect system calibration and calibration requirements.
- Sensor Size: effects on the system calibration and the signal that is acquired.
- Calibration Accuracy: in which the inherent limitations of various calibration techniques are stated.

These three factors are examined because of the diverse views held by the members of the various committees. It is generally agreed that small sensors and electronic systems which have a flat response with zero phase shift over a wide frequency range are necessary to accurately replicate the pressure-time history of the signal; e.g. a small sensor is one whose physical dimensions are small relative to the major features of the explosive signal. It is further agreed that the sensor-electronics system must have an adequate dynamic range and a linear pressure response; e.g. the system must

respond linearly to both the high levels of the shock wave and the much lower levels of the negative phases. The specific question is therefore to determine the acceptability of linear large sensors for measurements in the spectral domain; i.e., for use in determining spectrum levels.

2.1 System Steady-State and Transient Characteristics

The frequency and phase response of a data acquisition system is known to "color" (i.e., significantly change) the time domain waveform. In view of this time domain coloration it is appropriate to ask what are the effects in the frequency domain. In particular, we ask how frequency and phase response, as well as transient response of the measurement system, affect the results of a measurement of the energy spectrum of a transient signal. The answer to this question is widely presumed to be that the squared steady state frequency response is the only factor that affects the output of the measured energy spectrum, but we find no straightforward derivation of this fact for transient signals in the easily accessible literature. In view of this we reproduce here such a derivation.

Consider a time signal p(t) which has zero mean and bounded non-zero, mean-squared value in the interval 0 to T, and is identically zero outside this range, i.e.,

$p(t) = 0$ for $t < 0$, $T < t$ and

and

$$0 < \frac{1}{t_o} \int_{t-t_o/2}^{t+t_o/2} p^2(t)\, dt \leq M; \text{ all } t_o > 0,\ 0 \leq t \leq T$$

Next we consider applying this signal to the input of a linear filter, with impulse response $h(\tau)$, frequency response $H(f)$ (note that $H(f)$ is complex). $h(\tau)$, $H(f)$ are a Fourier transform pair[5], i.e.

$$H(\omega) = \int_{-\infty}^{\infty} h(\tau)\, e^{-j\omega\tau} d\tau \qquad (2.1a)$$

$$h(\tau) = \frac{1}{2\pi} \int_{-\infty}^{\infty} H(\omega)\, e^{j\omega\tau} d\omega \qquad (2.1b)$$

It may be shown that for a constant harmonic input signal $p_i(\omega t) = ae^{j\omega t}$, the output signal $p_o(\omega t)$ is given by:

$$p_o(\omega t) = H(\omega)\, p_i(\omega t)$$

Thus it is appropriate to call $H(\omega)$ the steady-state frequency response, since it describes the steady-state change in phase and amplitude that the filter applies to the harmonic input signal. Our input signal $p_i(t)$ has an energy spectrum $E_i(\omega)$ which may be defined from the time signal Fourier transform, i.e,

[5] For example E. B. McGrab and D. S. Bloomquist, The Measurement of Time Varying Phenomena, pp 52-53.

$$E_i(\omega) = 2\, S_i(\omega) S_i^*(\omega) = 2\left|S_i(\omega)\right|^2 \tag{2.2}$$

where

$$S_i(\omega) \equiv \int_{-\infty}^{\infty} p_i(t)\, e^{-j\omega t} dt \tag{2.3}$$

It is this energy spectrum that we wish to measure. The output of the linear filter may be represented as:

$$p_o(t) = \int_{-\infty}^{\infty} h(\tau)\, s_i(t-\tau)\, d\tau \tag{2.4}$$

or, applying the Fourier transform (Eq. 2.3)

$$S_o(\omega) = \int_{-\infty}^{\infty} \int_{-\infty}^{\infty} h(\tau)\, s_i(t-\tau)\, d\tau\, e^{-j\omega t} dt \tag{2.4a}$$

$$= \int_{-\infty}^{\infty} h(\tau)\, e^{-j\omega\tau} \int_{-\infty}^{\infty} s_i(t-\tau)\, e^{-j\omega(t-\tau)} dt\, d\tau \tag{2.4b}$$

$$= \int_{-\infty}^{\infty} h(\tau)\, e^{-j\omega\tau} d\tau\, S_i(\omega) \tag{2.4c}$$

$$= H(\omega) S_i(\omega)$$

Thus;

$$E_o(\omega) = 2\left|S_o(\omega)\right|^2$$

$$= 2\left(S_i(\omega) H(\omega)\, S_i^*(\omega) H^*(\omega)\right) \tag{2.5}$$

$$= 2\left|S_i(\omega)\right|^2 \left|H(\omega)\right|^2 = E_i(\omega)\left|H(\omega)\right|^2$$

We note that the frequency response function can be separated into magnitude and phase terms, i.e.:

$H(\omega) = A(\omega)\, e^{i\theta(\omega)}$ where $A(\omega)$ is real.

Then;

$$\left|H(\omega)\right|^2 = A^2(\omega)$$

and

$$E_i(\omega) = E_o(\omega)/A^2(\omega) \qquad (2.6)$$

Thus the magnitude of the steady-state frequency response is a sufficient calibration of the (linear) measurement system for determining the input energy spectrum at a frequency range of interest, if the output energy spectrum from the system is known.

2.2 Sensor Size Effects

As in the case of using steady-state frequency response to characterize a system's response to a transient signal, it is also appropriate to ask how the finite size of a transducer affects the system's ability to measure a signal whose spatial extent in the water is comparable to or smaller than the transducer dimensions. In this case, we will show for a linear measurement system that the pure tone frequency response calibration (ratio of squared voltage to squared pure tone pressure as a function of frequency) in the direction of incidence is a sufficient calibration to permit the computation of the exact energy spectrum for the incident wave form in the frequency range of observation.

Physically, this problem is sometimes analyzed as an integration of the sound field over the transducer surface, so that the transducer output for an arbitrary input has the

form;

$$p'(t) = \int_{S_o} p(\underline{x},t)\, dS$$

where $p(\underline{x},t)$ is the time and space varying pressure field

$p'(t)$ is the "apparent pressure" that a point transducer would see in order to produce the same output

S_o is the active area of the transducer

dS is differential element of surface area

A more useful representation, which can be used when the sound field has a particular direction of incidence say x_o, is the impulse response function, defined by;

$$v_o(t) = \int_{-\infty}^{\infty} h(\tau,x_o)\, p(t-\tau,x_o)d\tau \qquad (2.7)$$

The impulse response function $h(\tau,x_o)$ is the voltage response of the transducer to a unit amplitude plane wave pressure impulse arriving from the direction x_o. This formulation is equivalent to the former representation, where the integration over the transducer surface has been replaced by an integration over the time variation of the (plane wave) pressure wave form. Taking the Fourier transform as in Eq. 2.4a yields;

$$V_o(\omega) = \int_{-\infty}^{\infty} v_o(t)e^{-j\omega t}dt$$

$$= H(\omega,x_o)\, S_i(\omega,x_o) \qquad (2.8)$$

where: $H(\omega,x_o) = \int_{-\infty}^{\infty} h(t,x_o)e^{-j\omega t}dt$

is again the complex steady-state frequency response of the transducer (i.e. the output for a constant input sinusoid of unit amplitude, frequency ω).

$S_i(\omega,x_o)$ is the complex frequency spectrum of the input pressure signal.

The energy spectrum of the output voltage is;

$$E_v(\omega) = 2\ V_o(\omega)\ V_o^*(\omega)$$
$$= \left|H(\omega,x_o)\right|^2\ E_p(\omega)$$

where $\left|H(\omega,x_o)\right|^2 = \mu(2\pi f,x_o)$

is the transducer sensitivity (squared voltage response) as a function of frequency for the direction x_o.

Thus we see that the steady-state frequency response provides the only calibration necessary for determining energy density of an incoming plane pressure wave of arbitrary time dependence. Physically, this occurs because exactly the same integration process occurs for each frequency in the calibration as occurs for the respective Fourier frequency component in the incoming arbitrary wave form. The only assumptions necessary to prove this were that:

1. The incoming signal be preserved for the entire time during which it is non-zero.
2. The transducer is linear and its sensitivity is known as a function of frequency for the frequency

range of interest and the directions of incidence of the acoustic signal.

3. The signal consists of a plane or spherical wave whose direction corresponds to that for which the calibration is known.

The latter requirement concerning the spatial form of the wave front is necessary in order to uniquely assign an impulse response function for Eq. 2.7, unless the transducer is omni-directional.

2.3 Transducer Calibration Accuracy

The two major transducer types of interest are tourmaline gauges and hydrophones.

The tourmaline gauge and its calibration are described by Cole.[6] He cites comparability of static and reciprocity calibrations of within 5% or less than 0.5 dB. Bobber[7] describes hydrophone calibration procedures, of which the reciprocity method is considered the most accurate. Reproducibility of these calibrations is again typically within 0.5 dB.

Of potential significance is the fact that neither calibration is typically performed in the pressure regime of interest for this study (e.g., hydrophones are typically calibrated at significantly lower levels, while tourmaline gauges are usually calibrated

---

[6] R. H. Cole, Underwater Explosions, Dover, New York, 1948 Section 5.7

[7] R. J. Bobber, Underwater Electroacoustic Measurements, Naval Research Laboratory, Government Printing Office, Washington, D.C., 1970

at much higher levels). As a result, dependence on gauge and system linearity will be required in order to obtain the desired data.

In either case, a calibration accuracy for the transducer of less than 0.5 dB appears to be within reach.

3. A SUS SIGNAL PROCESSING MODEL

The analysis of transient signals using digital processing techniques has proceeded on the basis of analogy with the analysis of continuous signals. We are not aware of any systematic study of errors that may occur in the analysis which take into account some of the unique properties of transient signals (such as their bounded total energy).

In this section we present a comprehensive analysis of signal processing error as a function of the processing parameters so as to place quantitative estimates on those error sources. Other sources of variability or error in an actual experiment, including variation of the medium and background noise are not included.

The digital signal analysis process is represented as consisting of three distinct processes, which include:

- Sampling in the time domain (temporal sampling)
- Quantization of the time domain signal into discrete levels (quantization)
- Discrete Fourier Transform (DFT)

Each of these processes may introduce errors that reflect themselves as differences between the resulting estimate of the signal energy spectrum and the "true" spectrum that would result from performing a continuous analytic Fourier transform on the continuous, exact signal. We presume for the purposes of this study that these errors may individually be made sufficiently small that their interactions are negligible, and

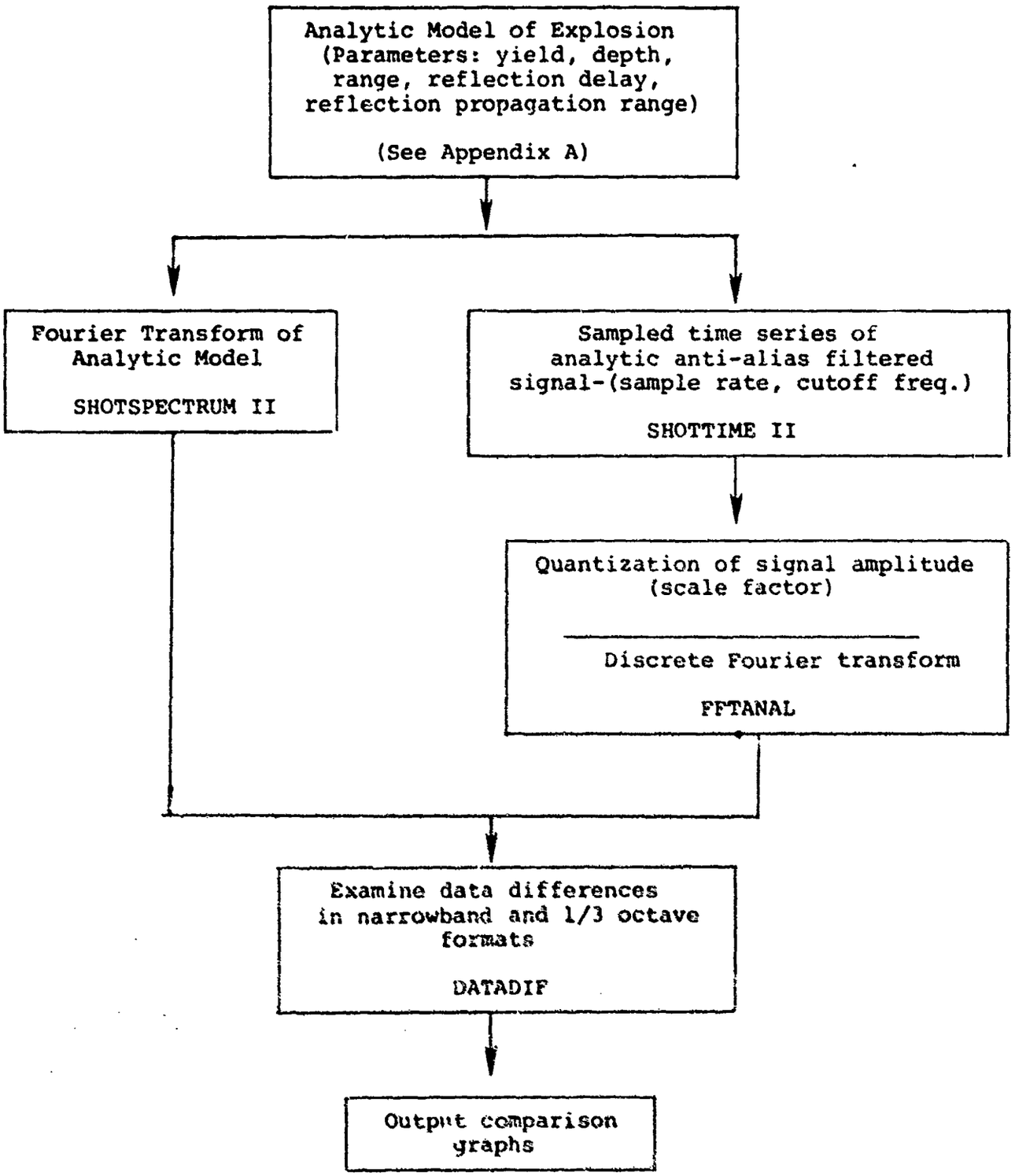

Figure 3-1. Schematic block diagram of computer experiments, identifying component programs.

the total mean-square error is the sum of the component mean-square errors.

This section includes, where possible, analytic estimates of an upper bound to the error for specific error sources. These error estimates are then compared with empirical error estimates derived from computer based experiments. The experiments are based on comparing the output of a simulation of a digital signal processing system, operating on a sampled analytic signal, with an exact Fourier analysis of that same analytic signal.

Figure 3-1 presents a schematic diagram of the data flow in the computer experiments reported in this section. The concept of the experiment is to use a superposition of analytic functions (exponentials, half-sines and constants) to represent the time series of an explosive signal. This function may be transformed analytically to obtain an exact expression for the energy spectrum of the time series. This exact transformed analytic expression is evaluated at discrete frequencies in the program SHOTSPECTRUM. SHOTSPECTRUM permits the computation of a spectrum for a single direct arrival, or the superposition of a direct arrival plus a surface-reflected arrival with arbitrary delay, propagation range and amplitude clipping (of the reflected shock wave). The program SHOTTIME provides the time series values of the analytic model signal after it has been operated upon by an analytic representation of a 4-pole Butterworth anti-aliasing filter. Input data to

this program includes: sampling time interval, shot yield, depth and range, filter cutoff frequency, reflected signal delay, range and shock amplitude clipping. The program FFTANAL operates on the output of SHOTTIME to quantize the amplitude representation of the signal, and then implements a Fast Fourier Transform (FFT) to provide the digital signal processor estimate of the signal spectrum. Finally, the program DATADIF takes the output from SHOTSPECTRUM and FFTANAL and plots the respective spectra and their differences in narrowband and 1/3 octave formats for the frequency ranges of 0 - 100 Hz and 0 - 500 Hz.

There are a number of different questions which can be examined using this model. As in the previous chapter, the questions selected for investigation are those which could not be definitively resolved by the various committees and Workshop. These questions, each followed by a short discussion are:

- What accuracy can be achieved with FFT processing? A comparison of spectral levels obtained by several organizations by applying FFT techniques to a set of SUS recordings is reported in Ref. 3. Differences of the order of a decibel were observed, but were not investigated in detail, since the goal was to attempt to explain reported differences of the order of 3 to 6 dB. Since this difference has since been reduced by 3 dB, Ref. 4, the remaining reported processing differences become

important, particularly in regard to the performance of an experiment. A series of investigations are therefore described which indicate the level of accuracy which can be achieved.

- What accuracy limitations are imposed by overlap of direct and surface-reflected signals? Received signals of SUS detonations include both direct and surface-reflected arrivals. For 60 foot 1.8 lb SUS it is not possible to avoid overlap of these signal components. The decorrelation of the received signals to determine the free field source levels is examined in the frequency domain. This investigation includes consideration of non-linear effects at the surface.

- What is the optimum measurement range? It is well known that the shock wave generated in a detonation propagates by shock laws rather than acoustic laws. The latter govern the other parts of the total signal. Consequently the signal spectrum is range dependent. It is believed that as the propagation range increases, and the shock wave amplitude decreases, a gradual transition between shock wave and acoustic wave propagation occurs. Further, it is believed that this occurs in the vicinity of a peak pressure of about 1 psi. This suggests that if the source levels are measured at sufficient range, they will adequately represent the "effective source level" for acoustic measurements at greater range, to within a fraction

of a decibel. However, as the range increases the accuracy of refraction corrections to propagation decreases and for that reason one would want to make the source level measurement at the shortest possible range. Accepting a peak pressure of 1 psi as being approximately correct for the transition, an investigation of potential errors is made in the vicinity of this value to determine whether it is desirable to experimentally account for our limited knowledge by making measurements at several ranges.

3.1 Analytic Representation of the Signal

As previously discussed, the investigation is performed by establishing an analytic signal which closely replicates the SUS signal but for which the Fourier Transform can be taken in closed form. No attempt has been made to develop an analytic model which represents "truth" in the absolute since. Rather it is sufficient for our purpose to closely replicate the recognized features of explosive signals in the time and frequency domains. Thus, the analytic pressure-time model and its Fourier Transform are used to represent a "relative truth" against which all other analyses are compared to permit the systematic development of error estimates.

Details of the analytic model and these programs are described in Appendix A. Figures 3-2 and 3-3 provide plots of the time series signal for one set of shot parameters,

showing the difference between the wide band signal and the anti-alias filtered signal. Figures 3-4, 3-5 and 3-6 show comparison spectra for this analytic model and other models. Of principal interest here is not detailed agreement, but rather the fact that the time series used in this study provide spectra that incorporate many of the features of the spectra to be expected from other models or from an actual experiment. Thus we expect that error analysis estimates made on the basis of studying this signal should be closely representative of what may be expected during analysis of field data.

3.2 Digital Processing

3.2.1 The Discrete Fourier Transform. The Discrete Fourier Transform (DFT) is the analytic construct that forms the basis of modern digitally-implemented signal processing. It is a close relative of the well known Integral Fourier Transform, but has some very distinctive properties of its own. As has been noted previously in this report, much of the present understanding of the significance of the DFT is based upon the study of spectral analysis of continuous, stationary, infinite time series.[8] In the application to noise time series, the squared magnitude of the DFT provides an estimate of the power spectrum of the infinite length time series. We will show that the DFT, when applied to the entire time interval

[8] For example see, "R. B. Blackman and J. W. Tukey, The Measurement of Power Spectra, Dover, New York, 1968.

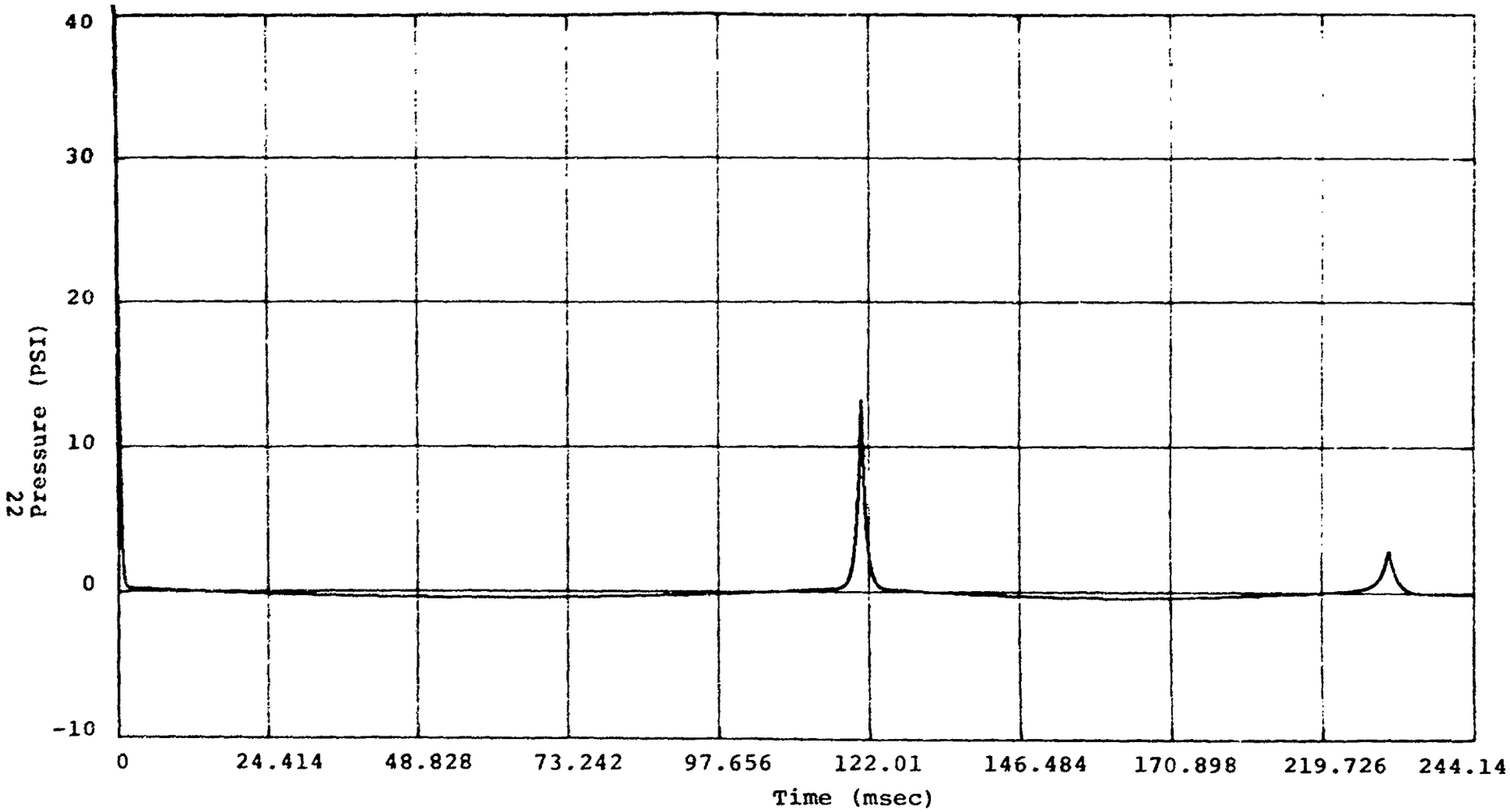

Figure 3-2. Time series for unfiltered analytic shot model. Model Parameters: Yield 1.8 lbs; Depth 60 ft, Range 100 yds.

Peak Pressures: Shock Wave 41.2 psi, 0.00 sec
First Bubble Pulse 13.4 psi, 0.1208 sec
Second Bubble Pulse 2.84 psi, 0.2060 sec
(not shown) Third Bubble Pulse 1.34 psi, 0.2751 sec
(not shown) Fourth Bubble Pulse 0.41 psi, 0.3394 sec

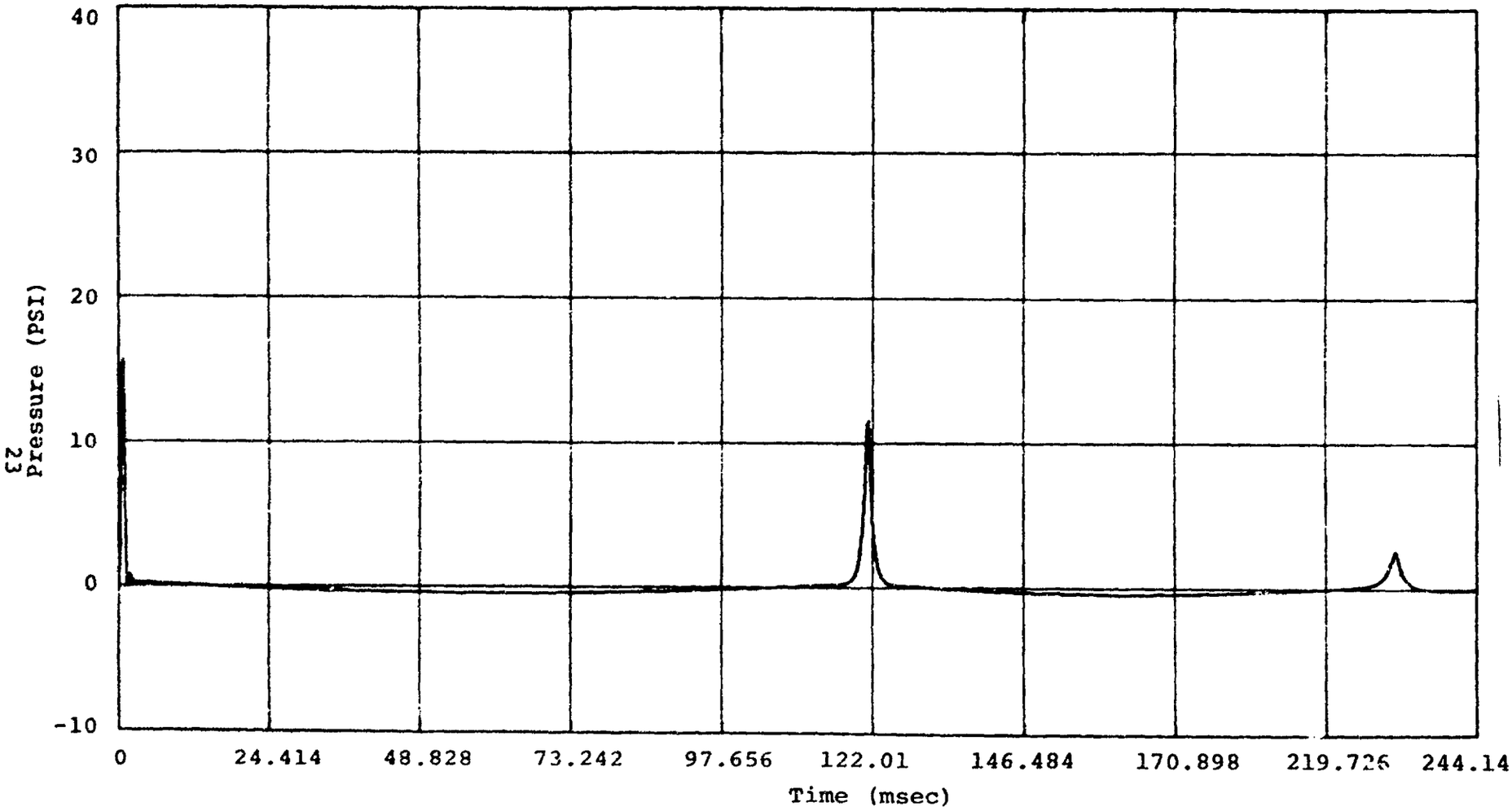

Figure 3-3. Antialias filtered time series. (Cutoff frequency = 2040 Hz), all other parameters same as Figure 3-2.

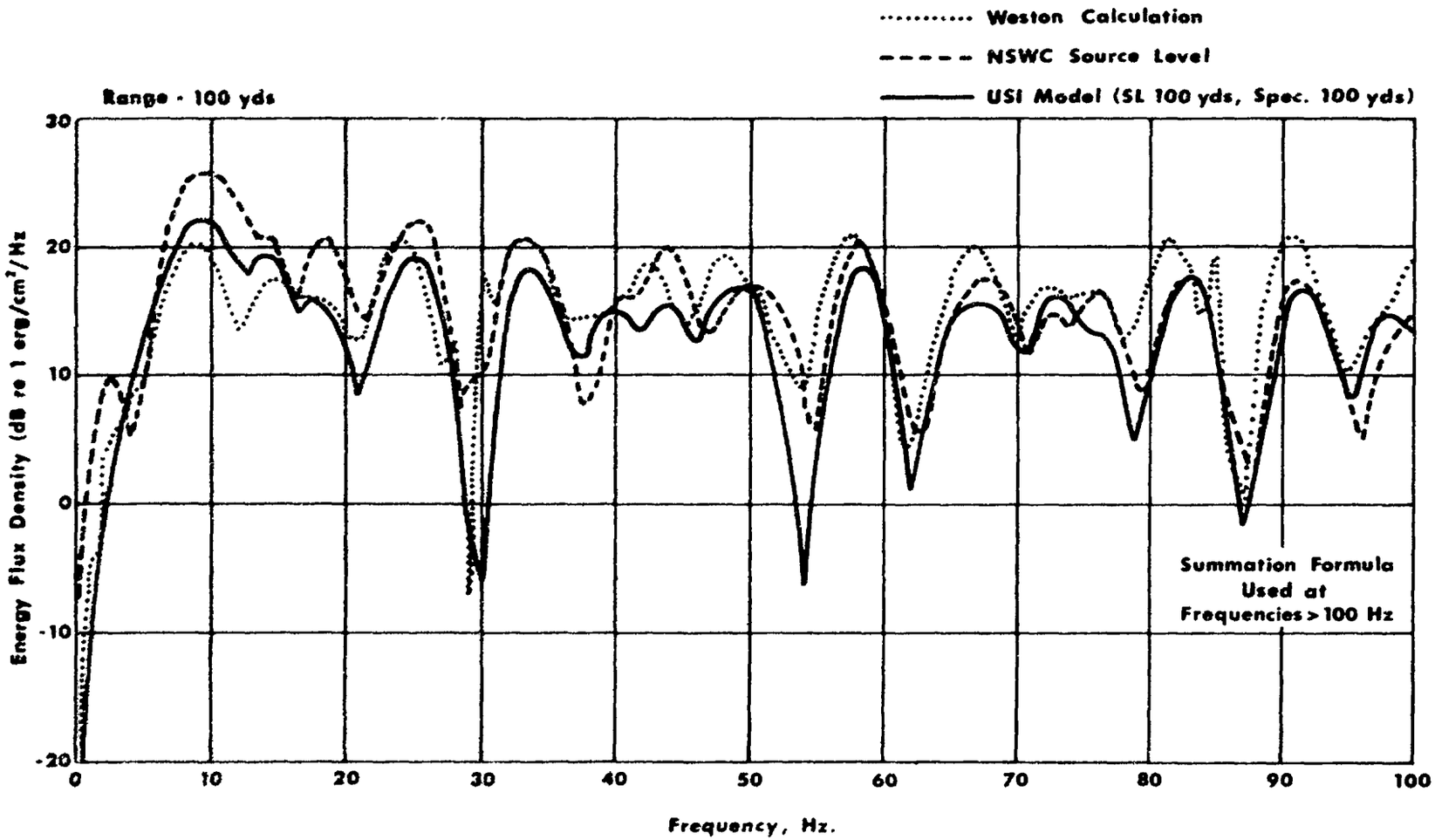

Figure 3-4 Comparison of USI model with Weston's analytic formulation and NSWC calculations - 1.8 lb of TNT at 60 ft depth.

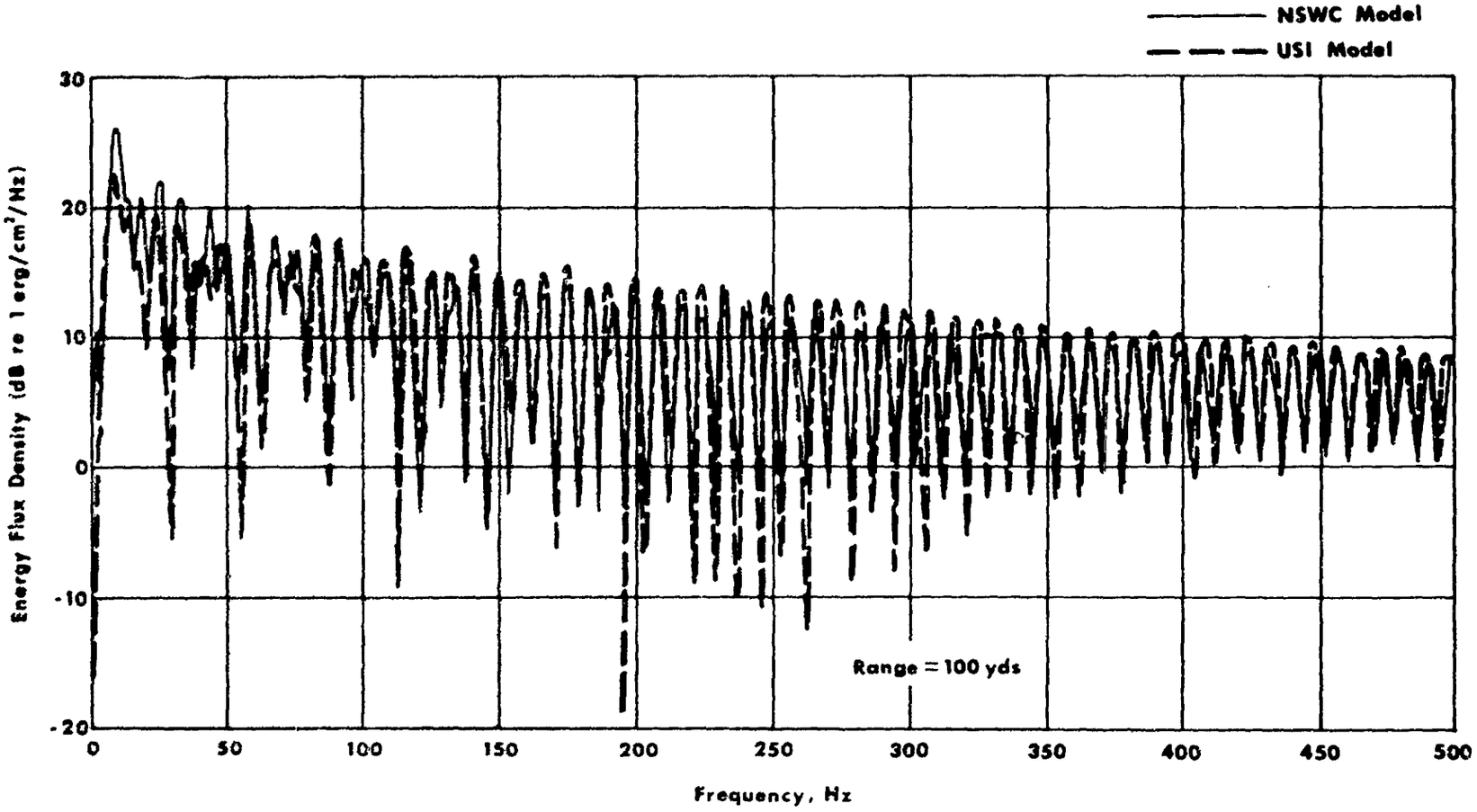

Figure 3-5 Comparison of USI model with NSWC model - 1.8 lb of TNT at 60 ft depth.

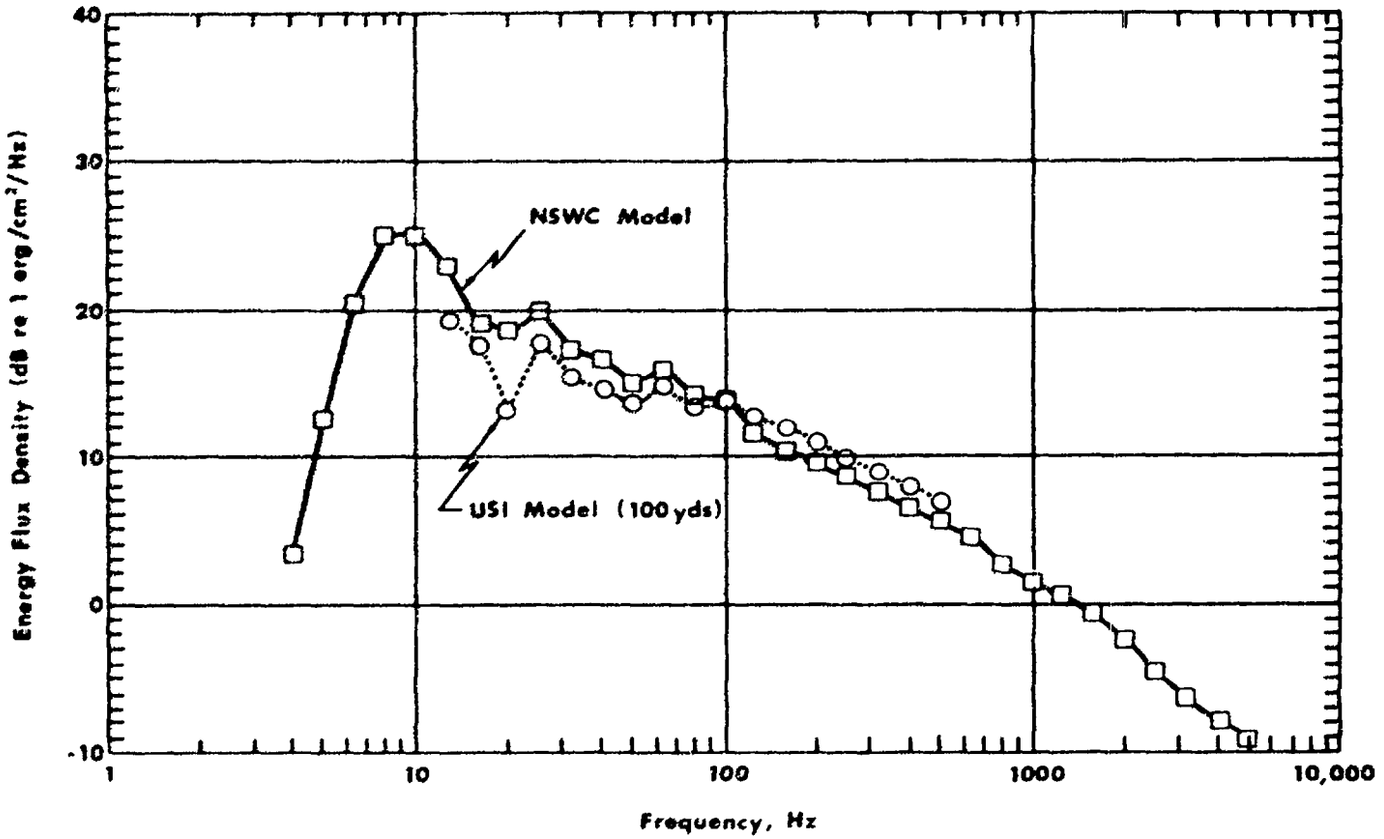

Figure 3-6 1/3 octave band source level comparison with NSWC - 1.8 lb of TNT at 60 ft depth.

of the finite duration transient, yields the exact Fourier transform of the signal at the discrete frequencies at which it is evaluated, and further, when sampled at sufficiently high rate, provides sufficient information to define the continuous Fourier transform at all values of frequency.

Let us introduce the discrete operator (after Blackman and Tukey,[8] paragraph A.2)

$$d(t) \equiv \sum_{q=-\infty}^{\infty} \Delta t \; \delta(t-q\Delta t)$$

which has the Fourier transform,

$$d(t) \leftrightarrow D(f) = \int_{-\infty}^{\infty} d(t)\; e^{-j2\pi ft}\; dt = \sum_{q=-\infty}^{\infty} \delta(f-q/\Delta t)$$

where: Δt is a non-zero time interval

q is an integer series index

δ is the Dirac delta function defined by;

$$\int_a^b f(t)\delta(t-c)dt = \begin{array}{l} f(c) \text{ if } a < c < b \\ 0 \text{ if } c < a \text{ or } b < c \end{array}$$

Now, if we take the discrete Fourier transform of a continuous bounded signal $p(t)$ we have,

$$\int_{-\infty}^{\infty} d(t)\; p(t)\; e^{-j2\pi ft}\; dt$$

$$= \sum_{q=-\infty}^{\infty} \int_{-\infty}^{\infty} \Delta t\; p(t)\; \delta(t-q\Delta t)\; e^{-j2\pi ft}\; dt$$

$$= \sum_{q=-\infty}^{\infty} \Delta t\; p(q\Delta t)\; e^{-j2\pi fq\Delta t} = P'(f) \qquad (3.1)$$

We name this function $P'(f)$. From the exact Fourier transform of p(t), i.e.,

$$P(f) = \int_{-\infty}^{\infty} p(t)\, e^{-j2\pi ft}\, dt$$

we observe that $P'(f)$ is the convolution of P(f) with D(f), (the Fourier transform of d(t)), according to the multiplication theorem. Thus,

$$P'(f) = P(f) * D(f)$$

$$= \int_{-\infty}^{\infty} P(f-\lambda)\, D(\lambda)\, d\lambda$$

$$= \sum_{q=-\infty}^{\infty} P(f - q/\Delta t) \qquad (3.2)$$

Equation 3.2 is a complex but extremely significant result. Let us first examine its significance for the case where the signal has no energy above a frequency $f_N = 1/2\Delta t$ (the Nyquist frequency) i.e.;

$$P(f) = \begin{cases} \text{arbitrary}, & f < f_N \\ 0, & f \geq f_N \end{cases}$$

Figure 3-7 is a plot of the resulting real part of $P'(f)$ resulting from the transform of a real time series. The real part of P(f) is an even function. $P'(f)$ is a continuous even function of frequency f, which is identical with P(f) in the region $f_N < f < f_N$. It is repeated an infinite number of times centered at the frequencies $\pm q/\Delta t$ where q = 1, 2 ...

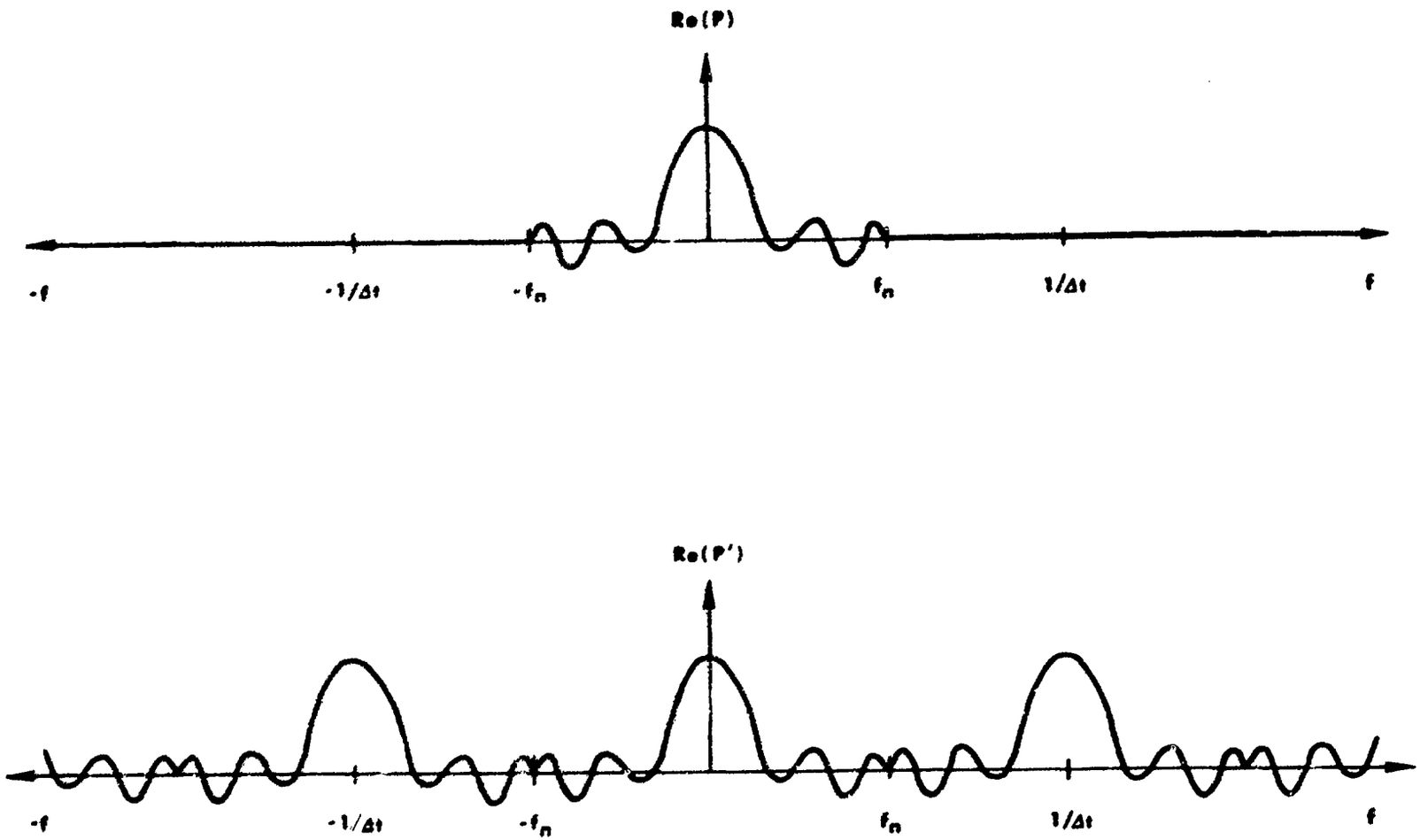

Figure 3-7 Comparison of discrete and integral Fourier transforms. The real part of a discrete Fourier transform (Re(P')) is shown plotted below the real part of an integral Fourier transform (Re(P)) for a time series with zero spectral energy components at frequencies f greater than $f_N = 1/2\Delta t$

Thus our condition that P(f) have zero value above f_N is a sufficient condition for $P'(f) = P(f), |f| < f_N$. Further, it is a necessary condition, since if $P(f) \neq 0$ for some f_1 greater than f_N but less than 2f, then at the frequency $f_2 = 2f_N - f_1$ we have from Equation 3.1,

$$\begin{aligned} P'(f_2) &= P(f_2) + P(f_2 - 1/\Delta t) \\ &= P(f_2) + P(f_2 - 2f_{max}) \\ &= P(f_2) + P(f_1) \\ &\neq P(f_2) \end{aligned}$$

The influence of signal above the Nyquist frequency on the resulting DFT is called aliasing, and its removal is called anti-alias filtering. Thus we see that appropriate anti-alias filtering is both necessary and sufficient to produce a DFT that is exactly equal to an IFT of a finite duration signal.

When we perform a Fast Fourier Transform (FFT), this amounts to an evaluation of a DFT (Equation 3.1) at discrete frequency intervals that are sub-multiples of f_{max}. If the total number of frequencies is N (usually a power of 2), we evaluate the complex value of $P'(f)$ at the frequency series,

$$f = \frac{n\, f_N}{N-1}, \quad n = 0, 1, 2, \ldots N-1.$$

It may be shown[9] that a necessary and a sufficient sampling for completely recovering the energy spectrum is obtained when

---

[9] W. T. Cochran et al, "Burst Measurements in the Frequency Domain", Proceedings of the IEEE Vol. 54, No. 6, pp 830-841 Appendix B.2.

the spectrum is computed at the frequency intervals 1/2T, where T is the total length of the time series. For a burst duration 0.5 seconds long, this requires spectrum sampling at every 1 Hz. If such a sampling is achieved, according to the Cardinal Series of Interpolation Theory[9a] the continuous Fourier spectrum can be constructed from the expression;

$$P'(f) = \sum_{n=-\infty}^{\infty} P'(n/t)\ \frac{\sin(\pi(f - n/T)T)}{\pi(f - n/T)T} \qquad (3.3)$$

where f is an arbitrary frequency in the range $|f| < f_{max}$

n is an integer series

T is the total period of the signal

Note in the above expression that although P' repeats cyclically at frequencies $2nf_{max}$, the sin x/x term rapidly damps out so that the computation can be achieved to an arbitrary level of accuracy with a finite number of terms.

Further, the energy density can be explicitly evaluated also,[9b] using a similar interpolation expression, i.e.,

$$E(f) \sim |P(f)|^2 = \sum_{n=-\infty}^{\infty} |P(n/2T)|^2\ \frac{\sin(2\pi(f - n/2T)T)}{2\pi(f - n/2t)T} \qquad (3.4)$$

where $|P(n/2T)|^2$ are discrete samples of the continuous energy density spectrum $|P(f)|^2$.

Thus we see that the DFT is an extremely powerful way of evaluating impulse spectra with the possibility of allowing

---

[9a] Cochran, op.cit., Appendix B.1

[9b] Cochran, op.cit., Appendix D

us, in a single evaluation of the data, to determine exactly, all of the information that is available in the energy spectrum, which can then be used to compute exactly the energy spectrum in any other bandwidth. The requirements for this exact analysis using any DFT are the following:

- The time series to be analyzed contains the entire event.
- The energy spectrum is computed at frequency intervals given by $\Delta f = 1/2T$, where T is the duration of the event. This can be achieved by adding zeros so that the total signal length analyzed is at least 2T. (This permits application of the interpolation formula.)
- The energy spectrum of the time series contains no energy at or above a maximum frequency $f_N = 1/2\Delta t$ (this elimates all aliasing error).

The third condition is virtually impossible to realize in practice, so in the following section we derive error estimates for realizable anti-aliasing filters, after a brief discussion of errors arising in the FFT computation due to finite word length.

3.2.2 Finite Word Length FFT Error. The procedure almost universally used to perform a Discrete Fourier Transform (DFT) is the "fast fourier transform" (FFT), which is a particular means of coding the DFT operation in a way that substantially reduces computation time over that of direct computation by taking advantage of periodicity in the computation procedure. It is inherently no more nor less accurate than any other means of computing the desired result. The fact that, in any computer, the numerical values used must be of finite length implies that in the process of performing the many additions and multiplications of data values, the rounding or truncation that must be performed at various levels will introduce errors in the computed results, independent of the errors in the input data to the program. In some sense then, the errors may be viewed as a noise term that is introduced within the FFT program. Unfortunately the magnitude of this noise is far from independent of the input signal. Extensive analyses of FFT error have been published in the literature, and will not be reproduced here, but their results will be quoted.[10]

For a fixed point FFT, where the data values are presented as integers and a special form of rounding is used (rounding a value up or down at the edge of the round-off interval is performed on a random basis) results in an upper bound error of,

---

[10] E. R. Rabiner and C. M. Rader, ed., Digital Signal Processing, IEEE Press, N.Y., 1972. See in particular: P. D. Welch, "A Fixed-Point Fast Fourier Transform Error Analysis", pp 470-476, C. L. Weinstein, "Round Off Noise in Floating Point Fast Fourier Transform Computation", pp 477-483.

$$\frac{\text{rms(error)}}{\text{rms(result)}} \leq \frac{C \cdot 2^{(M+3)/2} \cdot 2^{-B}}{\text{rms(initial sequence)}} \qquad (3.5)$$

where: rms(error) is the rms value of the computation error

rms(result) is the rms value of the resulting spectrum

C is a constant that depends on the machine arithmetic and varies between 0.4 and 0.9

M is the number of stages in the FFT ($M = \text{Log}_2 N$ where N is the number of FFT data words, so $N = 2^M$)

B is the maximum number of bits in the representation of a number in the machine (word length)

rms(initial sequence) is the rms value of the time series, scaled so that the magnitude of the maximum time series value is equal to unity. (Thus it is proportional to the inverse of a signal "crest factor".)

The rms error in dB of the fixed point FFT may be determined from the signal plus noise to noise ratio as,

$$\text{FFT}_F\text{ERROR(dB)} \leq 20 \text{ Log } \left(1 + \frac{C \cdot 2^{(M+3)/2} \cdot 2^{-B}}{\text{rms(initial sequence)}}\right) \qquad (3.6)$$

For a transient signal f(t), rms(initial sequence) in this context is;

$$\text{rms(initial sequence)} = \frac{\left(\int_0^T f^2(t)\, dt\right)^{\frac{1}{2}}}{|f_{max}(t)|\, T}$$

or in terms of acoustic parameters

$$= \frac{1}{T} \left(\frac{\text{(Total "intensity")}}{\text{Peak "signal"}}\right)^{\frac{1}{2}}$$

where T is the duration of the observation time interval.

For shallow SUS shots rms(initial sequence) is of the order of 0.003/T, unfiltered (0.01/T, filtered at 1 kHz). Thus the fixed point FFT error will be;

$$\text{FFT}_F\text{ERROR(dB)} \leq 20 \text{ Log } \left(1 + \frac{C \cdot 2^{((M+3)/2)-B}}{3 \cdot 10^{-3}/T}\right) \qquad (3.7)$$

For a 16 bit word length, a 4096 (2^{12}) word FFT of 1 second duration, and a 1 kHz filter, this yields a maximum error of,

$$\text{FFT}_F\text{ERROR} \leq 20 \text{ Log } \left(1 + \frac{0.4 \cdot 2^{((12+3)/2)-16}}{0.01/T}\right)$$

$$= 20 \text{ Log } 1.04$$

$$= 1 \text{ dB}$$

A lower bound estimate for the error of a spectrum, from Reference 10 gives,

$$\text{FFT}_F\text{ERROR(dB)} \geq 20 \text{ Log } (1 + (M-2.5)^{\frac{1}{2}}(.3)2^{-B})$$

which, for the above example, gives a minimum rms error of the order of 0.005 dB.

For the experimental data given in the same paper from

Reference 10, the error was between one tenth of the upper bound and the upper bound.

The error analysis expression predicts increased error for increased signal "crest factor", decreased machine word length, and increased number of FFT words.

For a floating point FFT, upper bound of the error is typically less, and is given by;

$$FFT_{FL}ERROR(dB) = 20\ Log\ (1 + 0.5 \cdot 2^{-m} \cdot M^{\frac{1}{2}})$$

where m is the number of bits used in expressing the mantissa of the floating point word, and M as before is the number of stages. For comparison with the previous example, a machine would use two integer words to represent a single precision floating point word, so that perhaps 20 bits might be used in the mantissa, giving an error of about $3 \cdot 10^{-5}$ dB, which is completely negligible for this analysis. The increased precision of the floating point FFT is achieved at the expense of substantially increased machine memory (2x) and a much longer computation time.

Figures 3-8a and b give plots comparing the FFT and exact spectra for a set of conditions that correspond to the above examples, performed on a Varian 620L minicomputer with 16 bit arithmetic, using a fixed point FFT routine. The signal analyzed corresponds to a shallow shot, direct signal only (1.8 lb, 60 ft depth, 300 ft range) 1024 Hz cut-off frequency, sampling rate 4096 Hz ($f_s = 2 \times F_N$), 1 second

of data, 16 bit representative). The agreement between the FFT and true spectrum is so good that these two curves superimpose on each other. The dashed line shows their differences on an expanded scale while the triangles show the differences in the 1/3 octave band spectral levels. Computations on the difference data indicate an rms error from 1 to 500 Hz of about 0.3 dB (excluding the 0 Hz term), which compares favorably with the above fixed point FFT upper bound error estimate of 1 dB . The mean bias of about 0.1 dB in both the 1 Hz spectrum and the difference in 1/3 octave band values is believed to be the result of round-off error in the FFT.

3.2.3 Aliasing Error. Figures 3-9a and b show the effect of increasing the antialiasing filter cutoff frequency to 2048 Hz, which is also the Nyquist frequency for this sample rate. The positive bias introduced is clearly obvious at high frequency (above 250 Hz). Using the theory of Appendix B the predicted error (ratio of signal plus noise to noise) is:

$$\text{ALIAS ERROR(dB)} = 10 \text{ Log } \frac{E_2'''(f)}{E_2(f)}$$

$$= 10 \text{ Log } \left[1 + \left(\frac{f_c}{f_N}\right)^{2n} \left(\frac{f}{2f_N}\right)^{2}\right] \qquad (3.8)$$

$$f_r < f << f_c,\ f_c \leq f_N$$

For $f_c = 1024$ Hz (i.e. $f_s > 2\ f_N$) , Equation 3.8 predicts an alias error of less than $6 \cdot 10^{-3}$ dB, which cannot be detected in Figure 3-8 in the presence of the FFT round-off error.

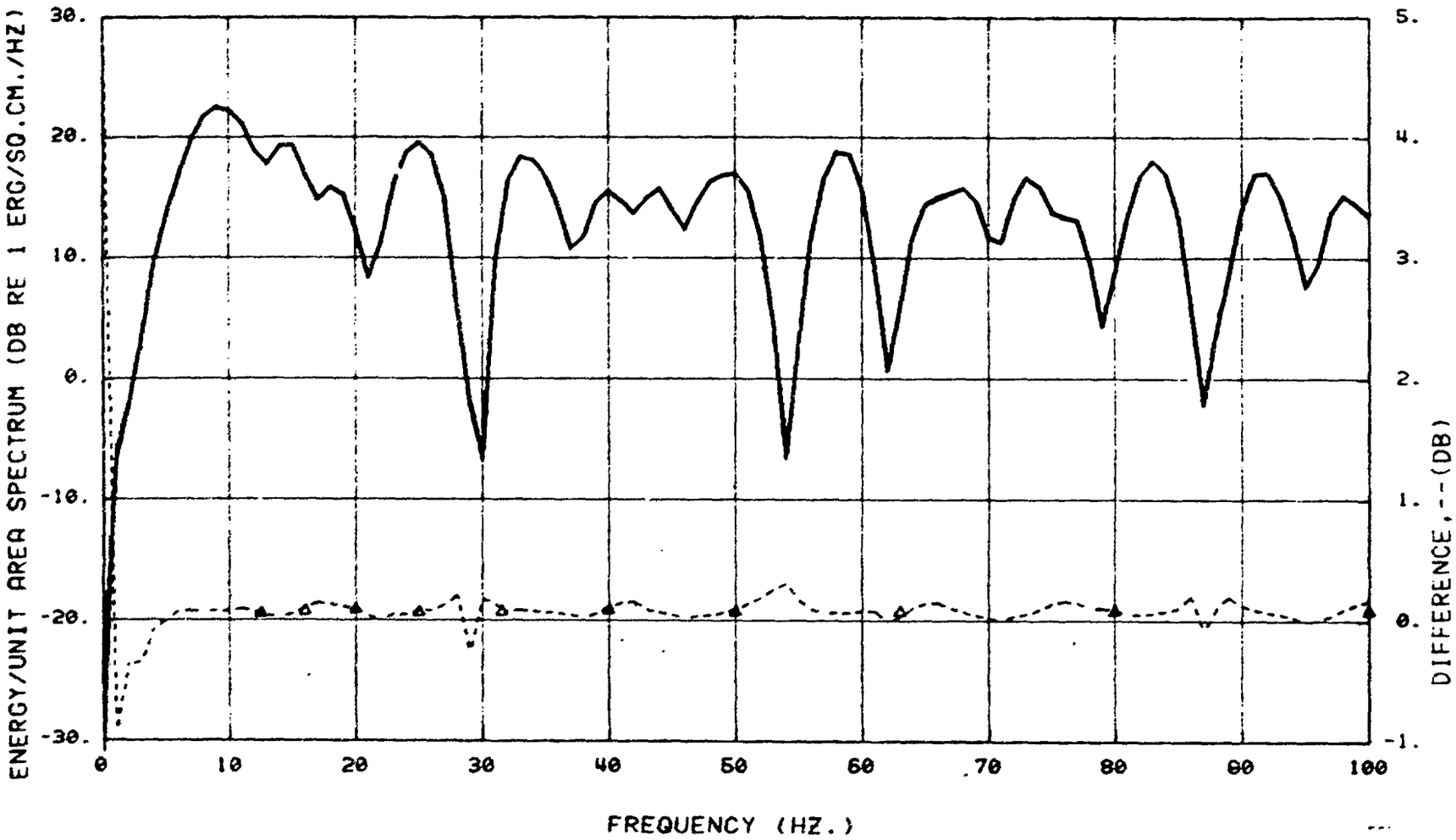

Figure 3-8a. Baseline 4096 term fixed-point FFT comparison. Shot Parameters: 1.8 lbs, 60 ft depth, 300 ft range; Analysis Parameters: Sample Rate 0.24414 msec (4096 Hz), antialias filter cut off 1024 Hz. Sample Quantization 16 bits, FFT implementation 16 bits (sampling starts at initiation of signal. Heavy Solid Line - FFT Spectrum; Light Solid Line - not visible in this figure) - Exact Spectrum; Dash Line - Difference between FFT and exact (expanded scale); Triangles Δ - difference between 1/3 octave band spectrum levels (expanded scale)).

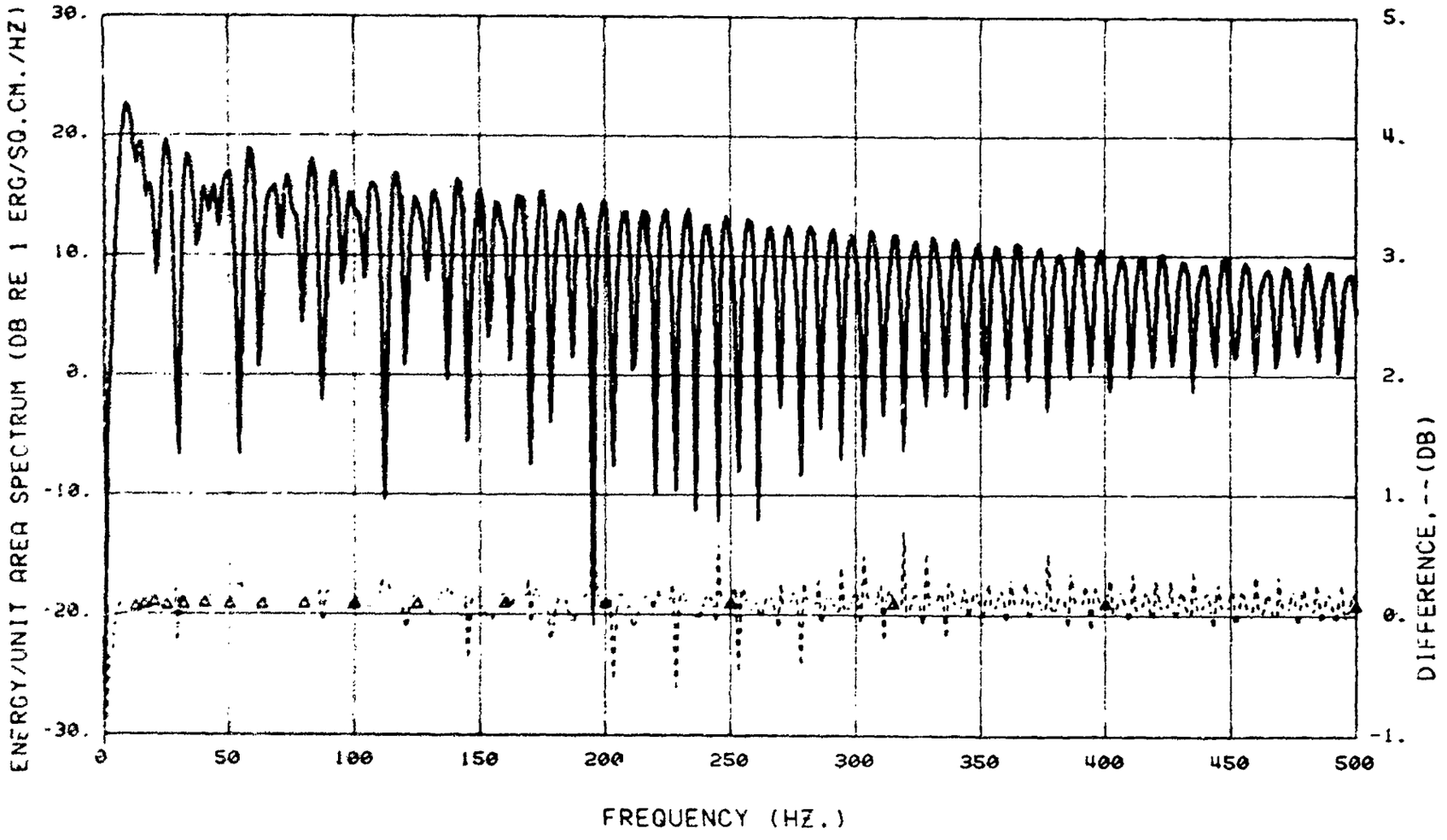

Figure 3-8b. Same as Figure 3-8a except frequency range 0 - 500 Hz.

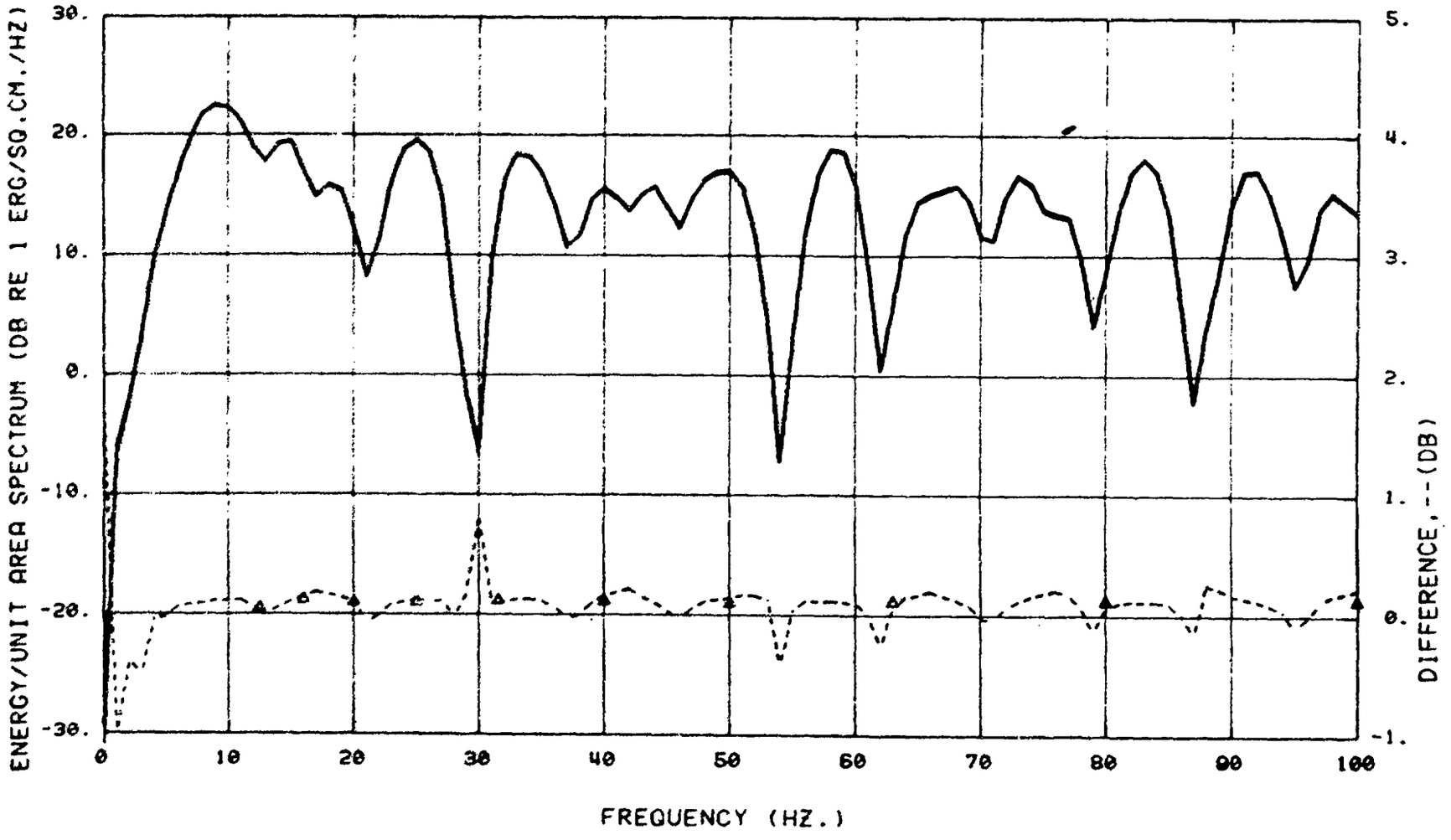

Figure 3-9a. Fixed point FFT comparison showing aliasing error. Shot parameters same as for Figure 3-8 except f_c = 2048 Hz.

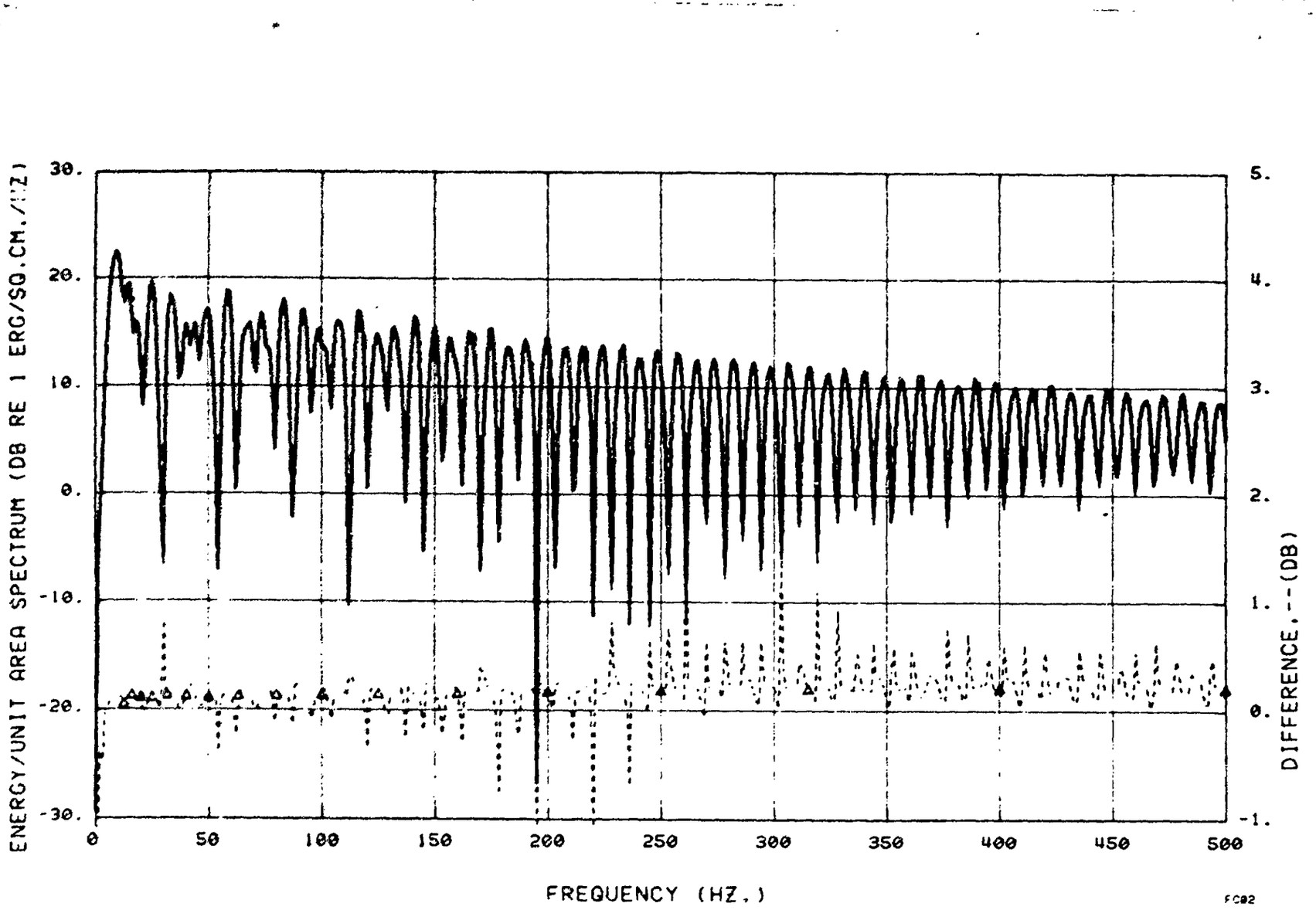

Figure 3-9b. Same as Figure 3-9a except frequency range 0 - 500 Hz.

For f = 500 Hz, $f_c = f_N$ = 2 kHz, Equation 3.8 predicts an aliasing error of about 0.2 dB, which is comparable to a 0.1 dB increase in error observed in the 500 Hz 1/3 octave band (compare Figures 3-8b and 3-9b). The increase in negative going errors at frequencies below 250 Hz in Figure 3-9b is attributed to interaction with the round-off error term.

3.2.4 Finite word length quantization error. Traditionally, when dealing with noise signals, quantization error has been treated as an additicnal noise process because the quantization process can be represented as the addition of a small oscillating signal (magnitude equal to half the quantization interval) that has a uniformly-distributed amplitude independent of the quantized time series. For a SUS signal, error is correlated with the signal. Here we find that, for times where the signal is rapidly varying (i.e. has high frequency content), it also has a relatively high amplitude, and conversely, low amplitude is correlated with low frequencies, so the signal cannot be uniformly well-described over the frequency range of interest by a few discrete steps. For the shot studied (1.8 lb, 60 ft depth, 300 ft range) the peak pressure (when filtered to 1 kHz) is about 16 psi, while the minimum negative-going pressure is about 0.4 psi. Thus a 4-bit representation would completely eliminate (set to zero) all time series values except those in the immediate vicinity of the shock wave and bubble pulse peaks. Since the long periods of low pressure

with very slow pressure gradients carry the low frequency information, it is this region that is affected most by low quantization resolution.

Figures 3-10a through 3-13b show the effects of progressive reduction in the number of bits (from 14 to 8) used to represent the signal (see Figure 3-8 for the 16 bit case). (Note: more than 50% overrange for the input signal was allowed (i.e. peak signal less than 66% of full scale).) The error shown in these figures is a combination of the FFT round-off error and the quantization error. Since the errors are of a related type, there is considerable interaction between the two. Table 3-1 shows a comparison of single number measures of the errors. The trend of the data is for a slight reduction in error going from the 16-bit (Figures 3-8a and b) to 14-bit representation, followed by a progressive increase in error for further reduction in number of bits. The FFT input data were not corrected to zero mean value in this analysis, so that the substantial growth in the DC (0 Hz) term in the FFT is also indicative of the fact that quantization is not an unbiased operator for this signal.

The net decrease in error of the FFT for a change from 16- to 14-bit signal representation is interpreted as a reduction in FFT round-off error while still preserving adequate signal representation. Unfortunately, the FFT error analyses in the

(Text continues on Page 52)

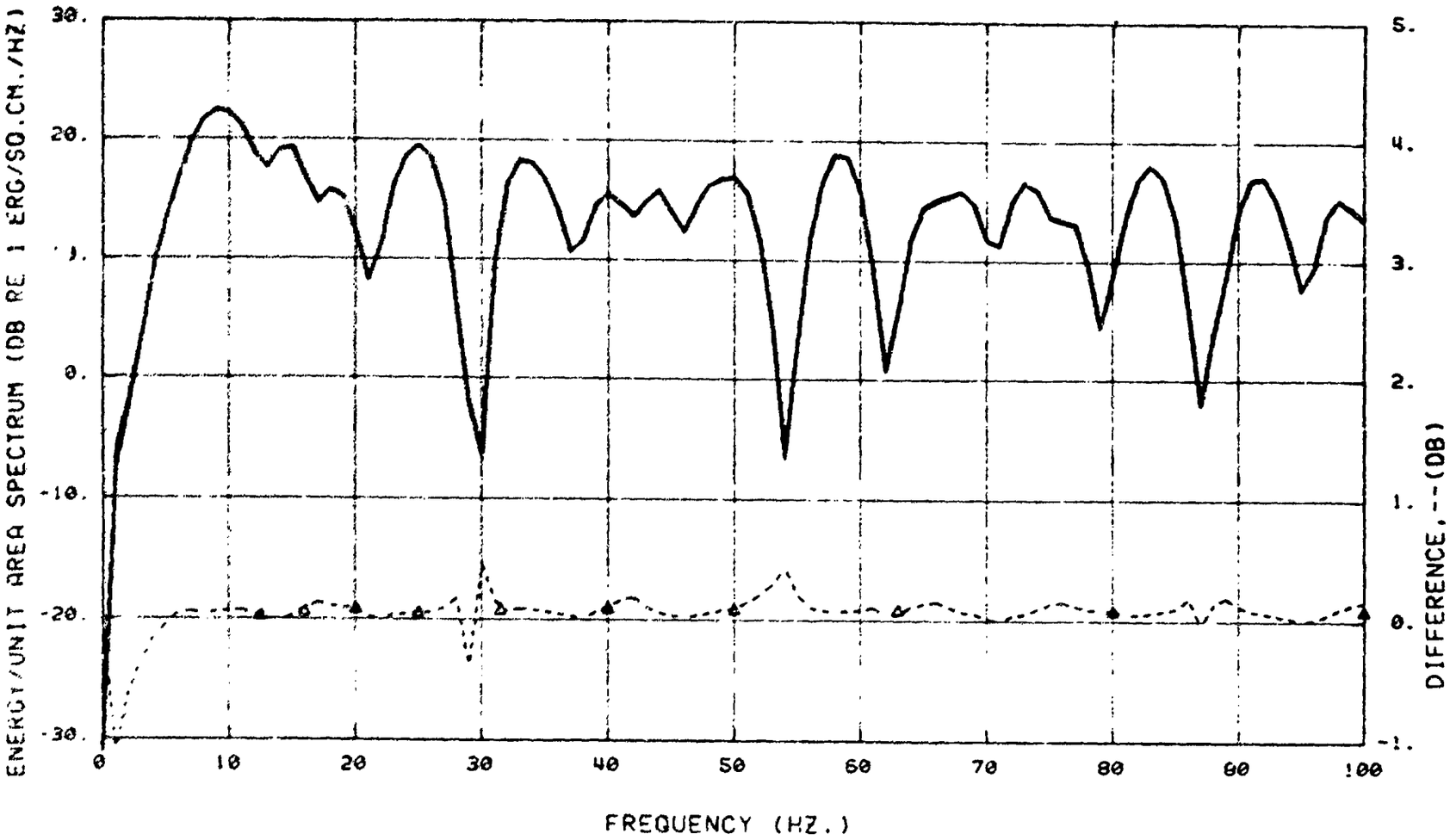

Figure 3-10a. Effect of quantization. Standard shot, all parameters same as Figure 3-8 except quantization 14 bits.

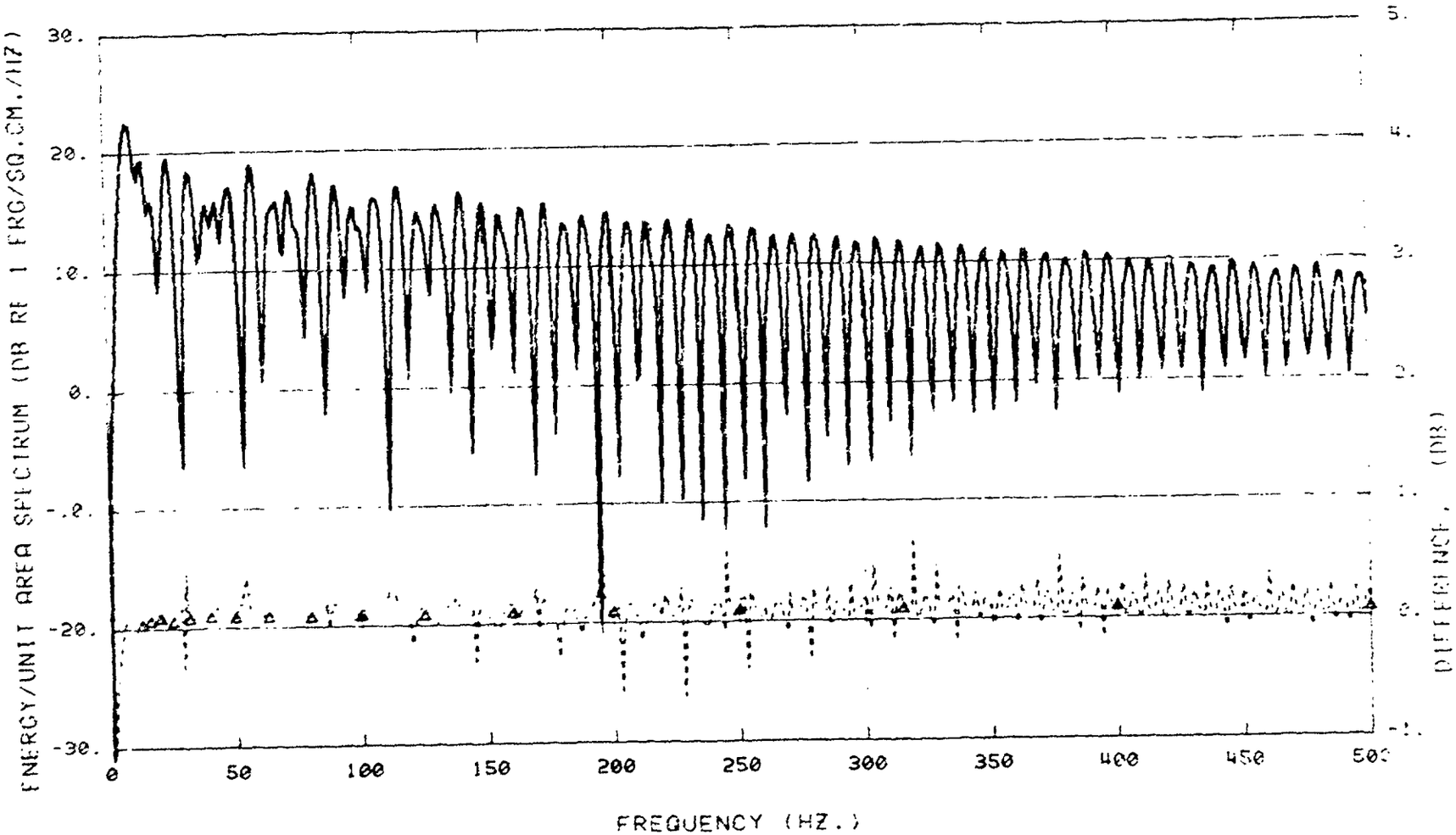

Figure 3-10b. Same as Figure 3-10a except frequency range 0 - 500 Hz.

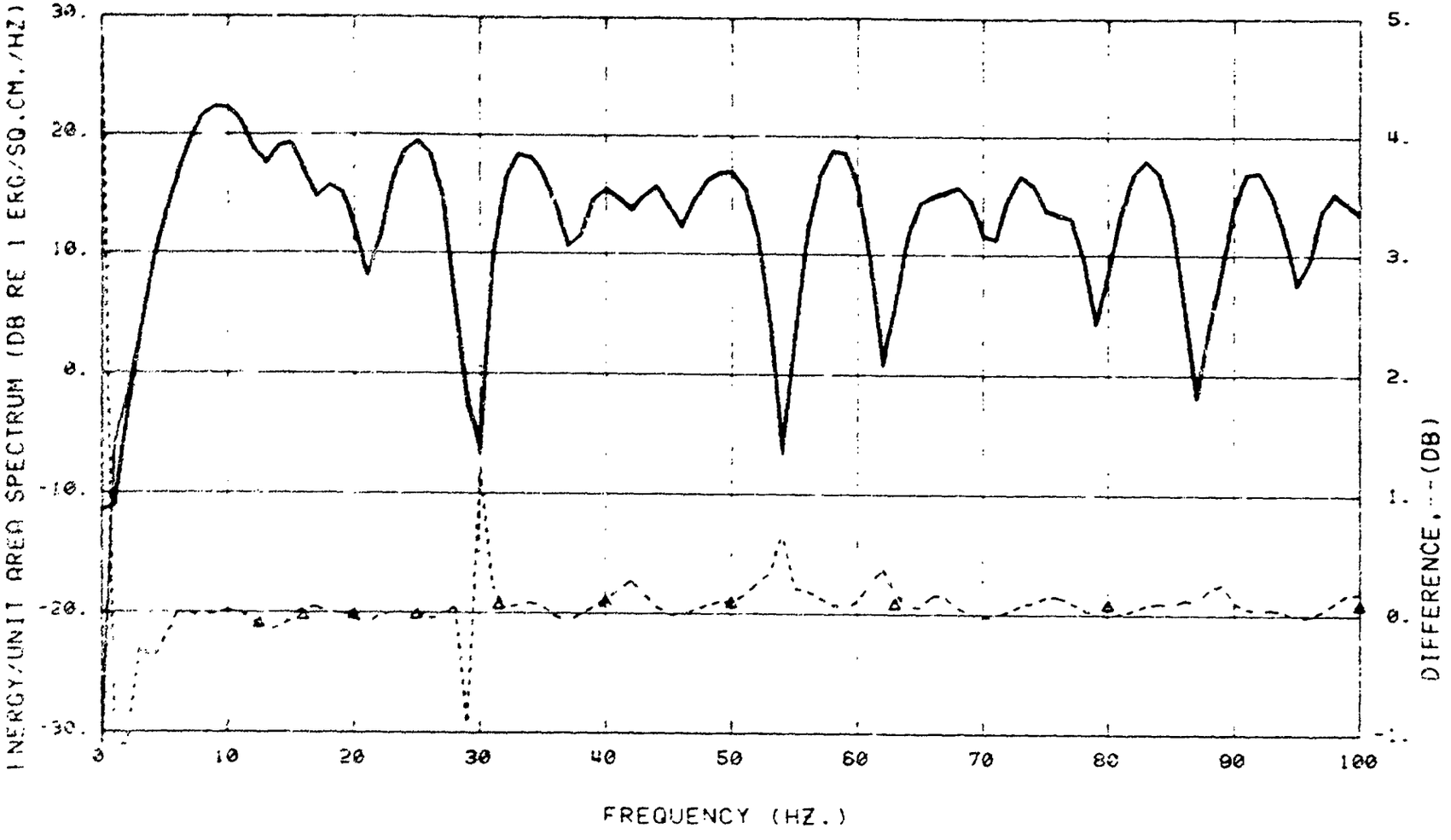

Figure 3-11a. Effect of quantization. Standard shot, all parameters the same as Figure 3-8 except quantization 12 bits.

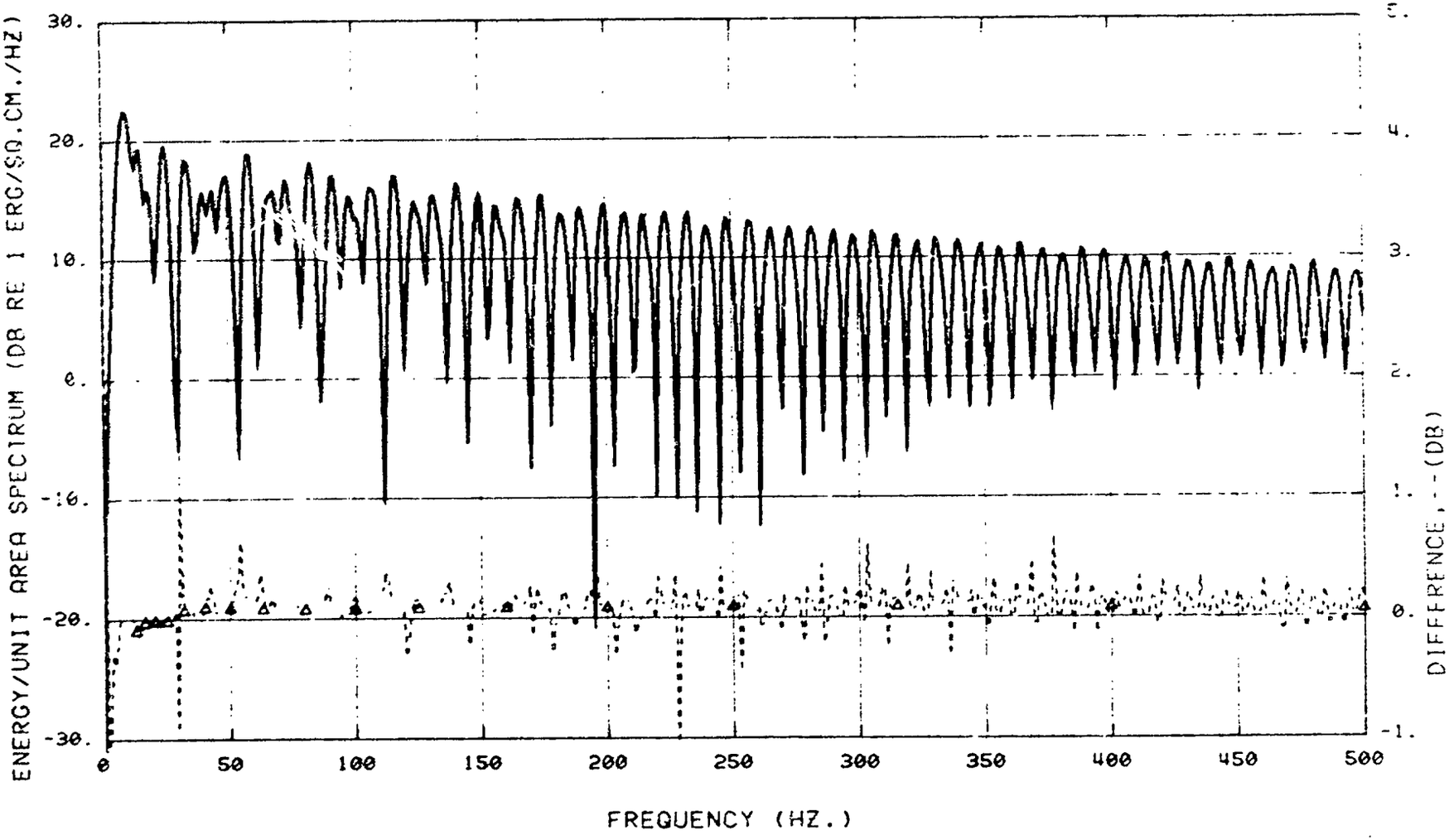

Figure 3-11b. Same as Figure 3-11a except frequency range 0 - 500 Hz.

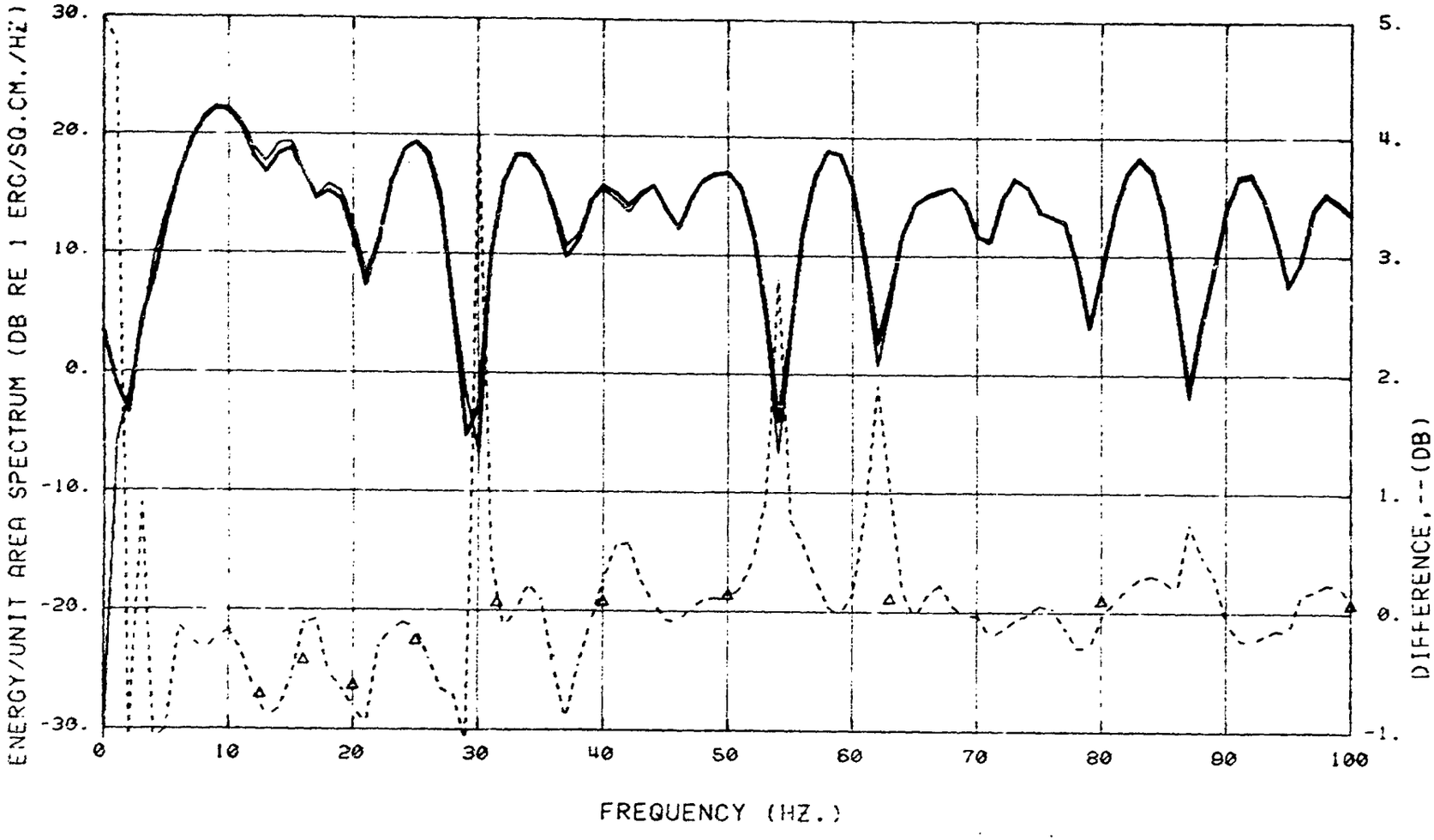

Figure 3-12a. Effect of quantization. Standard shot, all parameters as in Figure 3-8 except quantization 10 bits.

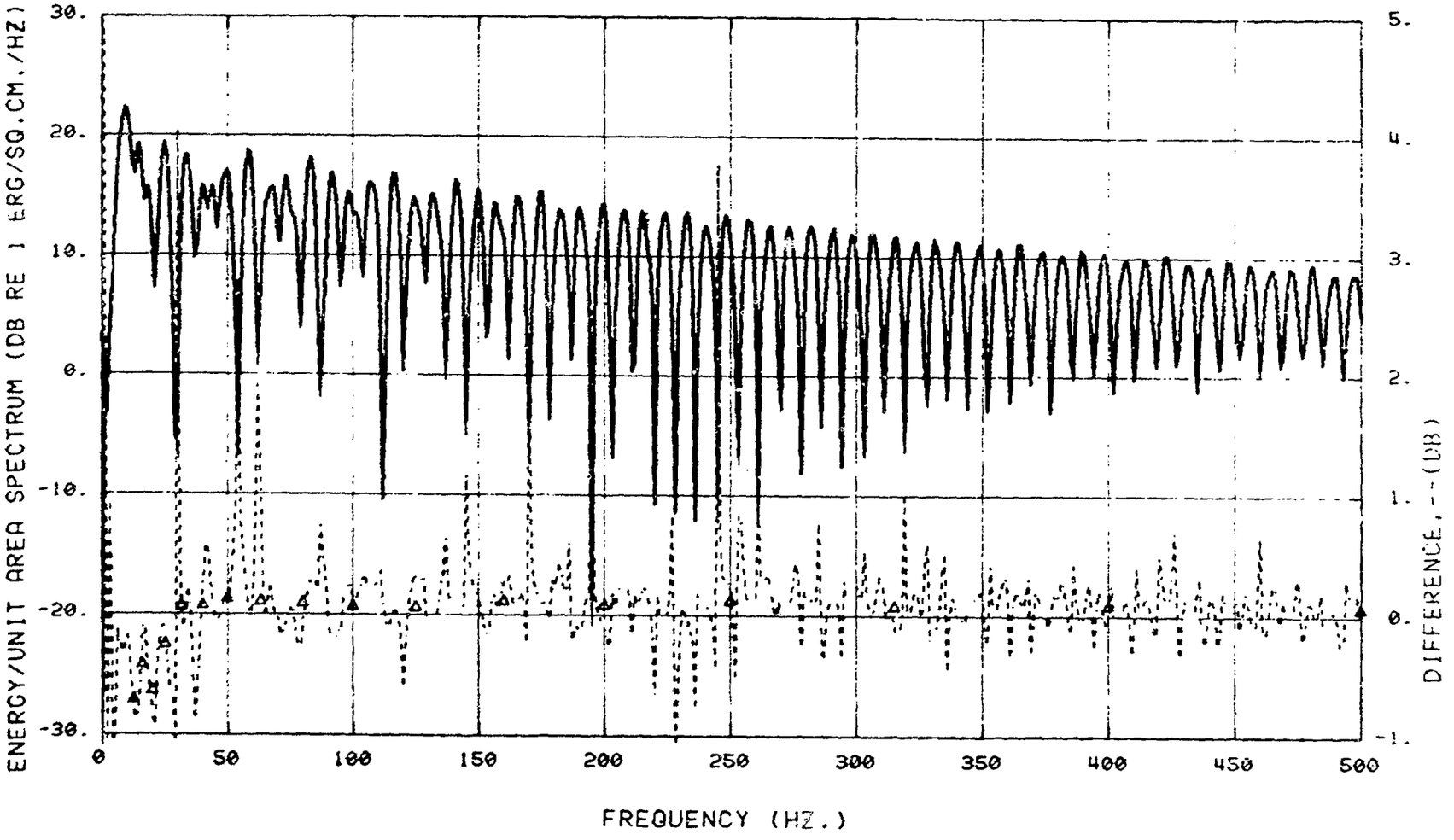

Figure 3-12b. Same as Figure 3-12a except frequency range 0 - 500 Hz.

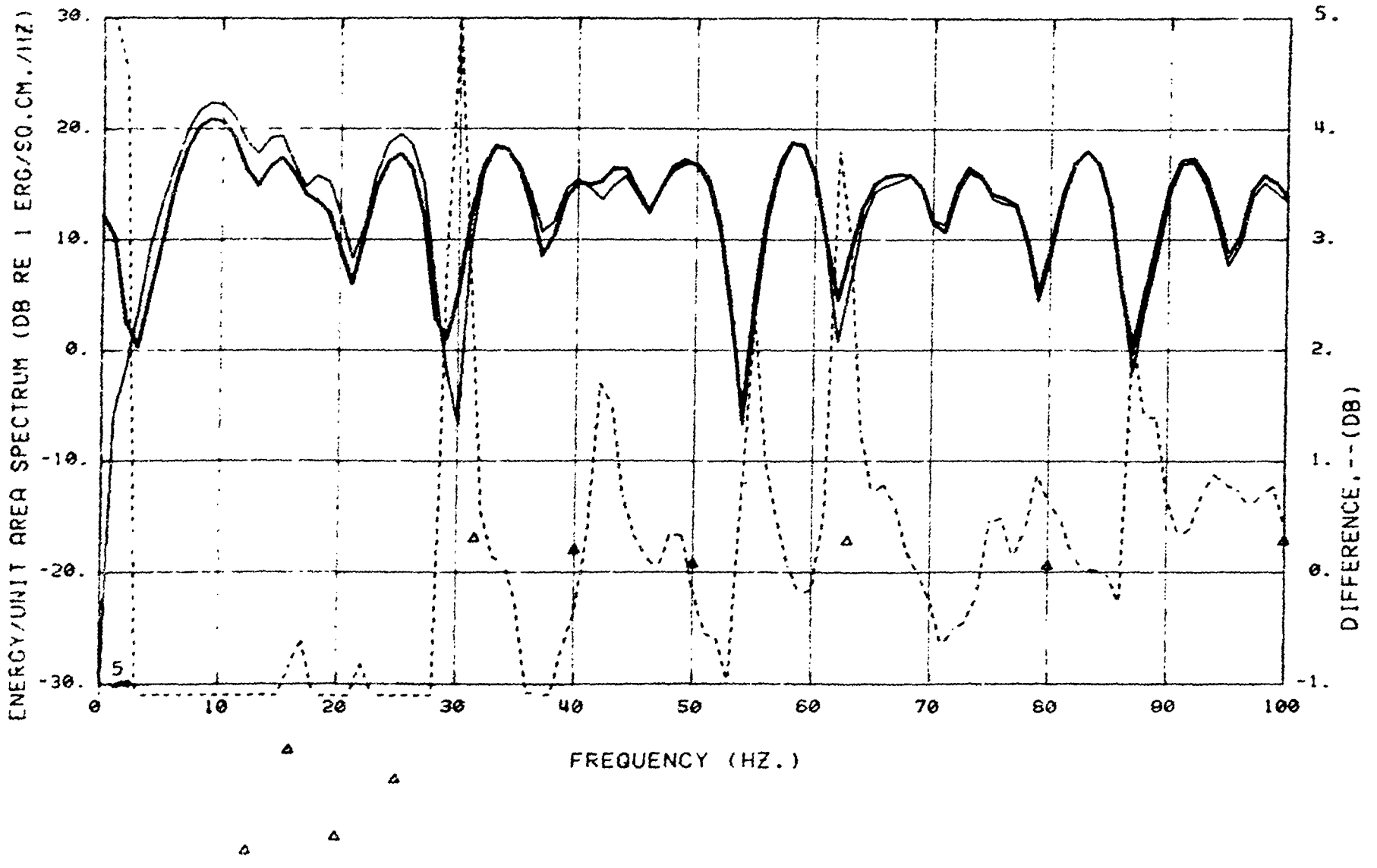

Figure 3-13a. Effect of quantization. Standard shot, all parameters same as Figure 3-8 except quantization 8 bits.

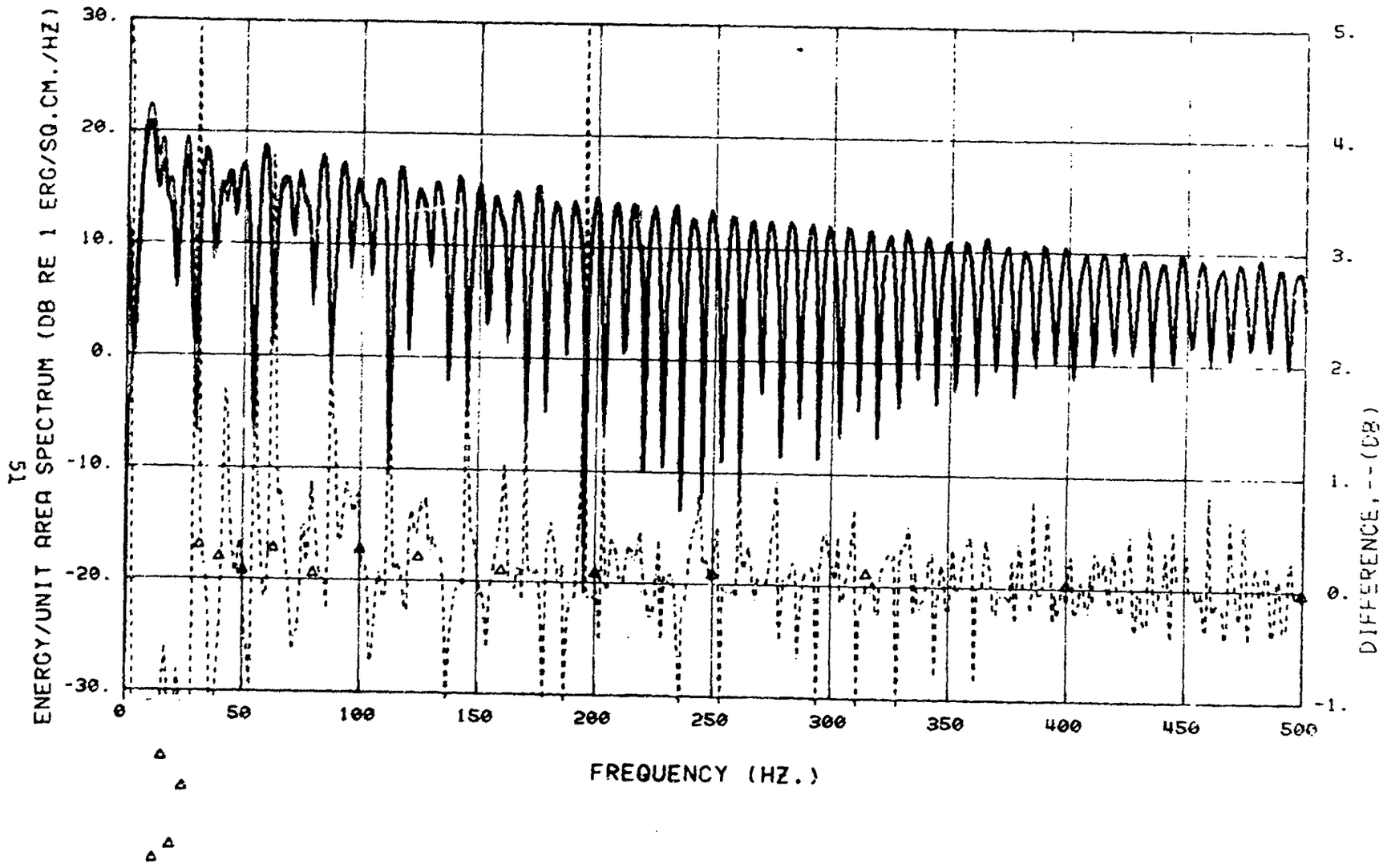

Figure 3-13b. Same as Figure 3-13a except frequency range 0 - 500 Hz.

literature do not incorporate this, but rather deal only in fully-scaled signals, so we are unable to predict this effect quantitatively. It can be understood intuitively from the fact that, with fewer bits in the incoming signal, there is less need for rounding the results of additions in the early stages of the FFT, thus reducing the errors that are propagated to later stages.

Table 3-1 gives the rms error for 1 Hz band spectra and mean error in 1/3 octave bands for the calculations shown in the previous figures. For a 16-bit, fixed point FFT, a 14-bit signal representation gives a minimum in combined round-off and quantization error and a 12-bit representation is almost as precise as a 16-bit representation. Neither of these conclusions is expected to apply to a floating point FFT since that would have a much lower FFT round-off error. In the floating point case, increasing the number of bits in the signal representation is expected to provide a more precise FFT; the rms errors in Table 3-1 would certainly be upper bounds. Further, the errors for 1/3 octave data are expected to represent accurate estimates of mean error for a floating point FFT, since the indicated biases are in large part due to data quantization, and so are not strongly dependent on the type of FFT.

This source of error can apparently be made sufficiently small, using readily available hardware, to be negligible for

Table 3-1

Total fixed point error in 16-bit FFT of a shallow shot (direct signal only) vs number of bits in digital representation of input signal.

Number of bits for input signal	1 Hz Band Rms ERROR (dB)		1/3 Octave Band Mean Bias dB	
	1-100 Hz	1-500 Hz	12.5-100 Hz	12.5-500 Hz
16	0.3	0.35	0.08	0.08
14	0.2	0.2	0.08	0.08
12	0.8	0.5	0.04	0.06
10	1.2	0.7	-0.15	0.03
8	2.6	1.2	-0.7	-0.4

the purposes of this study (e.g., minimum 12 bit "sample and hold" A-D with minimum 4 kHz sample rate).

We further note an interaction error that is present on some A-D converters, between sampling and quantization errors which perform the A-D by comparing against a "running" signal. The error manifests itself in the form of time base "jitter", due to the fact that this type of converter compares against the continuously-changing analog signal. Thus the particular time instant at which the sample value is taken is unknown, except that it is bracketed into a time window of some specified duration. This problem is completely avoidable, through hardware selection that uses "sample and hold" circuitry, and was therefore not considered in the analysis.

3.2.5 Registration effects and other signal processing questions. Registration is a term used in the context of signal processing to refer to the temporal location of the signal within the time window with respect to the time of some other event, such as the analysis start time or the time of occurrence of another signal. Since the analysis of the DFT processes as applied to transient events (Section 3.1) does not indicate the presence of any dependence on timing of the signal, other than that the signal is completely contained within the time window for the analysis, we expect no dependence on timing. Further, since the spectrum results from an error-free FFT

(no alias, FFT round-off or quantization errors) that is exactly correct and interpolatable exactly, any time domain information with respect to two or more signals present in the analysis window can be recovered exactly.

When error sources are present within the FFT, registration may be used to some advantage to modify these errors. Figures 3-14 through 3-16 illustrate these effects. In Figures 3-14 through 3-15, the signal is sampled with a ¼- and ½-sample-period time shift, while in 3-16a the signal is shifted 1,000 samples in the time domain by pre-filling the data sample with zeros. In Figures 3-14 through 3-15 we see subtle changes in the difference spectrum, but the mean and rms errors are not significantly altered from the corresponding values for the curve in Figures 3-8. In Figures 3-16 there is in fact a statistically-significant reduction in mean and rms error, which is attributed to a reduction in FFT round-off error in the early stages of the FFT calculation of low frequency components (i.e., less than 1 kHz).

Two other aspects of digital signal processing are appropriate to mention at this time. The first concerns the addition of zeros to round out the length of the time series to some convenient value, while the second concerns the use of windowing functions. Equation 3.1 clearly indicates that the addition or deletion of terms for which $p(q\Delta t)$ has zero value has no effect whatsoever on the value of the resulting spectrum. It is precisely this lack of effect, coupled with the finite

(Text continues on Page 62)

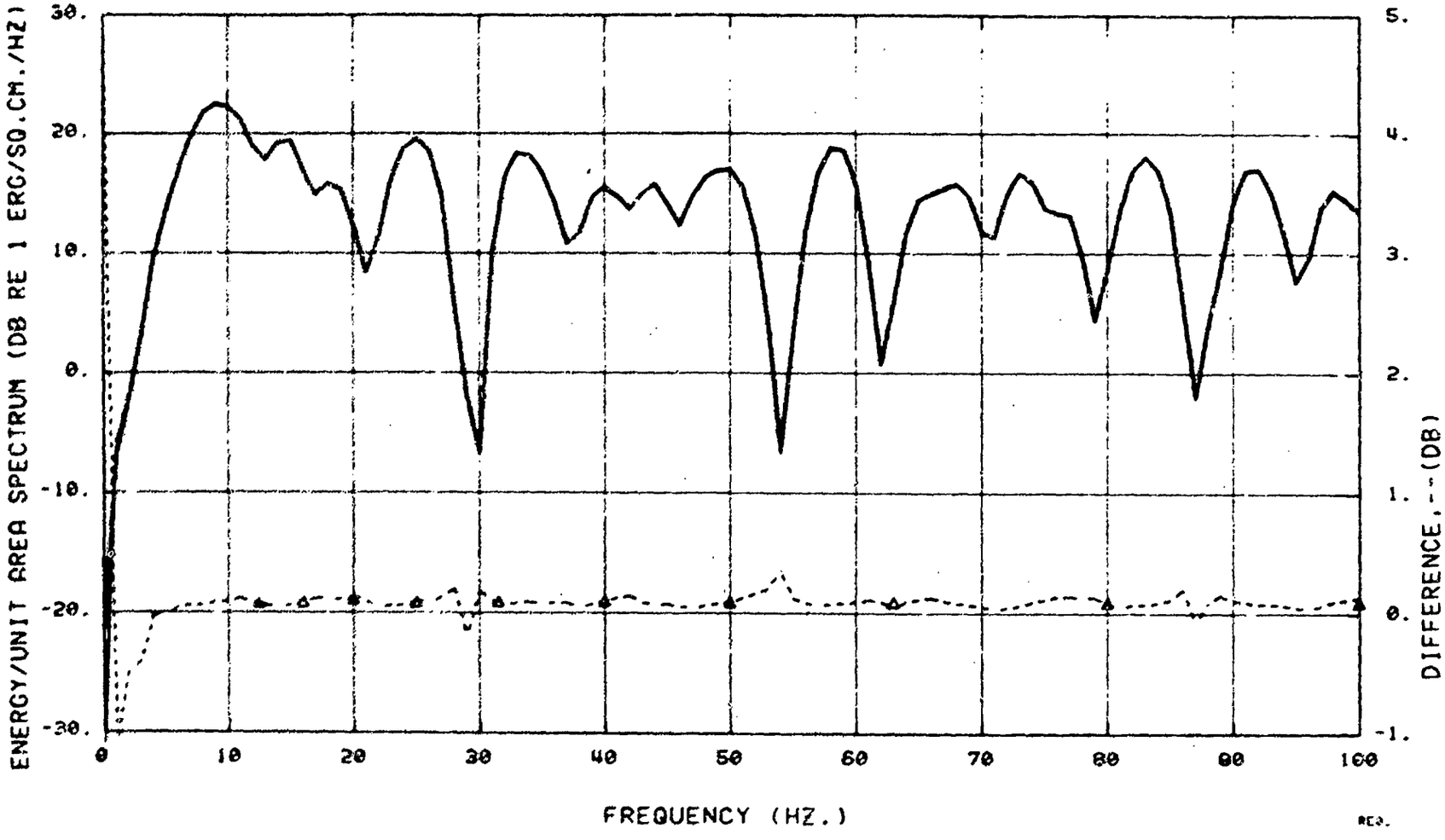

Figure 3-14a. Registration study. Standard shot, same as Figure 3-8 except time series starts at t = -0.061035 ms (-0.25 Δt) relative to start of shock wave.

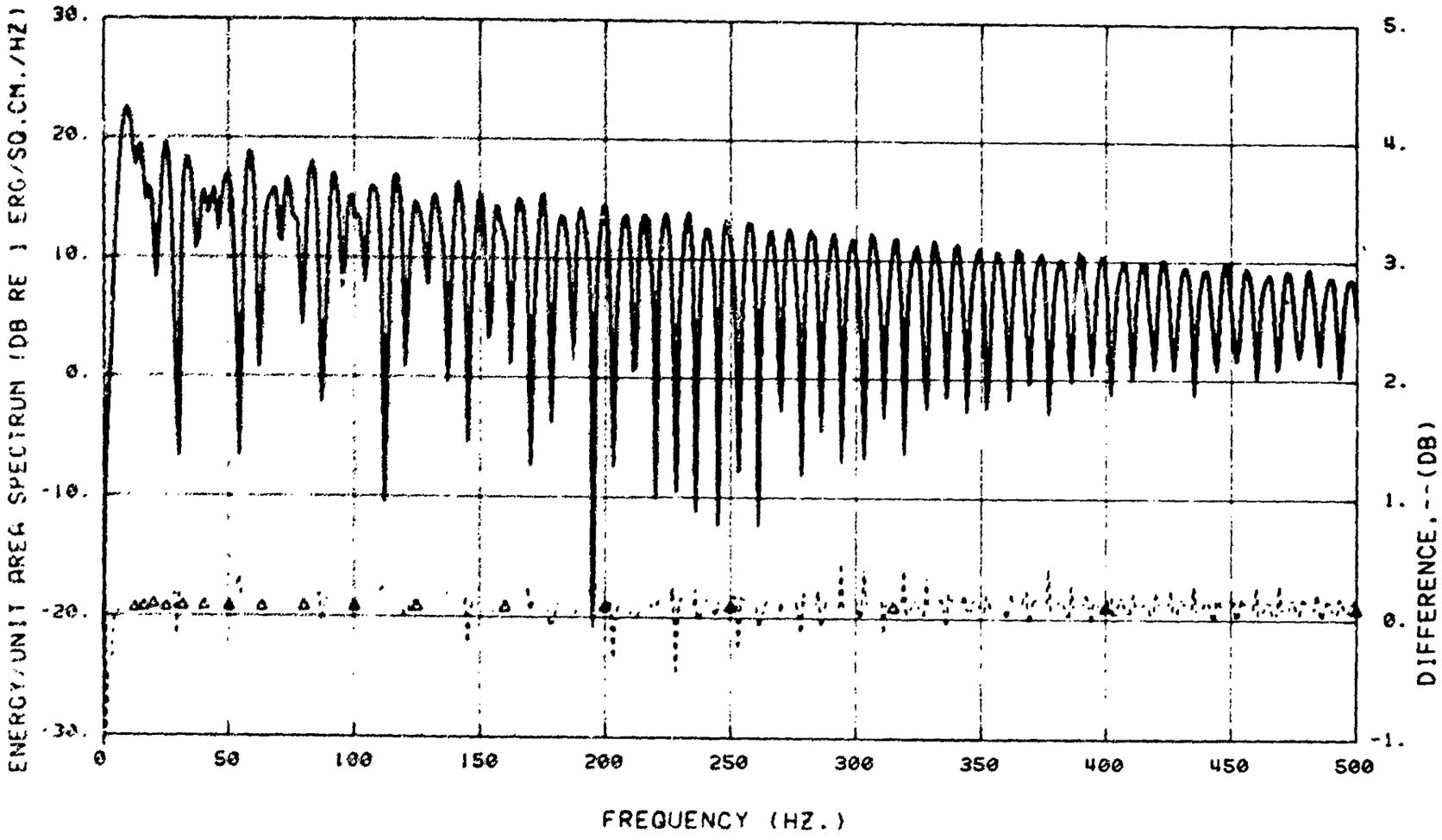

Figure 3-14b. Same as Figure 3-14a except frequency range 0 - 500 Hz.

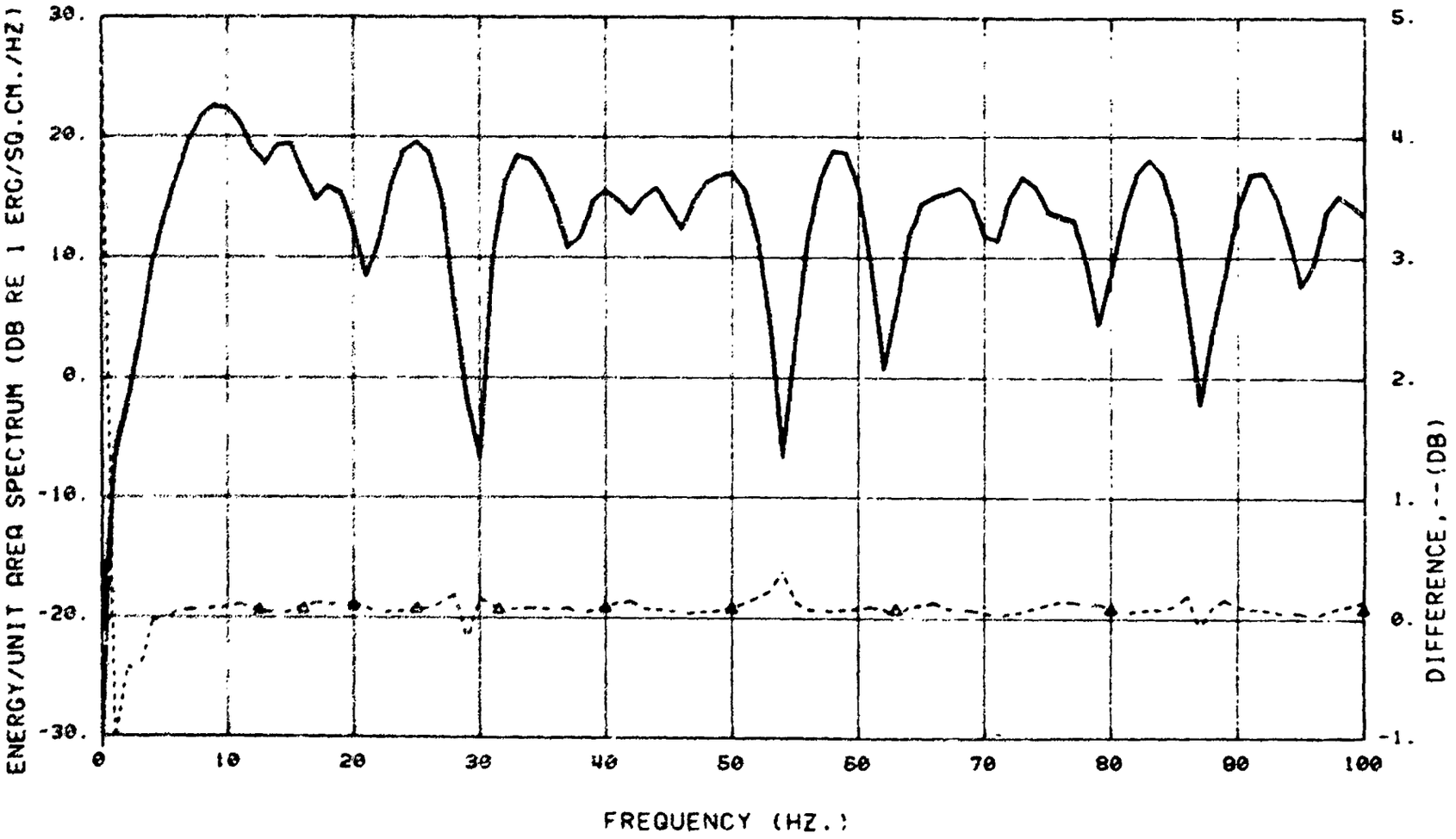

Figure 3-15a. Registration study. Standard shot (same as Figure 3-8) except time series starts at -0.12207 ms (-0.5 Δt) relative to start of shock wave.

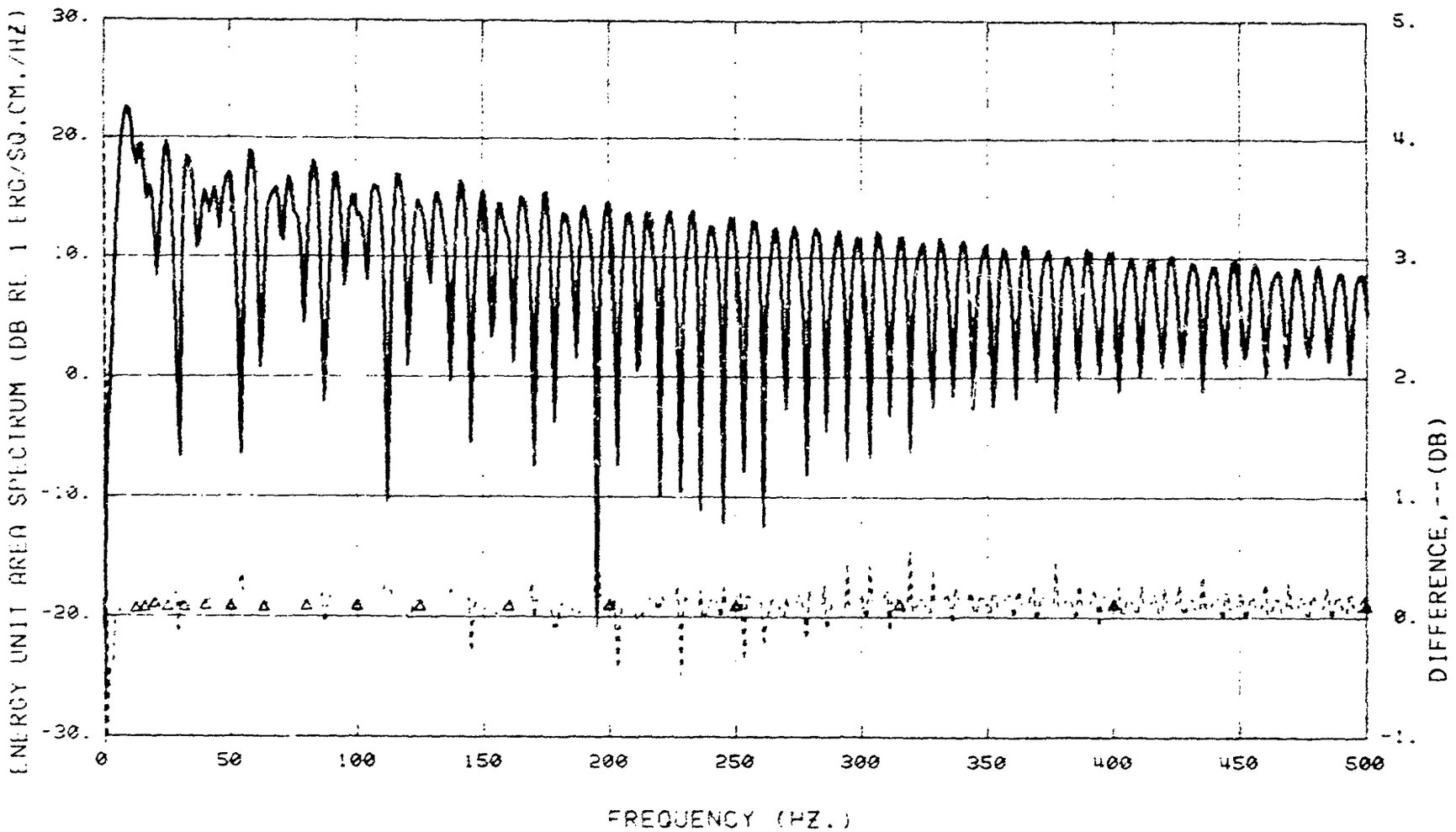

Figure 3-15b. Same as Figure 3-15a except frequency range 0 - 500 Hz.

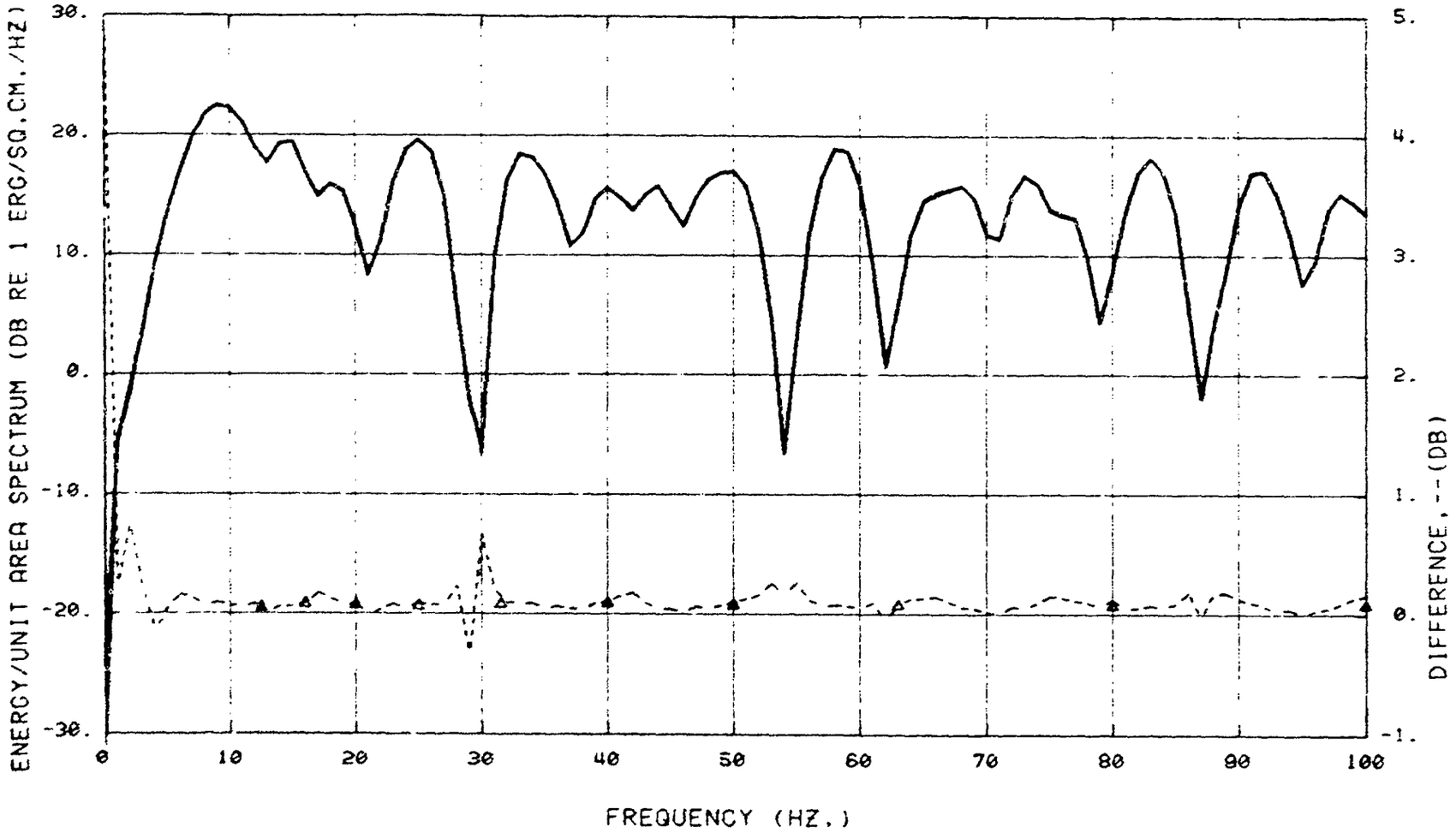

Figure 3-16a. Registration investigation. Standard shot (same as Figure 3-8) except time series starts at -244.1406 ms (-1000 Δt) relative to start of shock wave.

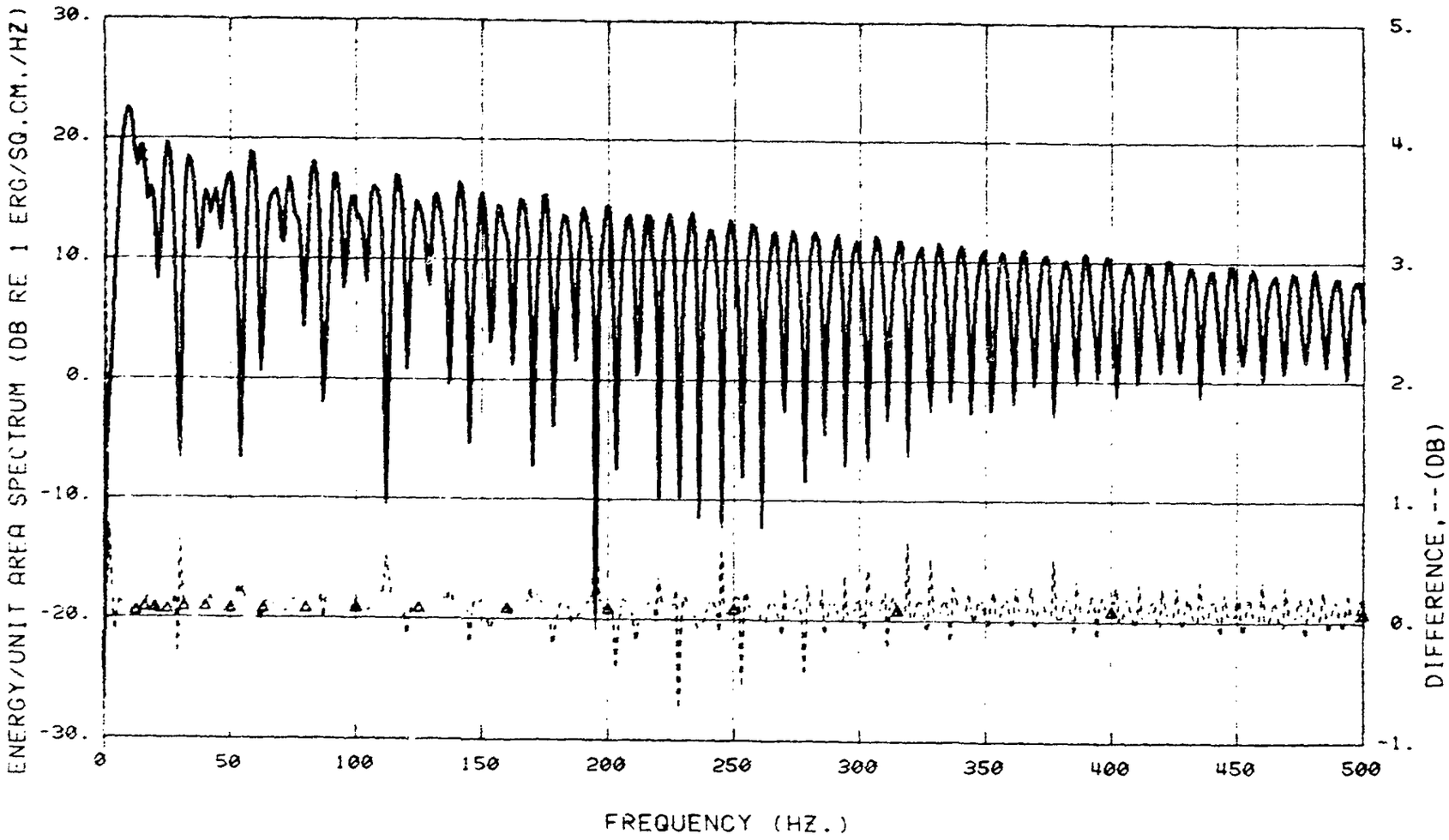

Figure 3-16b. Same as Figure 3-16a except frequency range 0 - 500 Hz.

time duration of the transient, that permits the exact realization of the summation with infinite end points. Further, when the time series is fully contained within the analysis time window, there are no signal discontinuities at the end points that are not already part of the signal, and therefore there is no need to "smooth" the signal by applying a window such as a Hamming or hanning smoothing function. Since the signal is by definition non-stationary, the application of such a weighting must give a result that depends on where the signal is in the window, with no hope of being able to appropriately correct the result for the weighting.

3.3 Surface Reflections

Having used the analytic model to examine signal processing parameters, it is appropriate to ask what other information might be learned. Two effects, clipping of the surface reflection and change of the spectrum shape with range, have been examined and are discussed in this and the subsequent subsection.

The effect of surface reflections on the resulting data is of critical importance for shallow (60 ft) shots because there is no receiver location for which the direct signal can be isolated in the time domain from the reflected signal. A further apparently unavoidable problem of shallow shots is the fact that the surface-reflected shock wave frequently is

truncated because of cavitation and the total signal may be further modified by the non-planar sea surface. In the model, because of lack of detailed data, this is treated as a truncation ("clipping") of the shock wave at some constant value with no compensation to the total impulse.

When the surface-reflected signal is an exact replica of the direct signal with the exception of a π phase change and a time delay τ, the resulting signal may be represented as follows:

$$p_{total}(t) = p_{direct}(t) + p_{sur\ ref}(t)$$

$$= p_{direct}(t) - p_{direct}(t-\tau)$$

$$= p_{direct}(t)(1 - e^{+i\omega\tau})$$

the energy spectrum takes the form;

$$E_{total}(\omega) = E_{direct}(\omega)\ (2 - (e^{+i\omega\tau} + e^{-i\omega\tau}))$$

$$= E_{direct}(\omega)\ (2(1 - \cos\ \omega\tau))$$

$$= 4\ E_{direct}(\omega)\ \sin^2\ (\frac{\omega\tau}{2})$$

Thus the sum of direct and linearly surface-reflected signals gives an energy spectrum which is modulated by a term of the form $4\ \sin^2(\frac{\omega\tau}{2})$. This term has alternate maxima and minima at frequencies corresponding to $\omega\tau = n\pi$, $n=0,1,2\ldots$ At the maxima (odd values of n), the total energy spectrum is 6 dB above the direct spectrum alone, while at the minima (even or zero n), the interference is complete. Thus the linear reflection case is well defined and accurately calculable from frequency domain information, except in the frequency intervals in the vicinity of minima of the $\sin^2\ (\frac{\omega\tau}{2})$ term. The principal problems for data

analysis are thus expected to be those associated with non-linear reflection processes (i.e. signal clipping).

To illustrate the effect of this clipping, the combined exact signal spectrum for the direct plus clipped, reflected signal is compared with the corresponding unclipped exact spectrum. Figures 3-17 through 3-21 show these comparisons for the case of the standard shot (1.8 lb, 60 ft depth, 300 ft range, shock peak pressure 42 psi) combined with a surface reflection that has no attenuation relative to the direct signal except for a truncation of the shock wave to 15 psi amplitude. The delay τ between the direct and reflected signal is the variable in this group, varying from 24 ms to 1.5 ms, corresponding to far-field radiation angles of 90° to 7° respectively. As can be clearly seen, the $\sin^2 (\frac{\omega\tau}{2})$ modulation dominates the general shape.

Of considerable interest is the fact that the clipped signal spectrum is significantly altered only at the minima in the $\sin^2$ modulation with relatively little change in wide band energy at other frequencies. The fact that the spectral changes due to clipping occur primarily only at the spectral minima is shown by the relatively small change (less than 1 dB) in 1/3 octave band levels except at those bands containing the $\sin^2$ modulation minima. This consistent behavior strongly suggests that the detection of a "clipped" surface reflection may be difficult using only spectral information in a system with a noise floor, but also that the effects of clipping on the low frequency 1/3 octave band spectrum may not be as large as previously suspected.

One significant departure from the above noted is the 20 Hz 1/3 octave band for short delays, where the error exceeds 3 dB for 1.5 ms delay. No conceptual explanation for this unique behavior has yet been identified.

(Text continued on Page 76)

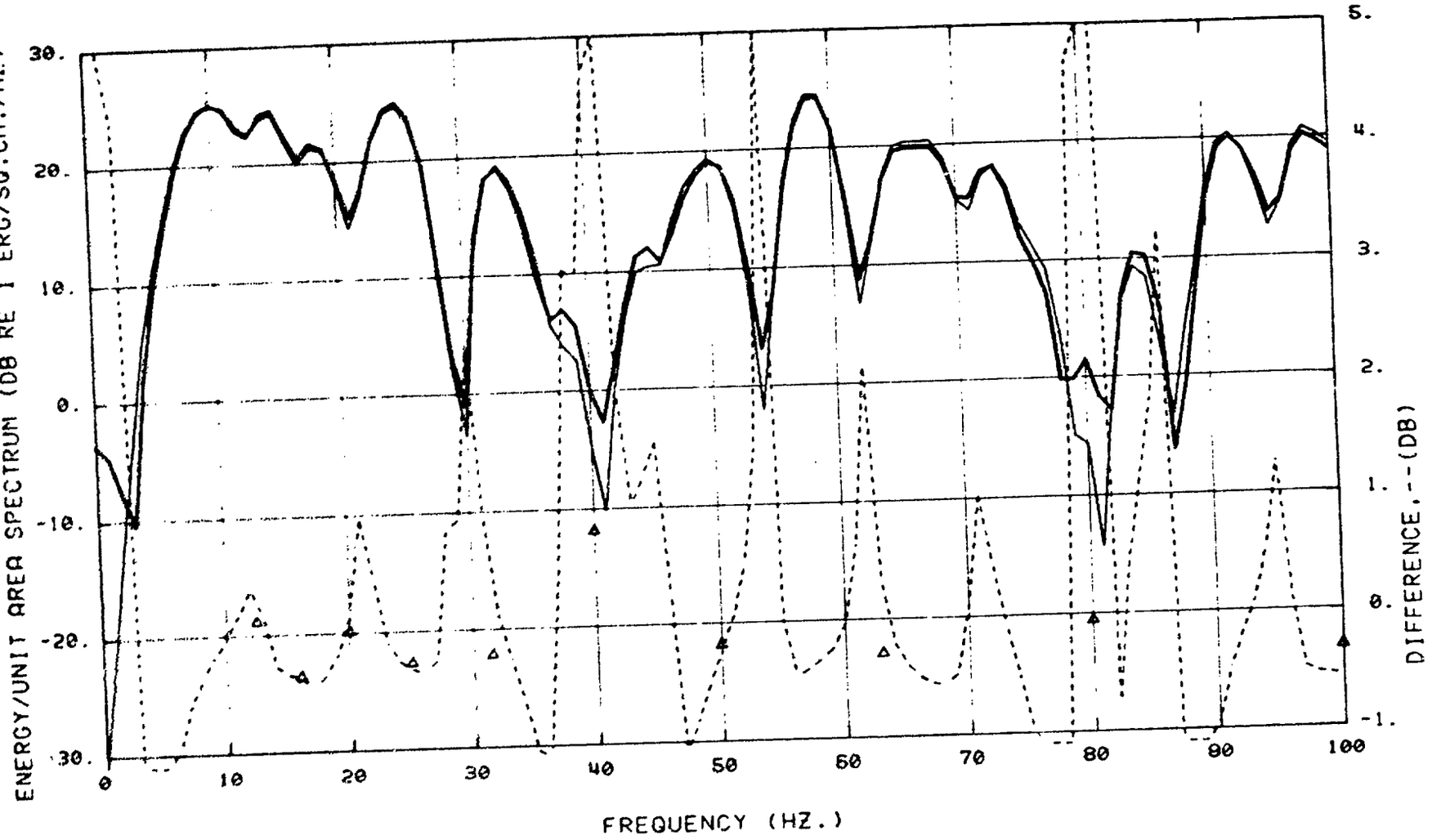

Figure 3-17a. Spectra of direct plus reflected waves with and without clipping of reflected shockwave signals to 15 psi. Delay 24 ms
light solid line - unclipped
heavy solid line - clipped shock wave
dash line - difference, Δ - difference of 1/3 octave band.

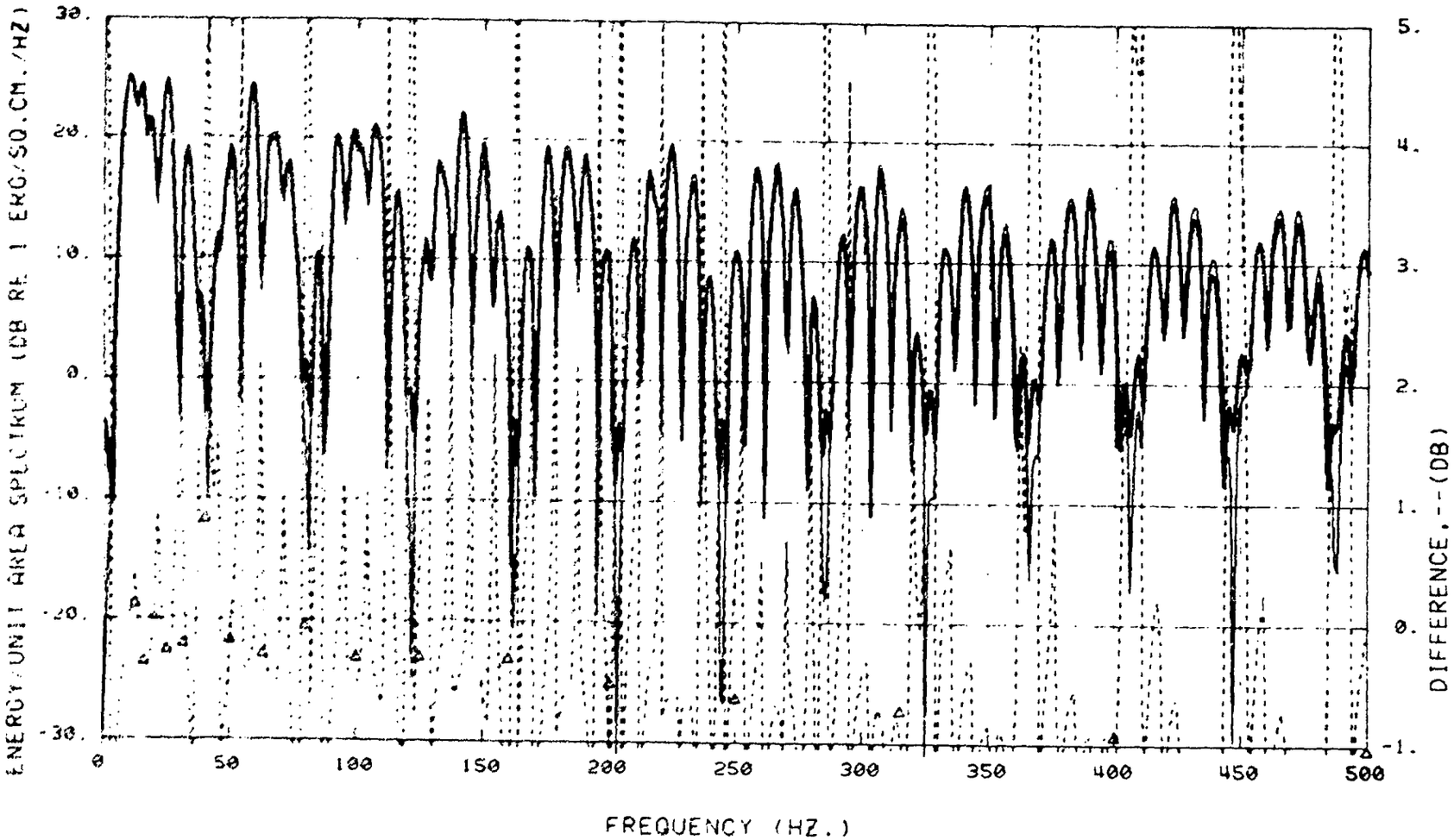

Figure 3-17b. Same as Figure 3-17a except frequency range 0 - 500 Hz.

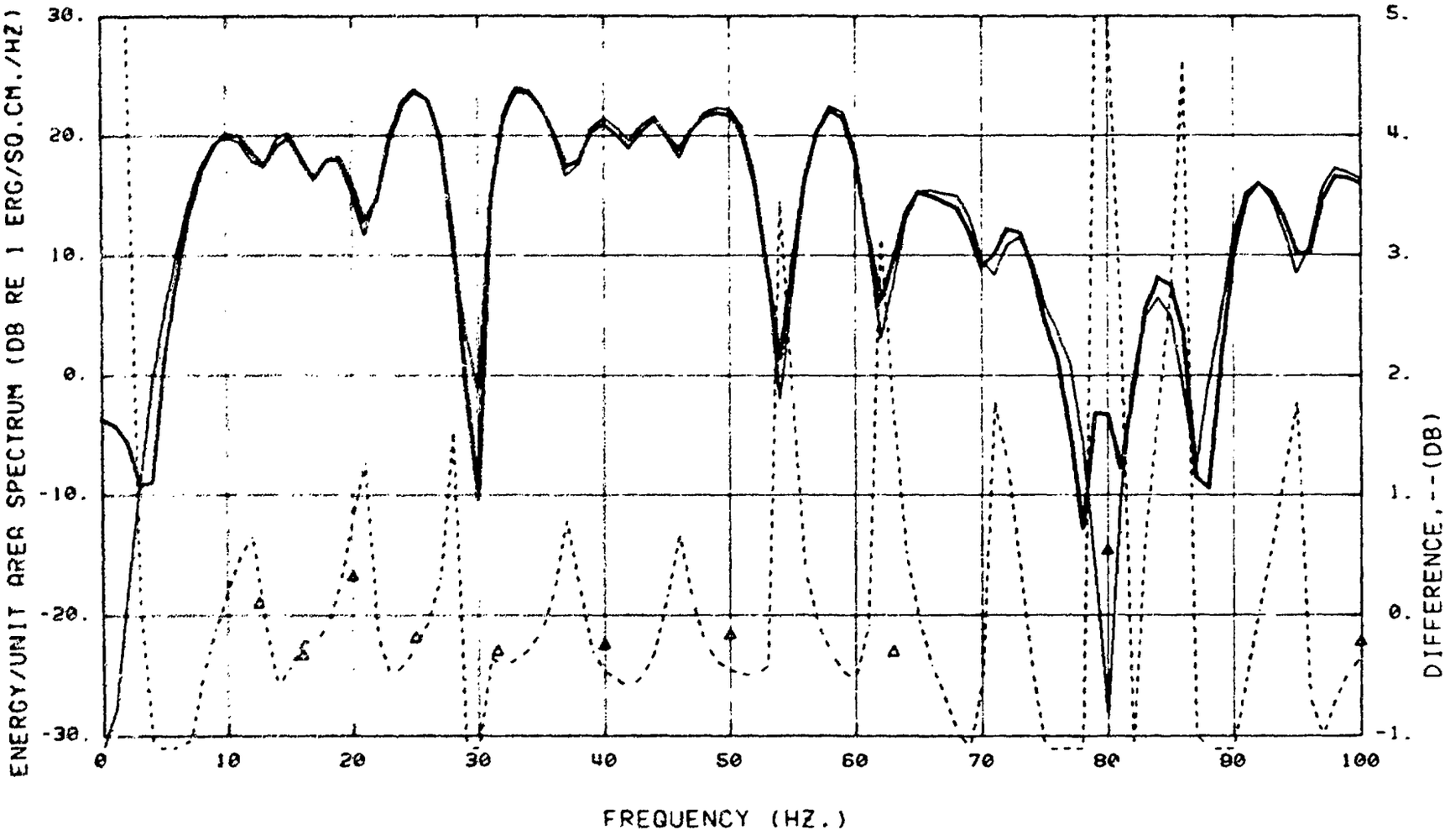

Figure 3-18a. Same as 3-17 except delay is 12 ms

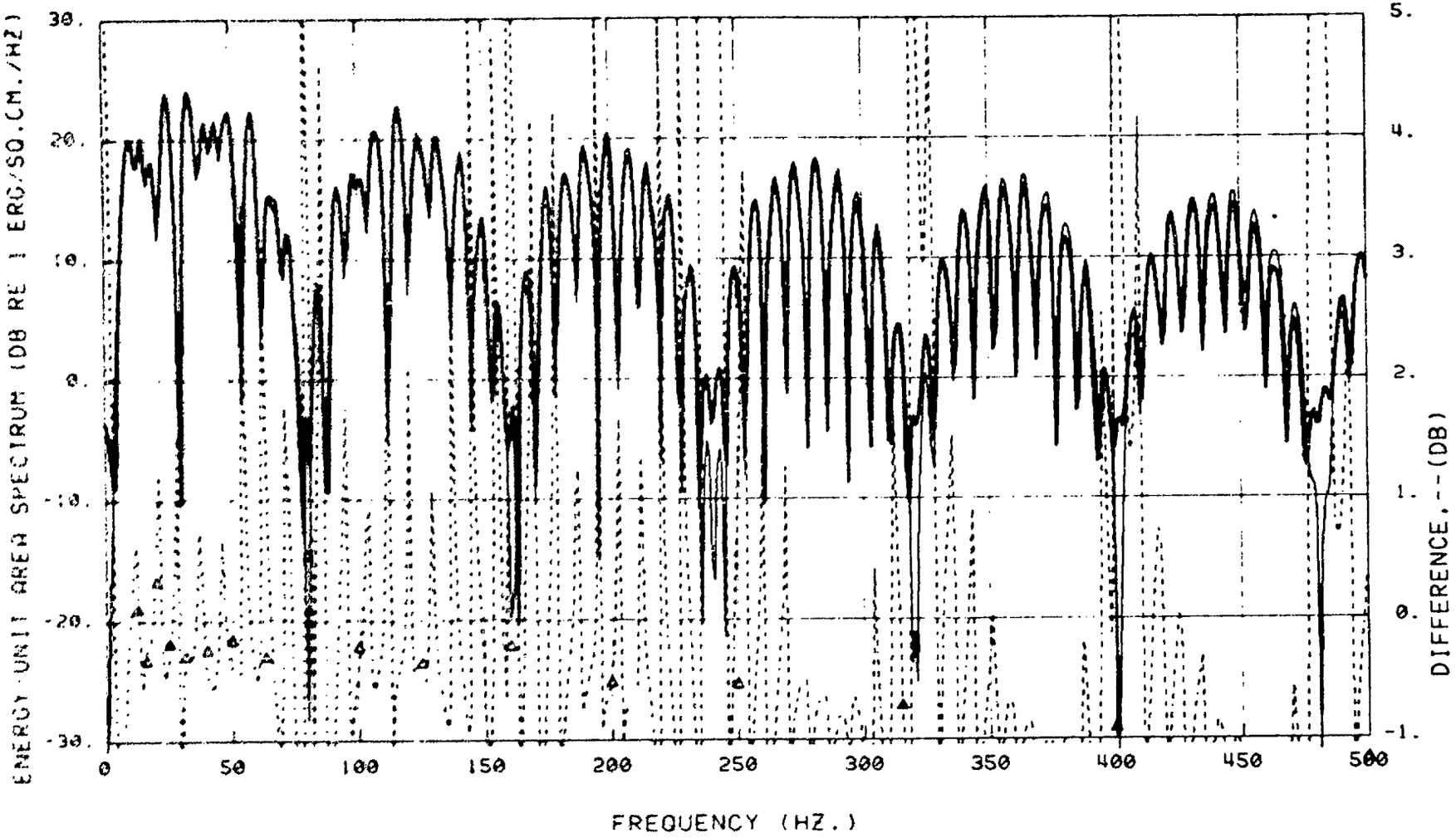

Figure 3-18b. Same as Figure 3-18a except frequency range 0 - 500 Hz.

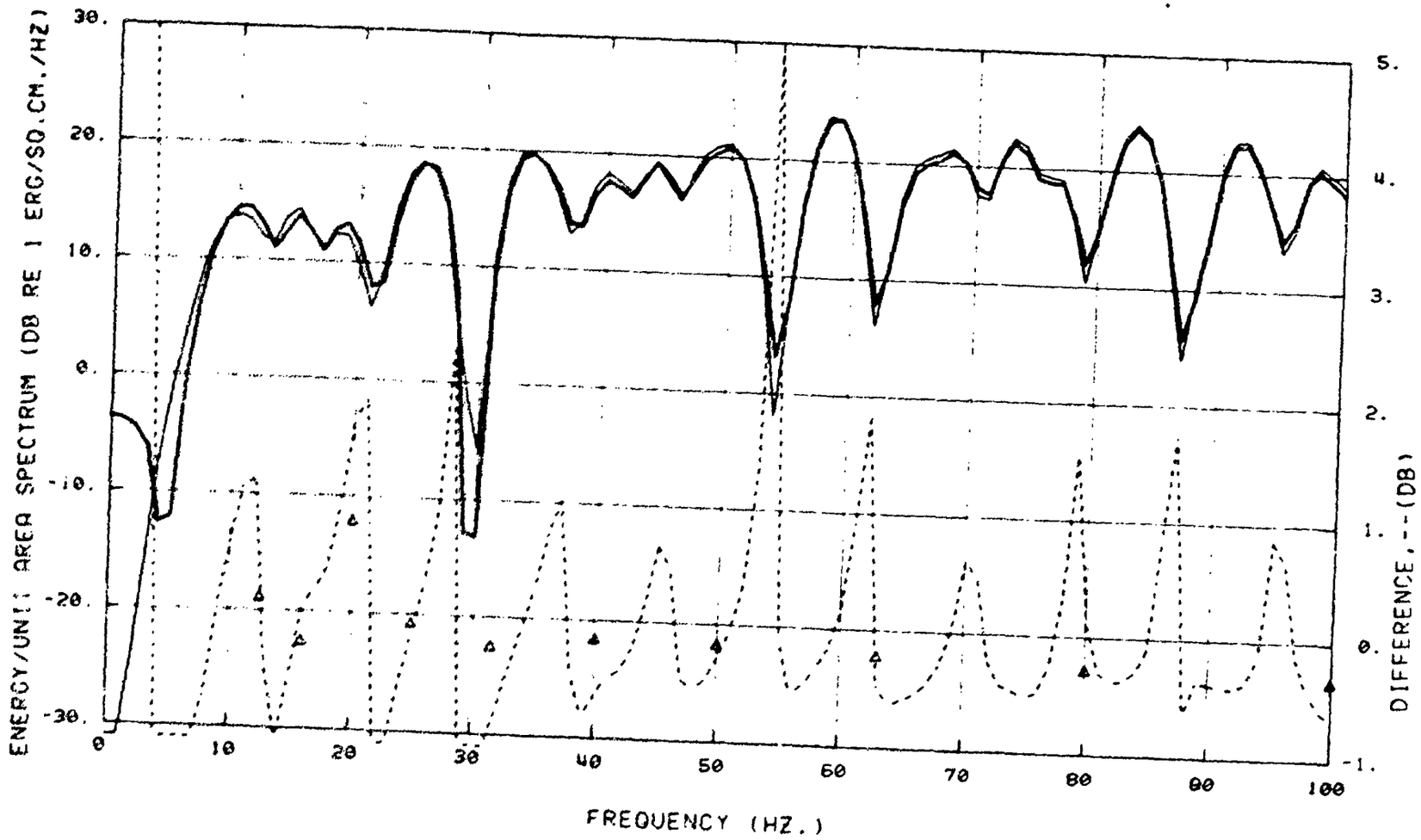

Figure 3-19a. Same as 3-17 except delay is 6 ms

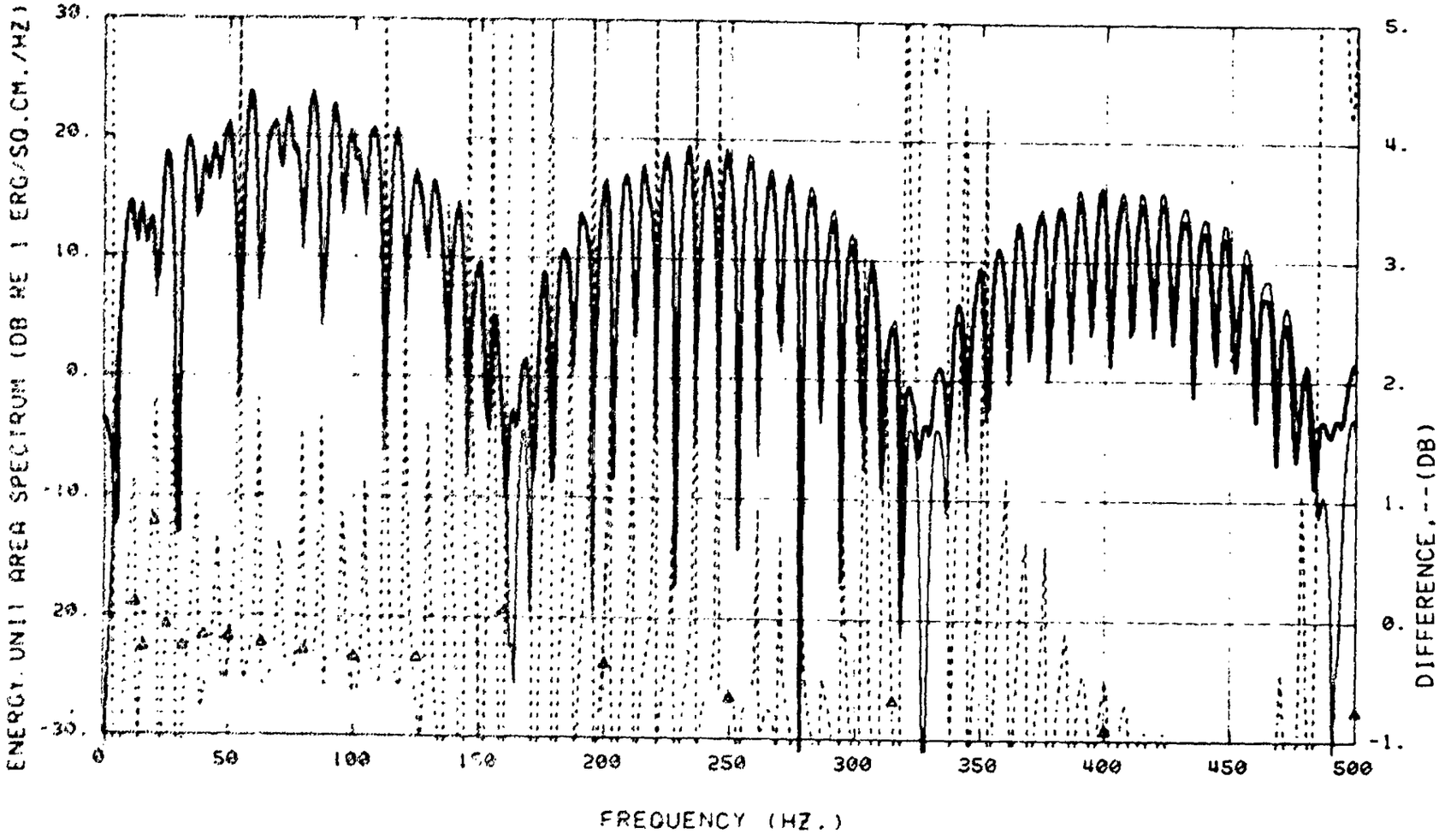

Figure 3-19b. Same as Figure 3-19a except frequency range 0 - 500 Hz.

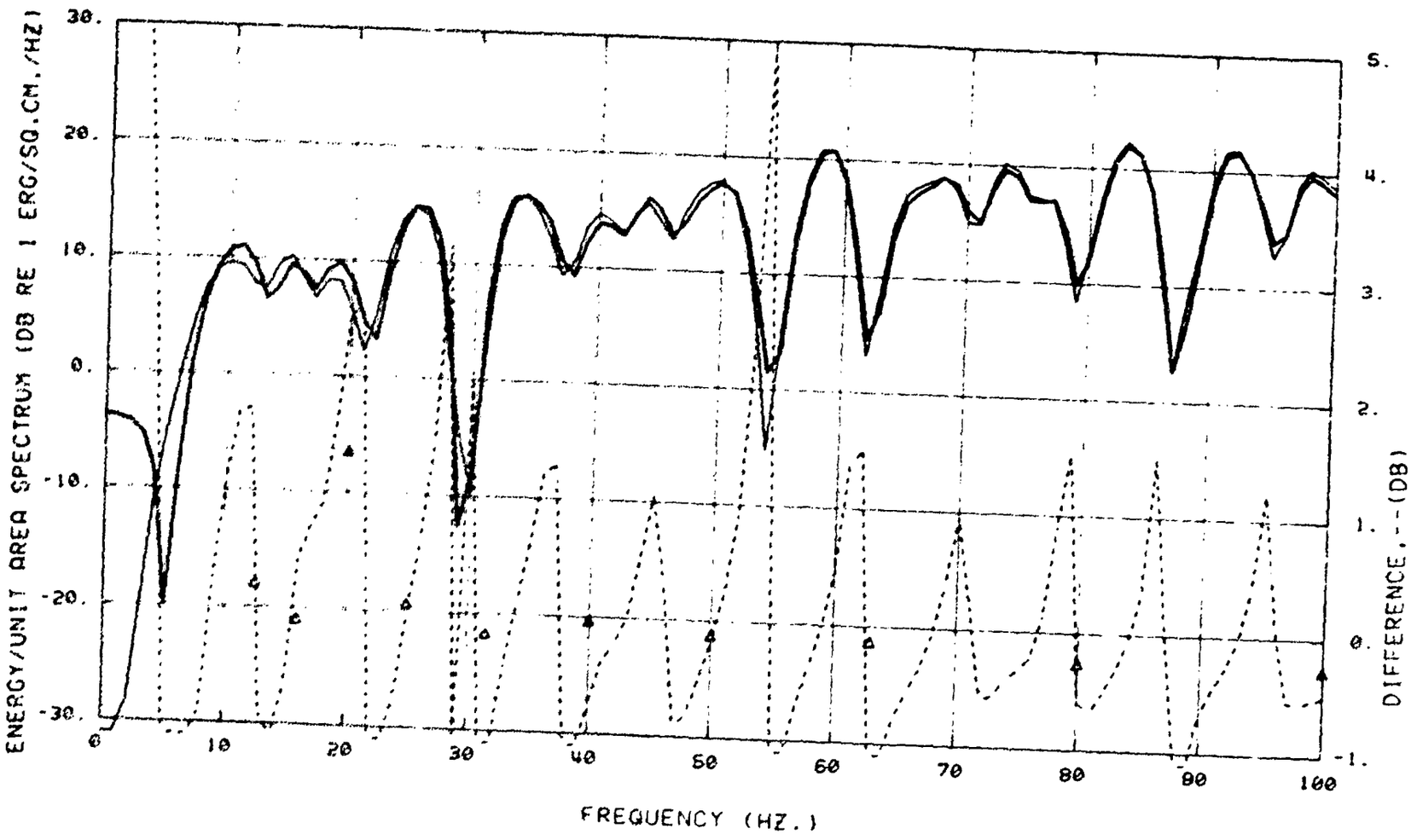

Figure 3-20a. Same as 3-17 except delay is 3 ms

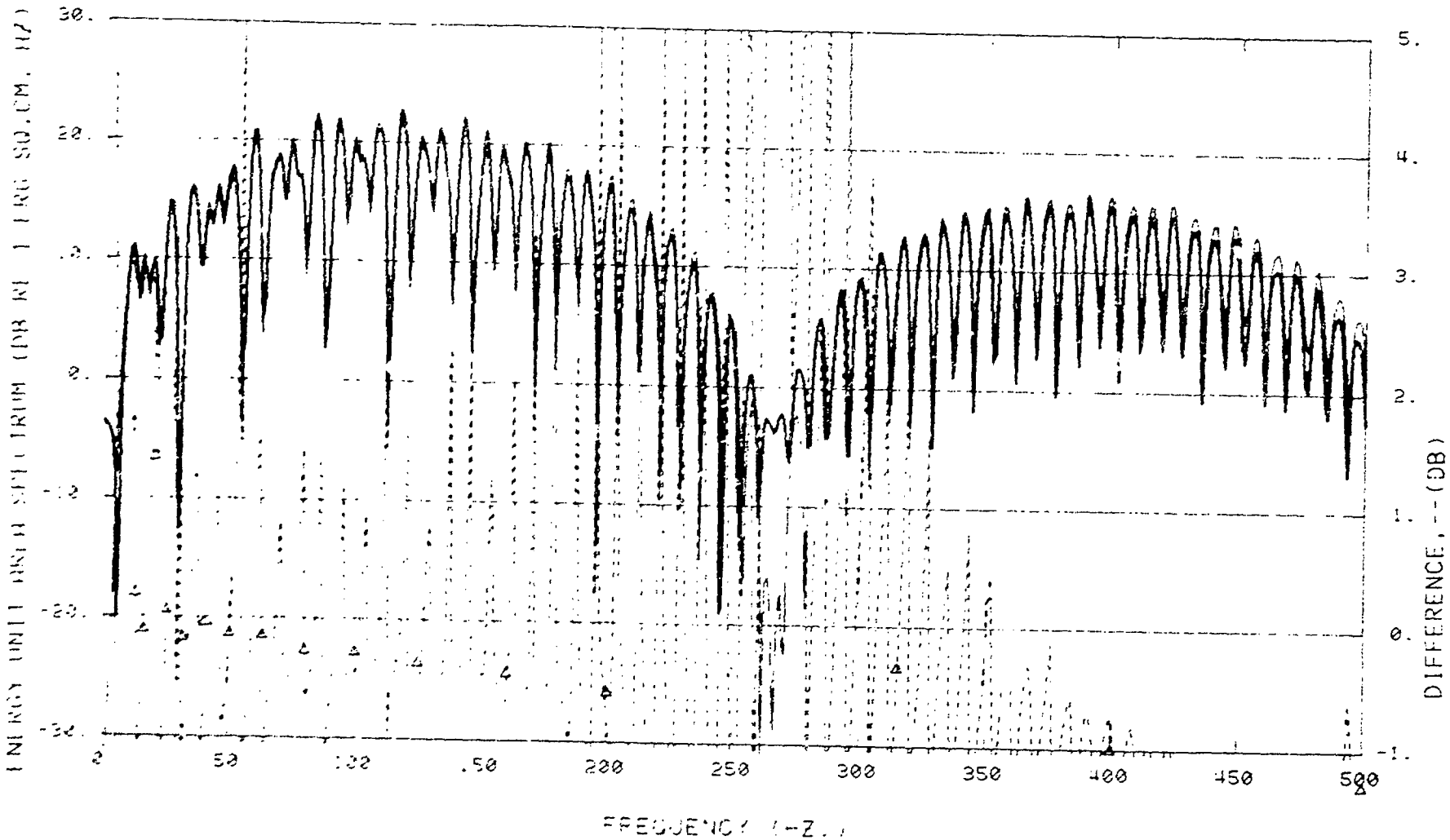

Figure 3-20b. Same as Figure 3-20a except frequency range 0 - 500 Hz.

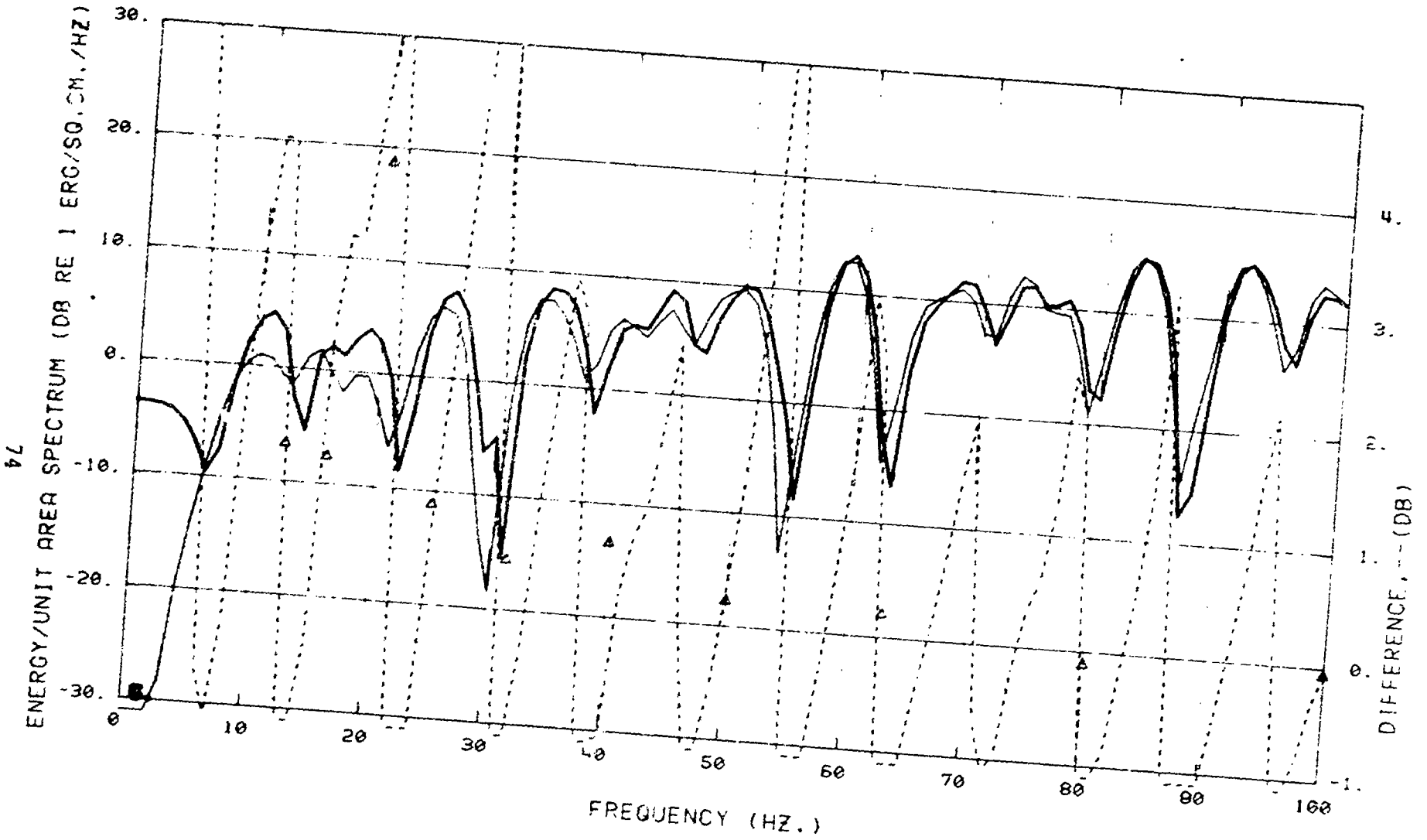

Figure 3-21a. Same as 3-17 except delay is 1.5 ms

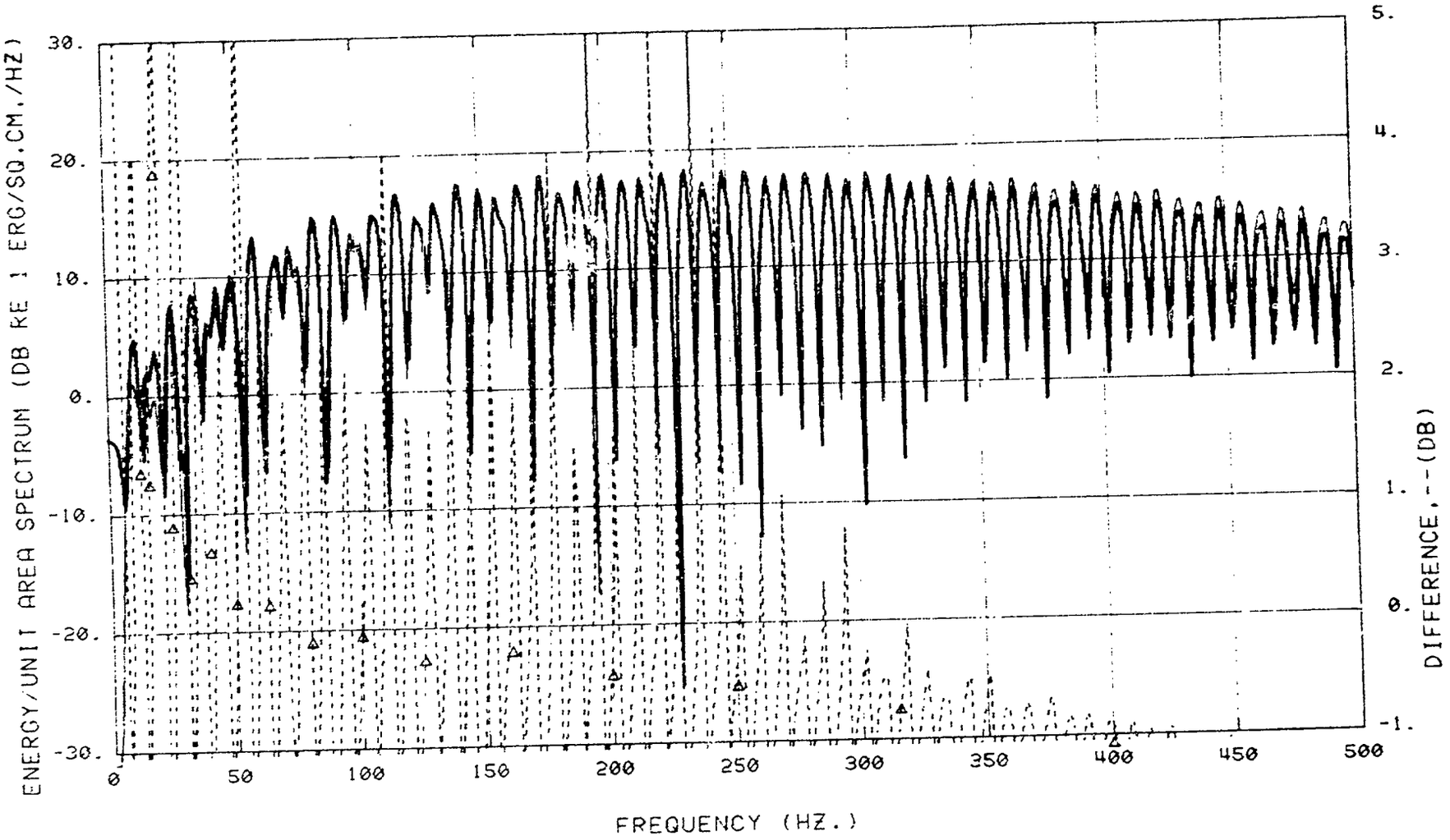

Figure 3-21b. Same as Figure 3-21a except frequency range 0 - 500 Hz.

3.4 Effect of Range

As noted in the introduction to this section, one of the significant factors which bears on the usefulness of explosive signals for use as sources in propagation experiments is the fact that the shock wave portion of the time series signal attenuates more rapidly than a small amplitude acoustic signal, at least for short ranges. Previous authors have experimentally determined the rate of change of amplitude and decay constant of the exponentially-decaying shock wave vs range. Since these experimentally-determined terms were used in the analytic model of the signal used in this study, the model can then be used to examine the way in which this model of the frequency spectrum of the signal changes with range. In particular, we seek an answer to the question, "If the shock wave propagation follows the empirically-determined attenuation law, what is the magnitude of the changes in the spectrum shape to be expected with range?" The answer to this question is

then used to phrase an answer to the question, "What is the expected variation from spherical spreading of the source level spectrum as a function of range?"

Figures 3-22 and 3-23 show calculated shock spectra at ranges of 1 kyd and 10 kyd compared to the baseline spectra at 100 yd for the direct arrival only of a 60 ft depth 1.8 lb shot. The computations were made using the exact SPECTRUM program with data scaled back to 100 yds assuming spherical spreading. The differences between the spectra reflect only the dependence on the programmed difference of the time series versus range. These differences from spherical spreading, as may be noted from Appendix A, are a decrease in the shock wave peak in proportion to $(\text{range})^{-.13}$ and an increase in the exponential decay time constant in proportion to $(\text{range})^{0.22}$. The nominal computed peak amplitudes of the shock wave at these ranges (assuming spherical spreading) are 3.05 psi and 0.226 psi respectively. With the exception of the slow conversion of several minima in the 100 yd spectra into minor peaks in the 1000 and 10,000 yd spectra, this seemingly large change in the time series wave form had a remarkably subtle effect on the spectra.

The present position of many workers in the field is that a transition from shock propagation (i.e. spreading loss not proportional to $(\text{range})^{-1}$) to acoustic propagation (spreading loss proportional to range^{-1}) would be expected to occur in the vicinity of 1 psi peak pressure in the shock wave. One type of experiment to evaluate the presence of this occurrence would involve a comparison

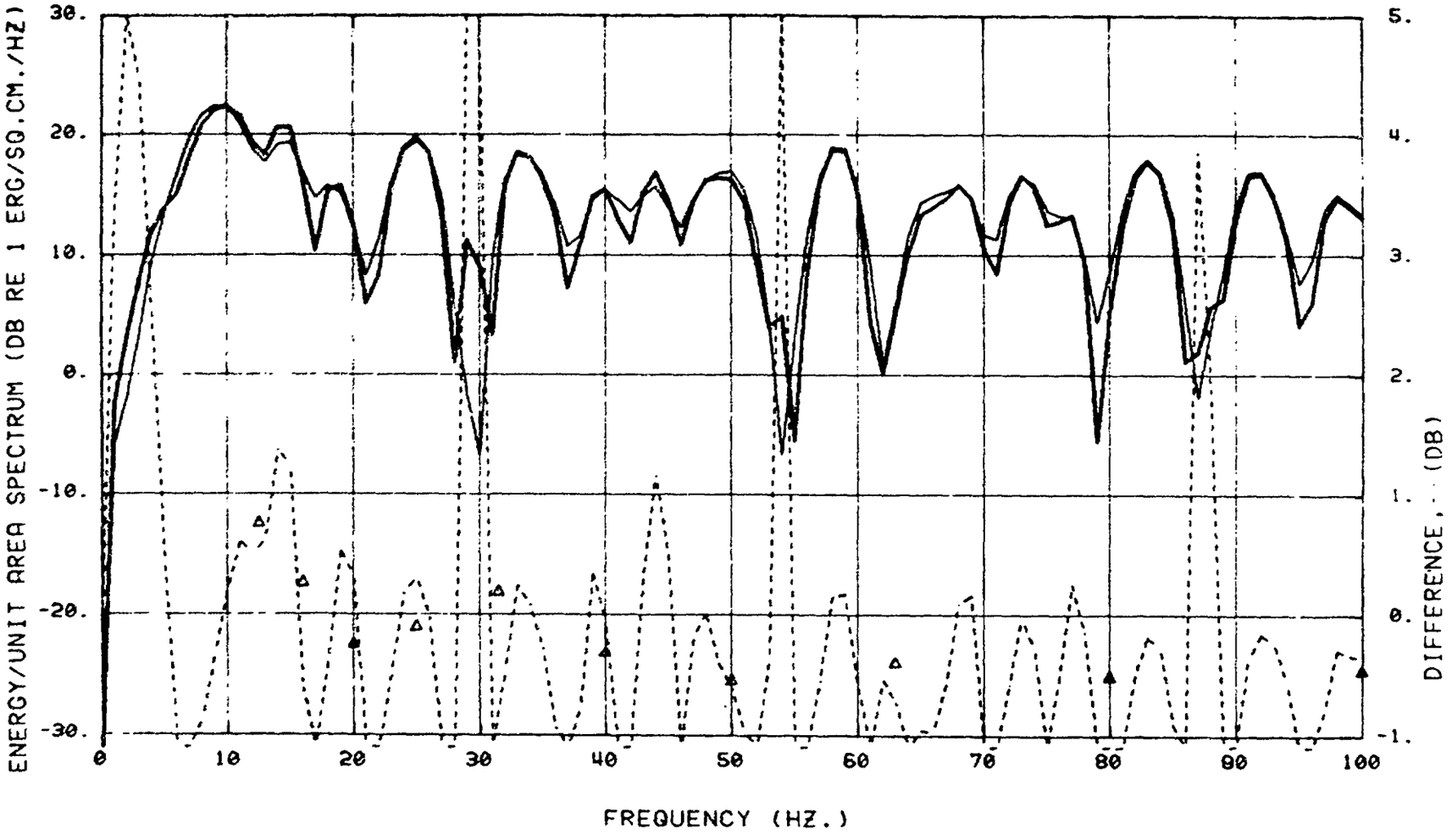

Figure 3-22a. Comparison of direct arrival spectra of 60 ft depth, 1.8 lb shot at 1000 yd and 100 yd. - Computed spectrum at 1000 yd scaled by spherical spreading to source level at 100 yd. - Computed spectrum at 100 yd. --- Difference in spectra (Note expanded scale on right.)
Δ Difference in 1/3 octave band levels.

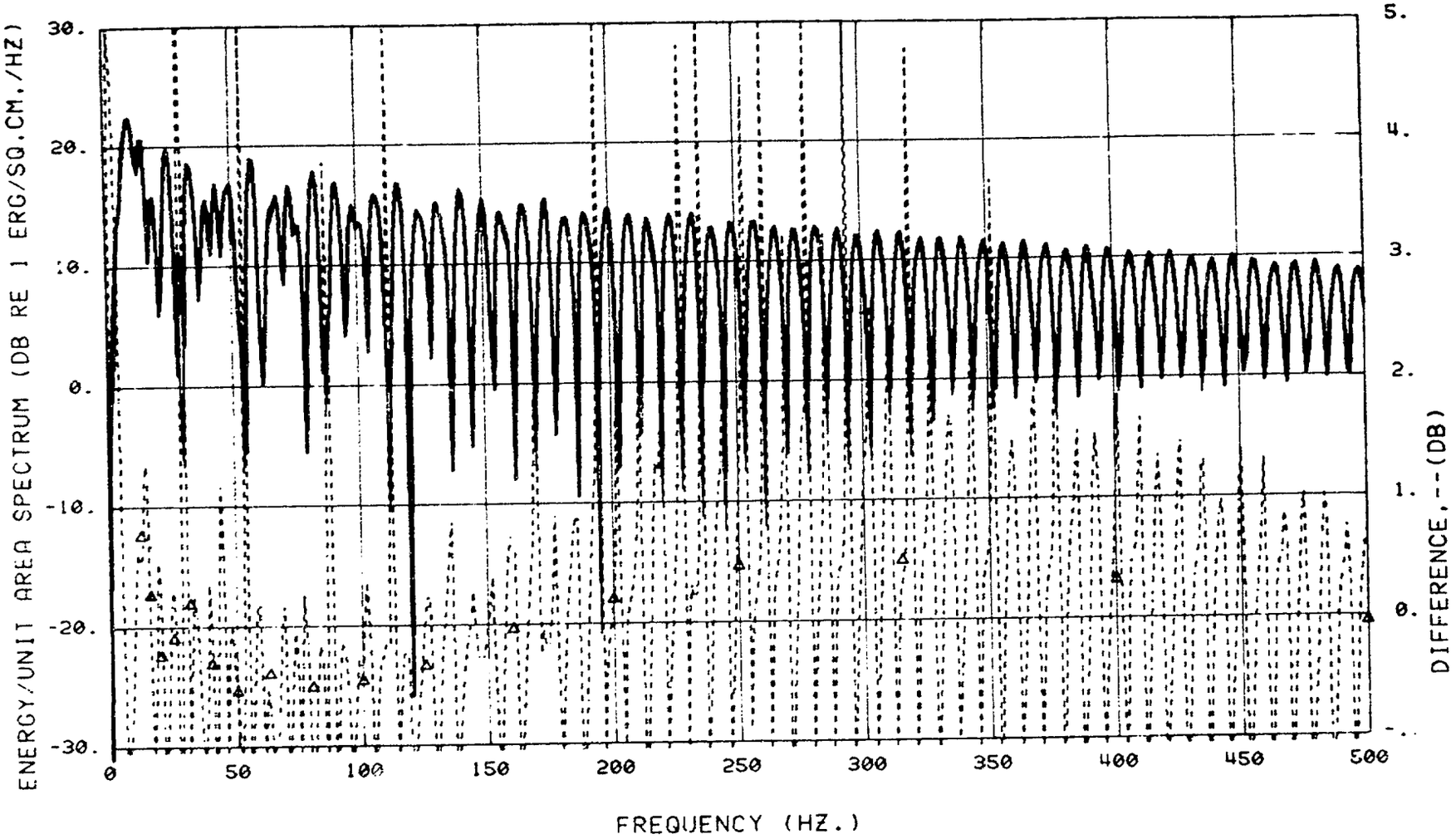

Figure 3-22b. Same as Figure 3-22a except frequency range 0 - 500 Hz.

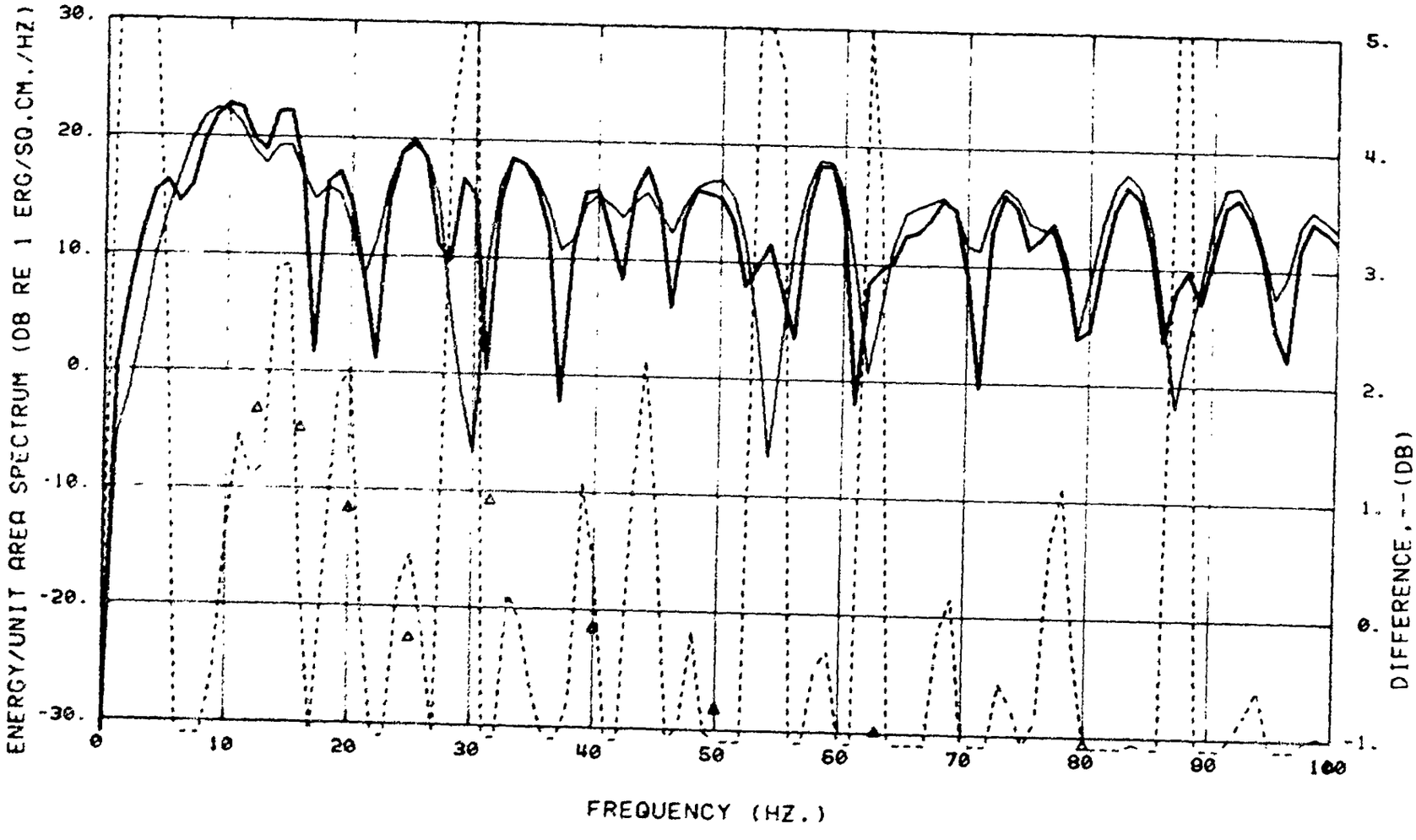

Figure 3-23a. Comparison of direct arrival spectra of 60 ft depth, 1.8 lb shot at 10,000 yd and 100 yd. - Computed spectrum at 10,000 yd by spherical spreading to source level at 100 yd. (Other data same as Figure 3-22).

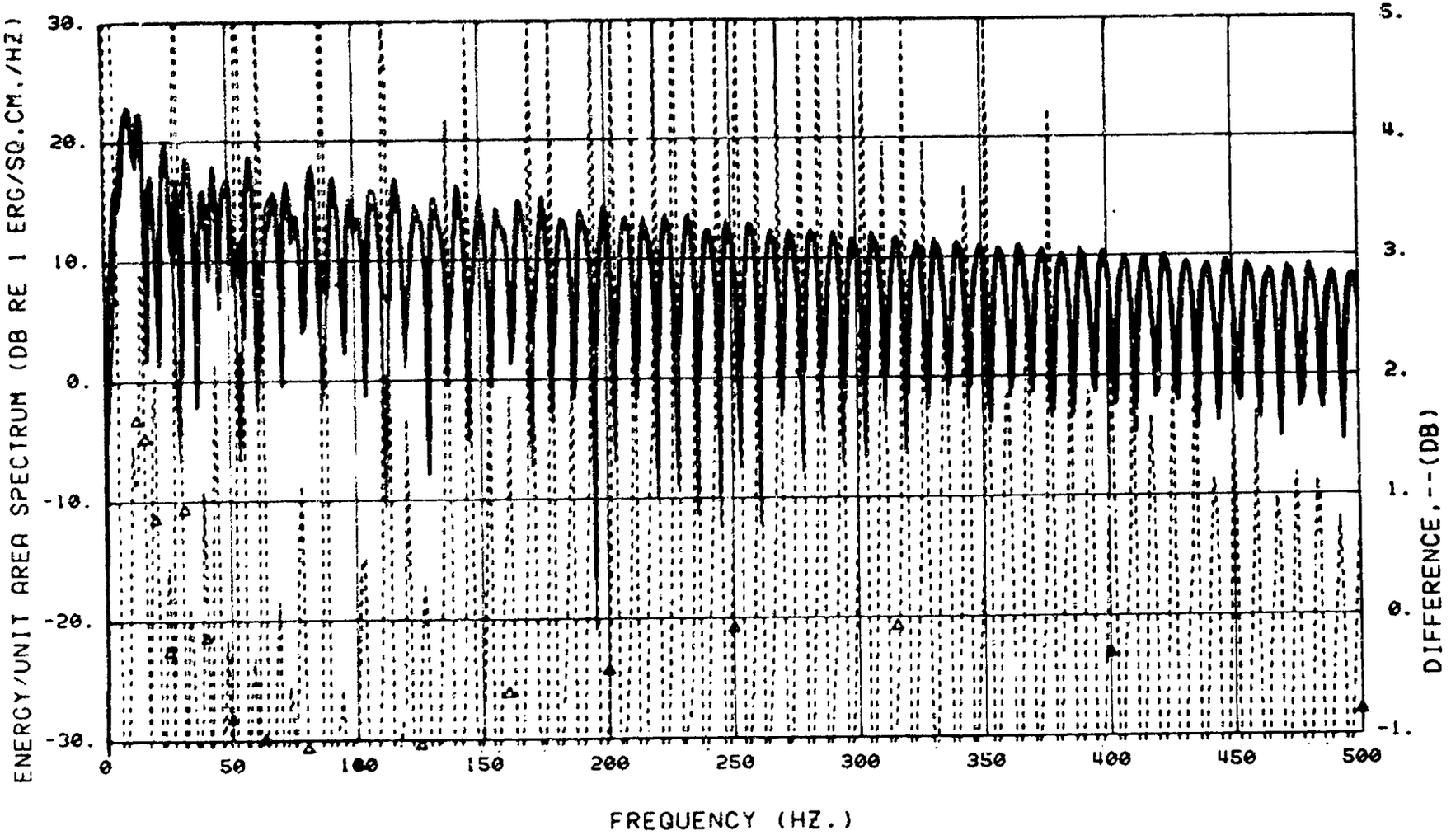

Figure 3-23b. Same as Figure 3-23a except frequency range 0 - 500 Hz.

of 1/3 octave spectral levels which have been corrected back to a common range via spherical spreading. Figure 3-24 provides a plot of the results to be expected from an error-free performance of such an experiment, performed under the assumption that shock wave propagation continues to a range beyond that shown in the figure. We have plotted 1/3 octave energy source level spectrum difference from that at 100 yds, with band center frequency as a parameter in this figure. The result of a transition to acoustic propagation on such a figure will show up as a transition of all curves to a horizontal slope at some common range. In the area of interest (i.e. 1000 yd range to 10,000 yd range, 20 Hz - 500 Hz), the slope of all curves is less than 1 dB per decade of range change. This already small slope, when coupled with the probable magnitude of experimental errors associated with propagation loss correction, source yield variation, etc, strongly suggests that this form of data reduction will not yield a powerful test of transition range.

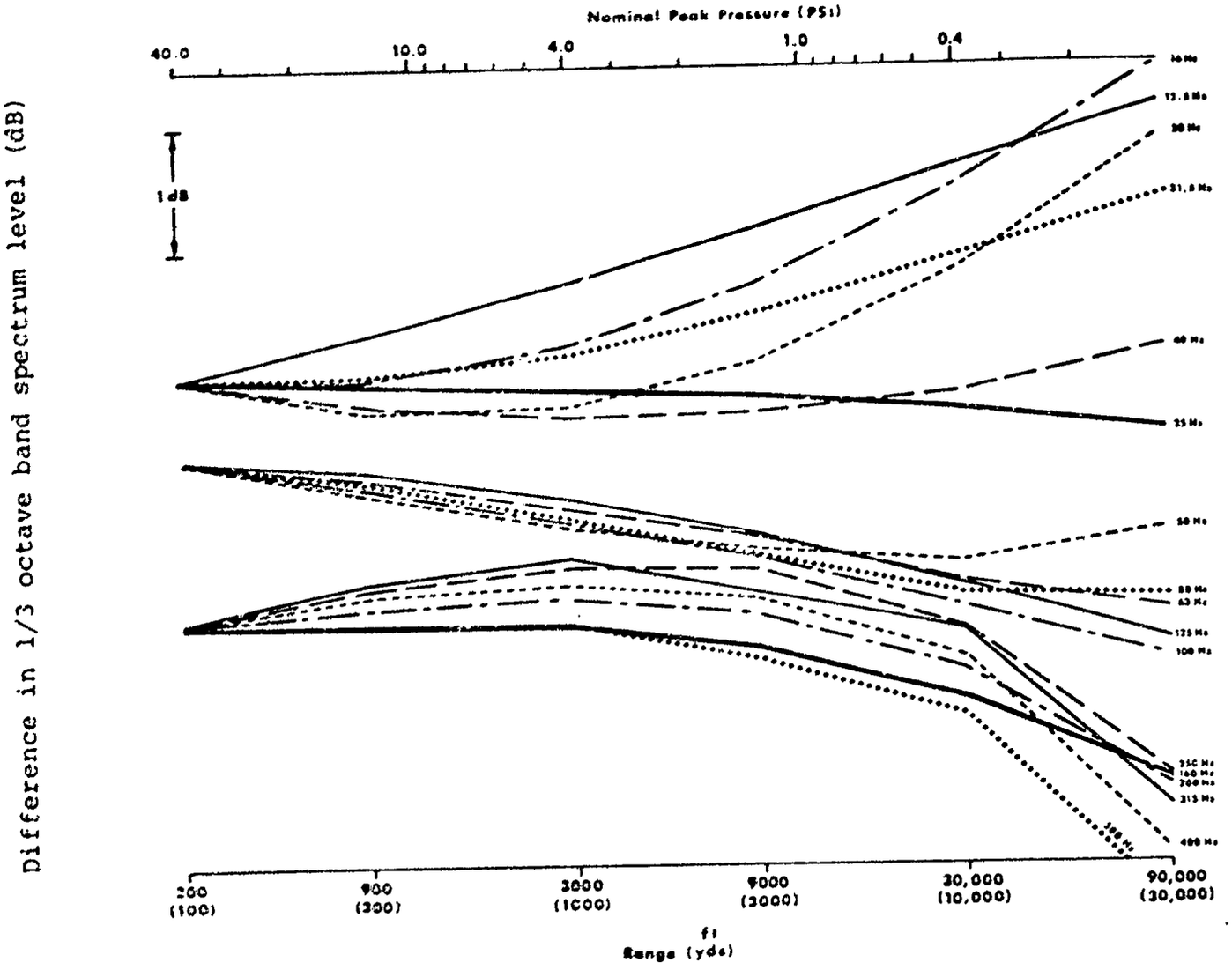

Figure 3-24 Change in 1/3 octave band spectrum level (normalized to 100 yard range) from spectrum at 100 yards versus range, (1.8 lb shot, 60 ft depth). Nominal peak pressure of shock wave shown on upper scale.

4. MINI-EXPERIMENTS

4.1 Introduction

The success of or need for the source level experiment is contingent upon the amount of knowledge that is at hand during the decision and planning phases. Such items as the sensitivity of results to A-D sampling rates, low pass filter frequencies, 1/3 octave levels, reflection deconvolution, and measurement range have been discussed above. The repeatability of the acoustic level from a SUS, the interaction of the SUS reflections at the surface and the water medium, and the effect of measurement range should be examined further. Although modeling of the last two effects was undertaken, the results are only estimates, since the exact physics controlling these phenomena are poorly known. It seems appropriate that these three items be examined by means of limited scope experiments, mini-experiments, to better quantify the achievable accuracy in source level measurements.

4.2 SUS Repeatability

The repeatability of the acoustic level from a standard SUS has been a question mark in most scientists' minds for a long time. Such variables as amount of explosive detonated, burst strength of the case, and potential aluminum vaporization are among the more often heard problems concerning SUS repeatability.

The amount of explosive detonated is a function of several things. The first question arises during casting the charge. The full 1.8 lbs is not cast at one time but is the result of two or three separate pours, the last one or two being made to make up for the shrinkage of the TNT when it solidifies. Thus one has the majority of the block as one unit with several thin layers poured on top. It is a well known fact in explosive experience that if a charge is cracked, the charge represented by pieces that cracked away from the main charge may or may not detonate. If they do detonate it can be with a slight time delay or with a low order, slow velocity detonation. The separate pours for the charge may result in a situation similar to the cracked charge. There is also the possibility of the TNT charge cracking between the time of the pour and the time it is used. The amount of explosive actually detonated affects two phenomena - the overall level, and the bubble pulse frequency. An overall change in level is proportional to the cube root of the weight. Thus a change from 1.8 to 1.6 lbs would result in a 0.3 dB change, which may or may not be considered tolerable. A change in the bubble pulse frequency can be more serious because of the octave processing that is presently in vogue. In the lower 1/3 octaves, i.e., 10 to 100 Hz, the 1/3 octaves are so narrow as to hardly span a complete amplitude cycle in the frequency domain. Therefore, the shifting of a null into or out of the fixed 1/3 octave band can result in significant errors. This situation is similar to the bubble

pulse variation as a function of depth, where a few percent change in depth can result in 1/3 octave level changes of the order of 0.5 to 3 dB.

The effect of the burst strength of the case on the acoustic source level has been questioned in recent years. The situation can be paraphrased as follows: energy that is expended to burst the case containing the explosives cannot contribute to the acoustic source level. Further, we know that there is a wide range of burst strengths for the case and this will cause the acoustic output to vary. The size of this effect is difficult to estimate, but in any case this concern by some members of the community should be borne in mind when planning a source level variability experiment.

Another concern that is heard from time to time is the possibility of vaporization of the aluminum case. One method of enhancing the low frequency components of an explosive spectrum is to add uniformly-distributed fine aluminum powder to the explosive. The result is a greatly increased bubble due to the aluminum vaporization and resultant increase in bubble pulse energy, which results in a much higher spectral level at the lower frequencies than would otherwise be obtained.

Following this line of reasoning, if the TNT in the SUS can actually vaporize small quantities of aluminum from the case, the source level at the lower frequencies could be affected. Another comment is usually added. This vaporization will take

place only part of the time to add to the uncertainty. This concern can be appreciated and is a potential cause of source level variation, but is difficult to evaluate.

The sources of small variations discussed above are difficult to separate except in very elaborate experiments. The reasons and causes of shot-by-shot variations are fine to contemplate but their understanding is not necessary to define the repeatability of the acoustic source level of a SUS as used for propagation loss purposes. Therefore, it is proposed that a number of SUS from different lots be detonated and their relative outputs measured to quantify the source level variation without regard for potential cause of the error.

4.3 Surface Reflection Non-Linearity

When shallow-detonated SUS are used as acoustic sources, the surface reflection problem is ever present. Experiments purport to have observed the reflected shock wave truncated in the pressure range of approximately 15 psi to essentially no truncation, as is theoretically predicted for deaerated water. Such a variation in the behavior of the surface reflection brings up several problem areas.

1. Can deconvolution techniques adequately handle the range of variation in the surface reflection?
2. How does this variation reflect in the use of source levels for PL measurements?

3. Is there any correlation between angle of encounter with the surface and the shock wave truncation process?

The truncation process for the reflected shock wave can be described as a cavitation process; i.e., when the negative pressure of the shock wave overcomes the tensions the water can support, it is pulled apart with the forming of small bubbles, or in the case of large charges a layer cavity that will later collapse. In any case the energy that is represented in that part of the shock wave that has been "cutoff" has been dissipated in the cavitation process. The tensional stress that water will maintain is a function of the dissolved gas in the water. For totally degasified water the tensional stress that is supportable far exceeds the tensional stress required of the medium for the reflected shock wave. However, with increasing gas content the tensional stress supportable by the water medium rapidly decreases so that truncation of the shock wave can be expected as a normal occurrence. Therefore, the expectation is that there will be varying truncation of the shock wave due to the gas content of the water.

Deconvolution techniques were tested in the analytical portion of this study and the results presented there. One of the objectives of the experiment is to determine whether or not the deconvolution error estimates developed above are realistic for a real measurement. Such a set of data can be easily acquired by measuring the same shot at two locations, one where

deconvolution is required and the second where it is not, i.e., the reflection arrives after the second bubble pulse.

The second area of concern is the effect of variability in the surface reflection for the ray paths that are reflected from the surface near the detonation point. The amount of variation will be measured so that an estimate of the variation on the two close-in reflected ray paths can be made for a 4-ray path bundle.

4.4 Effect of Measurement Range

A preferred experimental investigation of the transition to acoustic propagation would be self-correcting for propagation loss and shot yield. If that experiment were also self-correcting for small calibration differences in the transducer system, the accuracy would be improved even further. One such experiment would involve the use of two wideband transducers to receive signals from shots dropped in an annular region above one of the transducers, which is placed deep. The second transducer is placed shallow and at a significant horizontal range from the source drop area. This latter range, plus the radius of the drop area, is selected to span the horizontal range region of interest. The deep transducer is used to record signals at nominally constant source range, as a reference. To illustrate the data reduction scheme, we require an estimate of the signal, which we take as follows (from the analytic model used here; see Appendix A).

Shock wave peak pressure = $P_1 = 2.08 \times 10^4 (W^{1/3}/R)^{1.13}$

First bubble pulse peak pressure = $P_2 = 3.3 \times 10^3 (W^{1/3}/R)$

Using our analytic model (SHOTTIME) as a representation of a band-limited signal, it has been determined that these signals for a given shot can be detected with a relative inaccuracy of less than 5% for systems, with an upper cutoff frequency in the range of 10-20 kHz. The need for such a wideband system arises from the desire to study peak pressure independent of the decay rate of the exponential terms, which are integrated into the data in narrower bandwidth systems. The data reduction consists of determining the peak pressure of the shock wave and bubble pulse at each of the transducers, and forming their ratio. The result at each transducer if shock wave propagation holds is:

$$P_1(R_1)/P_2(R_1) = \frac{2.08 \times 10^4}{3.3 \times 10^3} \frac{(W^{1/3}/R_1)^{1.13}}{(W^{1/3}/R_1)}$$

$$= 6.3 \, (W^{1/3}/R_1)^{0.13}$$

We note that this ratio will be independent of transducer calibration constant, as long as the system response is linear. We now form the ratio of this quantity for the same shot, at two different ranges, R_1 and R_0, i.e.;

$$\frac{P_1(R_1)/P_2(R_1)}{P_1(R_0)/P_2(R_0)} = \left(\frac{W^{1/3}/R_1}{W^{1/3}/R_0} \right)^{0.13} = \left(\frac{R_0}{R_1} \right)^{0.13}$$

for shock wave propagation at R_1, R_2.

The result of the data reduction is an experimental value that, for the case of shock wave propagation, is now independent of shot yield, and depends only on the relative range of the two measurements. Consider now a case where both R_1 and R_0 are such that acoustic propagation of the shock wave occurs. One representation of this for the shock wave is;

$$P_1(R_1) = 2.08 \times 10^4 \ (W^{1/3}/R_m)^{1.13} \ (R_m/R), \qquad R \geq R_m.$$

This expression equals shock wave amplitude at range R_m, but follows acoustic propagation for $R > R_m$. If both R_1 and R_0 above are greater than R_m, then the ratio is;

$$\frac{P_1(R_1)/P_2(R_1)}{P_1(R_0)/P_2(R_0)} = \frac{(W^{1/3}/R_m)^{0.13}}{(W^{1/3}/R_m)^{0.13}} = 1; \qquad R_1, R_0 > R_m$$

If $R_0 < R_m < R_1$ we have;

$$\frac{P_1(R_1)/P_2(R_1)}{P_1(R_0)/P_2(R_0)} = \frac{(W^{1/3}/R_m)^{0.13}}{(W^{1/3}/R_0)^{0.13}} = \left(\frac{R_0}{R_m}\right)^{0.13} < 1; \qquad R_0 < R_m < R_1$$

In the above, if R_0 is the nominally constant range distance, the ratio of interest is nominally constant at a value less than unity, which permits computation of the range R_m where the transition to acoustic propagation occurs. A plot of this data vs log (variable range R_1) that spans the transition range R_m is expected to show a slope of -0.13 below R_m, and approach a constant value above R_m.

In summary, the above discussion suggests that an experiment to evaluate range dependence in the frequency domain is fraught with difficulty because of the small differences that are under study. A direct experiment in the time domain is suggested, and a data reduction scheme is outlined that is self-correcting for yield and range and that could provide the desired information. Further study to define equipment requirements is necessary, however, before a final experiment plan can be defined.

4.5 Specific Experiments

During October 1977, PAR wet tests were performed. To take advantage of that opportunity, an experiment plan was prepared to investigate SUS repeatability, decorrelation and non-linear surface reflection effects and, to a lesser extent, the effect of measurement range. This experiment plan is given in Appendix C.

5. CONCLUSIONS AND RECOMMENDATIONS

The foregoing analyses and discussions support a number of conclusions concerning the errors to be expected in an experimental determination of SUS Source level.

- Transducer calibration errors of less than 0.5 dB can be achieved.
- Signal processing errors using an FFT analysis system can be reduced to less than 0.1 dB bias in 1/3 octave bands, and less than 0.5 dB rms error in 1 Hz bands in the frequency range 12.5 Hz to 500 Hz, using a system consisting of:
    1) Minimum 12 bit or more Analog to Digital converter with negligible time base jitter (to minimize quantization error).
    2) Antialias filtering at a cutoff frequency of one-half or less of the Nyquist frequency with at least a 24 dB/octave roll-off of the low-pass filter skirt (to minimize aliasing error).
    3) Rectangular windowing of the time series with the entire event included in the window.
    4) An FFT algorithm that uses at least 16 bit fixed point computation representation (to minimize computation roundoff error).
- Physical knowledge of the laws governing a transition from shock to acoustic propagation is presently limited,

but even shock propagation produces less than a ±0.3 dB range dependence for the 1/3 octave spectrum in the range of 1000 - 10,000 yds. Taking this as an upper-bound to the variability due to range dependence provides one estimate for this source of variability that should be verified through a range dependence mini-experiment.

- Similarly, physical understanding of the variability of spectra due to the deconvolution of a signal including a direct signal and a clipped surface-reflected signal suggests that while the variations in 1 Hz bands are large, the 1/3 octave band spectra vary from the idealized (i.e., unclipped) spectra by less than 0.5 dB on the average in the frequency range 25 Hz - 250 Hz without <u>any</u> correction for clipping (see Figures 3-16b to 3-20b). This suggests strongly that some very simple analysis algorithms based on propagation delay only can be used to "deconvolve" shallow shot data regardless of clipping. This suggestion must also be tested in the physical world, and a mini-experiment is described in this report to evaluate it.

Using the above error estimates permits an estimate of overall confidence level in an experimental determination of SUS source levels.

We assume that the above errors are random and non-interacting and sum their squared values to arrive at a mean square error estimate for the completed experiment. One additional factor that deserves consideration is the data record-playback system.

We estimate that with current state of the art and individual gain setting calibrations that this error should be less than 0.5 dB. The root-sum-squared of the above five errors (range 0.3 dB, calibration 0.5 dB, record-playback 0.5 dB, processing 0.1 dB, deconvolution with clipping 0.5 dB) is about 0.9 dB. This indicates to us the potential feasibility of an experimental determination of SUS source level to within an absolute error of $\pm$1 dB, subject only to the positive verification of the error limits for surface clipping and range dependence in mini-experiments.

The above error estimate applies to the certainty with which the source level from a carefully observed SUS shot can be known. One further factor in the uncertainty in using this data to predict the source level of another shot is the yield-depth variability from shot to shot. A mini-experiment to shed further light on these statistics for SUS is also described. Since there is no data or a priori evidence currently available on this portion of the uncertainty, experimental study is our only approach to this factor. Since it could have some influence on future usability of a SUS calibration, it should be undertaken prior to final commitment to the calibration experiment.

Thus our recommendations from this study concerning SUS calibration include:

- Perform a mini-experiment to identify bounds for range dependence of SUS spectra.
- Perform a mini-experiment to identify the bounds for

error due to clipping and deconvolution of shallow shot spectra.

- Perform a mini-experiment to evaluate the statistics of shot-to-shot variability of SUS.
- Evaluate the significance of the data from the above experiments prior to committing to the performance of an experiment to improve SUS calibration accuracy.

References

1. D. E. Weston, "Underwater Explosions as Acoustic Sources", Proceedings of the Physical Society, 76, p 233-249, 1960.

2. J. B. Gaspin and V. K. Schuler, "Source Levels of Shallow Underwater Explosions", Naval Ordnance Laboratory Report, NOLTR, 71-160, October 1961.

3. "SUS Source Level Committee Report", MC Report 112, prepared for LRAPP by Underwater Systems, Inc., November 1975.

4. Report of SUS Source Level Workshop, Airlie Conference Center, 7-8 July 1976, prepared for LRAPP by Underwater Systems, Inc. and Tracor, Inc., July 1976.

5. E. B. McGrab and D. S. Bloomquist, The Measurement of Time Varying Phenomena, pp 52-53.

6. R. H. Cole, Underwater Explosions, Section 5.7, Dover, New York, 1948.

7. R. J. Bobber, Underwater Electroacoustic Measurements, Naval Research Laboratory, Government Printing Office, Washington, D.C., 1970.

8. R. B. Blackman and J. W. Tukey, The Measurement of Power Spectra, Dover, New York, 1968.

9. W. T. Cochran, et.al., "Burst Measurements of the Frequency Domain", Proceedings of the IEEE Volume 54, No. 6, pp 830-841, Appendix B.2.

10. E. R. Rabiner and C. M. Rader, ed., Digitel Signal Processing, IEEE Press, New York, 1972. See in particular P. D. Welch, "A Fixed-Point Fast Fourier Transform Error Analysis", pp 470-476, and C. L. Weinstein, "Round Off Noise in Floating Point Fast Fourier Transform Computation", pp 477-483.

11. J. Wakeley, Jr., "Letter to the Editor - Pressure-Signature Model for an Underwater Explosive Charge(U)", U.S. Navy Journal of Underwater Acoustics, Vol. 27, No. 2, pp 445-449, April 1977.

12. M. Abramowitz and I. A. Stegun, Handbook of Mathematical Functions, National Bureau of Standards, Applied Mathematical Series, Chapter 23.2 and Table 23.3, June 1964.

APPENDIX A

AN ANALYTIC FUNCTION MODEL OF AN EXPLOSION SIGNAL AND PROGRAMS FOR COMPUTATION OF ITS TIME SERIES AND SPECTRUM

APPENDIX A

An Analytic Function Model of an Explosion Signal and Programs for Computation of its Time Series and Spectrum.

The explosion signal used in this model is intended to represent a shock wave and four successive bubble pulses. The model uses all currently available scaling information for describing the time series signal.

The characteristics included in the signal representation are the following:[2]

- peak pressure of shock wave
- peak pressure of four bubble pulses
- maximum first negative phase pressure
- time of zero crossings during shock wave and first bubble pulse.
- exponential decay constant of shock wave
- time to peaks of first four bubble pulses

The decision to represent the time series as piecewise analytic using simple functional forms was based on the desire to make an exact Fourier transform of the time series so that the spectrum could be known analytically, and further, that Fourier transform techniques could be used to provide a simulation of anti-alias filtering. A similar approach for signal modeling was taken in Reference 11 independent from this effort.

[2] J. B. Gaspin and V. K. Shuler, op.cit.

A.1 The Unfiltered Time Series

Figure A-1 shows the components of the signal model. The time axis was divided (at the cusps in the time series curve) into epochs, and four different functions defined in each epoch are summed to define the time history. The four functions consist of an exponential decay at the beginning of the epoch, an exponential rise at the end, a positive constant and a negative-going half sine wave.

In addition to the peak pressure and time values identified earlier, several additional constraints and assumptions were imposed in order to define the values of the constants, including;

1. Pressure is continuous across the end of each epoch (a physical constraint).
2. Zero mean value of pressure was assumed within each epoch (except that epoch five is merged with epoch four to apply this).
3. The exponential decay constant was assumed to have the same value on both sides of each bubble pulse.

These twelve constraints and assumptions plus the values of the thirteen constants supplied as data were still insufficient to define the thirty independent constants of the model, so the following arbitrary selections of values were made:

$$PC(1) = PC(2)$$

$$PC(3) = PC(4) = 0$$

$$\theta B(2) = \theta B(3) = \theta B(4) = \theta A(3) = \theta A(4) = \theta A(5)$$

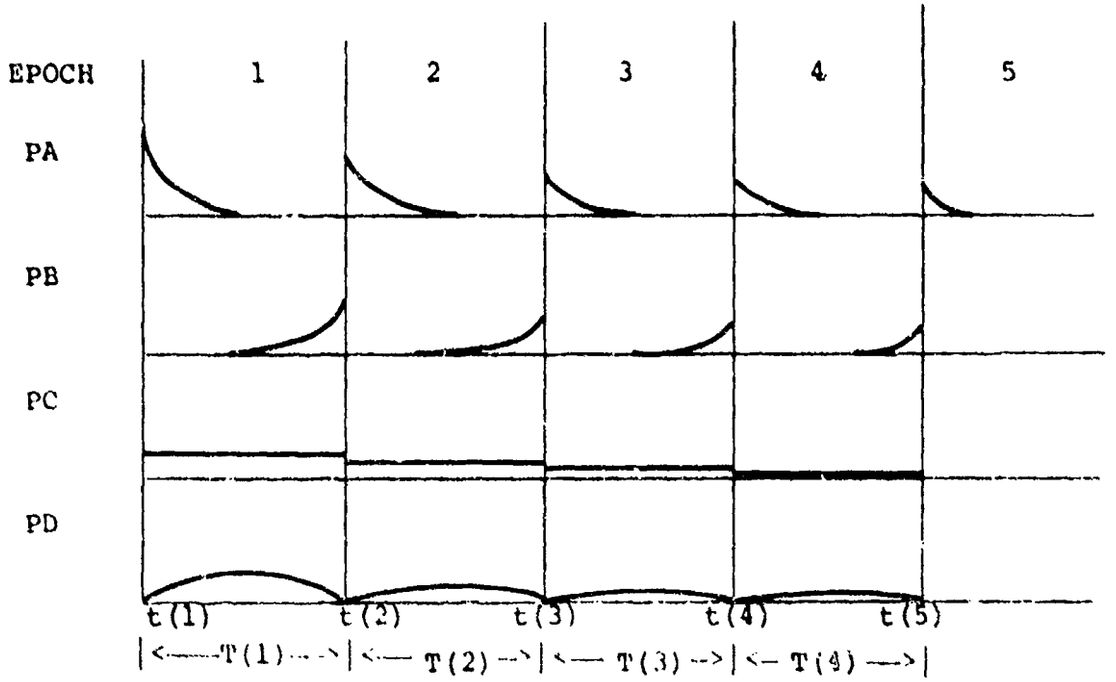

Components in the time domain:

$PA_i = PA(i)\ \exp[(t(i)-t)/\theta A(i)]$

$PB_i = PB(i)\ \exp[(t-t(i)/\theta B(i)]$

$PC_i = PC(i)$

$PD_i = PD(i)\ \sin[(t-t(i))*T(i)]$

i is the epoch number

t is elapsed time

t(i+1) is the elapsed time to the end of epoch i

T(i) is the duration of epoch i.

All functions are defined to be zeros outside their epoch of definition.

Figure A-1 The Unfiltered Time Series

As a result of these considerations, all of the constants of the model could then be put in the form of shot parameter dependent variables through the similarity expressions, giving the expressions shown in Table A-1.

A.2 The Fourier Spectrum and the SPECTRUM Program

The Fourier spectrum is computed from the standard Fourier integral:

$$S(\omega) = \int_{-\infty}^{\infty} p(t)\ e^{-j\omega t} dt \qquad (A.1)$$

The expressions given in Section A.1 were used for p(t), with the approximation that the domains of the exponential terms were extended to plus or minus infinity as appropriate. This approximation is believed to have negligible impact on the spectrum so long as the exponential time constant is less than about one fifteenth of the bubble pulse interval. This approximation limits the applicability of the program to shot parameters such that;

$$Z < 1700\ Y^{1/4}$$

For a 60 ft SUS shot this implies a range limit of about 30,000 ft.

The seventeen terms of p(t) were evaluated analytically using Equation A.1. The results for the generic types of terms are as follows:

Shock wave:

$$S_s(\omega) = \frac{PA(1)\ \ \exp(i\omega t(1))}{(1/\theta A(1) - i\omega)}$$

Table A-1

Shot Model Parameters

Z = D+33 where D is shot depth in feet

W = shot yield, lbs of TNT

R = shot range, feet

$X = W^{1/3}/Z^{5/6}$

$Y = W^{1/3}/R$

$P1 = 3300\ Y$

$PA(1) = 2.08 \times 10^{4}\ Y^{1.13} - PC(1)$

$PB(1) = P1 - PC(1)$

$PC(1) = .403\ PD(1)$

$PD(1) = 8.0\ Z^{2/3}\ Y$

$\theta A(1) = 5.8 \times 10^{-5}\ W^{1/3}\ Y^{-0.22}$

$\theta B(1) = PB(1)^{-1}\ [(\frac{2}{\pi} - .403)PD(1)T(1) - PA(1)\theta A(1)]$

$T(1) = 4.34X,\ t(2) = 4.34X + t(1)$

$PA(2) = PB(1)$

$PB(2) = .22P1 - PC(1)$

$PC(2) = PC(1)$

$PD(2) = 2.42\ (PC1 + PA(2)\ \exp(-.135T(2)/\theta A(2)))$

$\theta A(2) = \theta B(1)$

$\theta B(2) = ((\frac{2}{\pi}\ PD(2) - PC(2))T(2) - PA(2)\theta A(2))/PB(2)$

$T(2) = 3.06X,\ t(3) = 7.40X + t(1)$

$PA(3) = .22\ P1$

$PB(3) = .10\ P1$

Table A-1 Con't

$PC(3) = 0.0$

$PD(3) = .16\ \pi\ P1\ \theta A(3)/T(3)$

$\theta A(3) = \theta B(2)$

$\theta B(3) = \theta B(2)$

$T(3) = 2.48X,\ t(4) = 9.88X + t(1)$

$PA(4) = PB(3)$

$PB(4) = 0.03\ P1$

$PC(4) = 0.0$

$PD(4) = 0.08\pi\ P1\ AA(3)/T(4)$

$\theta A(4) = \theta B(2)$

$\theta B(4) = \theta B(2)$

$T(4) = 2.31X\ t(5) = 12.19X + t(1)$

$PA(5) = PB(4)$

$\theta A(5) = \theta B(2)$

Symmetric bubble pulse of amplitude B and decay constant θ:

$$S_b(\omega) = \frac{2B \exp(i\omega t)}{\theta\,(1/\theta^2 + (\omega)^2)}$$

Rectangular wave of amplitude C, start time t, duration T:

$$S_r(\omega) = \frac{C \exp(i\omega t)(\exp(i\omega T)-1)}{i\omega}$$

Half-sine pulse of amplitude D, period start time t, period T:

$$S_h(\omega) = \left(\frac{\pi}{T}\right) \frac{\exp(i\omega t)(\exp^{i\omega T}+1)}{\left(\left(\frac{\pi}{T}\right)^2 - \omega^2\right)}$$

A listing of an interactive Fortran program used to compute a 1000 point spectrum on a Varian 620L minicomputer is shown in Table A-2, while sample output listing is given in Table A-3. The program will compute the spectrum of a direct signal, or direct plus surface-reflected signal or just a surface-reflected signal, with an option to truncate the magnitude of the surface-reflected shock wave.

The input parameters for the program are:

1. Shot yield, depth and range of the direct signal (English Units).
2. Reflected signal range, time delay between direct and reflected signal, and the pressure for truncation of the reflected shock wave.
3. Spectrum parameters (start frequency, number of frequency values and interval between frequencies.

The output listing includes;

1. shot data
2. a list of the model parameter values
3. a listing of the complex Fourier pressure spectrum, the energy spectrum and the energy level spectrum

Table A-2 Listing of SHOT SPECTRUM

```
C     NAME SHOTSPECTRUM2A     **********RC=32000 **************
C     COMPUTES FOURIER SPECTRUM OF DIRECT PLUS REFLECTED
C     AND OUTPUTS RESULTS TO MAG TAPE
C
C
C        IF DIRECT RANGE (RD)<=0. DO REFLECTED ONLY
C        IF PCLIP<=0. DO NOT COMPUTE REFLECTED
C
C        STARTING FREQ MUST ALWAYS BE >= 0.0
C        START TIME=0 BY DEFINITION
C
C
      COMMON T(5),TT(4),PA(5),PB(4),PC(4),PD(4),AA(5),AB(4),XIMFP(1)
      DIMENSION TH(5),REFP(1000)
      COMPLEX CFP,EI,U2,U3,Z
      PI=3.141592654
      EMAX=0.
      EI=(0.,1.)
C     CEN=2(DYNE/SQ CM/PSI)**2/ROC
      CEN=61720.368
C     INPUT SHOT DATA
   15 WRITE (3,31)
      READ (2,33) W,D,RD
        IF(W.EQ.0.) GO TO 1010
      WRITE (3,32)
      READ (2,33) RR,TDL,CLIPP
   31 FORMAT(43H GIVE YIELD(LBS),DEPTH(FT),DIRECT RANGE(FT),/,
     *20H SEPARATED BY COMMAS)
   32 FORMAT(45H GIVE REF. RANGE(FT),TIME DELAY(SEC),CLIP PSI,/,
     *20H SEPARATED BY COMMAS)
   33 FORMAT (3F13.6)
C     INPUT FREQ. VALUES
      WRITE (3,3)
      READ (2,2)F0,FREQ,DFREQ
    2 FORMAT (3F13.4)
    3 FORMAT(56H GIVE FREQUENCY PARAMETERS:STARTING FREQUENCY,NUMBER OF
     *44HFREQUENCIES AND INTERVAL BETWEEN FREQUENCIES/15H REAL,SEPARATED
     *32H BY COMMAS:(MAX 512 FREQ VALUES))
C     PREPARE OUTPUT DEVICE
      WRITE (3,4)
    4 FORMAT(24H MOUNT DATA TAPE ON MT01)
      PAUSE 10
C        PROCESS INTERNAL PARAMETERS NEEDED FOR CALCULATION MODEL
C        USING TSVAL SUBROUTINE
      T0=0.0
      DO 51 K=1,1000
      REFP(K)=0.0
   51 XIMFP(K) = 0.0
C     CHECK TO SEE IF REFLECTED ONLY
      IF(RD.LE.0.0) GO TO 971
      PASS=1.0
      R=RD
      TCC=0.0
      PCLIP=0.0
      TC=0.0
   61 CALL TSVAL(W,D,R,T0)
        WRITE(11,41)
   41   FORMAT(23H DIRECT SHOT PARAMETERS)
```

Table A-2 Con't.

```
C      OUTPUT DATA HEADING
   63    WRITE(11,5)
         WRITE(11,7)F0,FREQ,DFREQ
         WRITE(11,40)T0
         WRITE(11,6)W,D,R
   64    WRITE(11,8)
         DO 900 I=1,4
900        WRITE(11,9)TT(I),PA(I),AA(I),PB(I),AB(I),PC(I),PD(I)
         WRITE (11,10)PA(5),AA(5)
         WRITE(11,12)
         DO 65 I=1,5
   65    TH(I)=1./AA(I)
C
C          FIND SPECTRUM FROM DATA
C      COMPUTATION START
       NST=1
       OM=2.*PI*F0
       OM0=OM
       NFREQ=FREQ
       DELOM=2.*PI*DFREQ
C      CHECK FOR ZERO FREQ
  953  IF(OM.GT.0.0) GO TO 960
C      COMPUTE ZERO FREQ
       RE=PA(1)*AA(1)*EXP(-TCC/AA(1))+PC(1)*AA(3)+TCC*PCLIP
       RE=RE+PC(1)*(T(3)-TC)
       RE=RE-PD(1)*(1.+COS(PI*TCC/TT(1)))/(PI/TT(1))+2.*PA(2)*AA(2)
       DO 954 K=2,4
       L=K+1
  954  RE=RE+2.*PB(K)*AA(L)-2.*PD(K)*TT(K)/PI
       REFP(NST)=REFP(NST)+PASS*RE
       OM=OM0+DELOM*FLOAT(NST)
       NST=NST+1
       GO TO 953
C
C
C      FOR POSITIVE FREQUENCIES
  960  CONTINUE
       DO 970 I=NST,NFREQ
       Z=EI*OM
       CFP=PA(1)*CEXP(Z*TC-TCC*TH(1))/(TH(1)-Z)
      *+PC(1)*CEXP(Z*T(3))/(TH(3)-Z)
      *+PC(1)*(CEXP(Z*T(3))-CEXP(Z*TC))/Z
      *+PCLIP*CEXP(Z*T(1))*(CEXP(Z*TCC)-1.)/Z
       XI=PI/TT(1)
       CFP=CFP-PD(1)*XI/(XI**2.-OM**2.)*(CEXP(Z*T(2))+
      *CEXP(Z*TC)*(COS(TCC*XI)-EI*SIN(TCC*XI)))
       DO 962 K=1,4
       L=K+1
  962  CFP=CFP+PB(K)*U2(TH(L),OM,T(L))
       DO 963 K=2,4
       L=K+1
  963  CFP=CFP-PD(K)*U3(OM,T(K),TT(K))
       REFP(I)=REFP(I)+REAL(CFP)*PASS
       XIMFP(I)=XIMFP(I)+AIMAG(CFP)*PASS
       EEST=REFP(I)**2+XIMFP(I)**2
       IF (EEST.GT.EMAX) EMAX=EEST
       XI=I
       OM=XI*DELOM+OM0
```

Table A-2 Con't.

```
117     970 CONTINUE
118         IF(PASS.EQ.-1.) GO TO 1000
119   C
120   C
121   C       SECOND PASS NEEDED?
122   C           IF NECESSARY, PROCESS CLIPPED SIGNAL INFORMATION
123    971     PCLIP=CLIPP
124             IF(PCLIP.LE.0.) GO TO 1000
125         T0=TDL
126         R=RR
127         CALL TSVAL(W,D,R,T0)
128         IF(PCLIP.GE.PA(1)) GO TO 972
129         TCC=-AA(1)*ALOG((PCLIP-PC(1))/PA(1))
130           PCLIP=PA(1)*EXP(-TCC/AA(1))+PC(1)-PD(1)*SIN(PI*TCC/TT(1))
131           WRITE(3,38)PCLIP,TCC
132      38     FORMAT(12H PCLIP(PSI)=,F13.6,10X,8H  TCLIP=,F13.6,4H SEC)
133            WRITE(11,39)PCLIP,TCC
134      39     FORMAT(2H  //,12H PCLIP(PSI)=,F13.6,10X,8H  TCLIP=,F13.6,
135         *4H SEC//)
136         GO TO 973
137     972 TCC=0.
138         PCLIP=0.
139     973 TC=T0+TCC
140         PASS=-1.
141           WRITE(11,42)
142      42     FORMAT(22H REFL. SHOT PARAMETERS)
143           IF(RD.LE.0.0) GO TO 63
144         GO TO 64
145    1000 ETST=CEN*EMAX*1.E-8
146         ENDFILE 11
147   C
148   C
149   C       OUTPUT COMPUTATION RESULTS
150         DO 910 I=1,NFREQ
151         XL=(I-1)
152         FREQ=XL*DFREQ+F0
153         ENRG=CEN*(REFP(I)*REFP(I)+XIMFP(I)*XIMFP(I))
154         IF(ENRG.LT.ETST)ENRG=ETST
155         XLEVL=10.*ALOG10(ENRG)
156     910 WRITE(11,20)FREQ,REFP(I),XIMFP(I),ENRG,XLEVL
157         ENDFILE 11
158         WRITE(3,21)
159       5 FORMAT(1H1,30H FOURIER SPECTRUM OF SHOT DATA)
160       6 FORMAT(/12H YIELD(LBS)=,F8.2/11H DEPTH(FT)=,
161        *F9.2/11H RANGE(FT)=,F9.2)
162       8 FORMAT(/25H CONSTANTS OF TIME SERIES/,
163        *45H IN FORM PRESSURE-TIME CONSTANT FOR EACH TERM/,
164        *7H PERIOD,8X,2HPA,8X,9H(THETA A),8X,2HPB,6X,9H(THETA B),
165        *10X,2HPC,9X,2HPD)
166       9 FORMAT(1X,2(F8.5,3X),1H(,E9.4,1H),3X,
167        *F8.5,3X,1H(,E9.4,1H),2F13.5)
168      10 FORMAT( 9H INFINITE,F11.3,3X,1H(,E9.4,1H)/1H1)
169       7 FORMAT(19H STARTING FREQ(HZ)=,F10.2/
170        *12H NO.OF FREQ=,5X,F12.0/
171        *19H FREQ INTERVAL(HZ)=,F10.2)
172      12 FORMAT(54H FREQUENCY SPECTRUM(PSI/HZ)      ENERGY     ENERGY LEVEL/
173        *3X,4H(HZ),6X,14HREAL       IMAG,4X,23H(ERG/CM2/HZ) (DB RE 1.))
174      20 FORMAT(F10.2,1X,2E10.4,E12.6,F14.2)
175      21 FORMAT(34H DATA HAS BEEN TRANSFERRED TO MT01)
176     40      FORMAT(1H ,12HT0(SEC)=      ,F13.8)
177           GO TO 15
178    1010 STOP
179         END
  0 ERRORS COMPILATION COMPLETE
```

Table A-2 Con't.

```
 1  C
 2        COMPLEX FUNCTION U2(THIN,OM,ELT)
 3  C     COMPUTES COMPLEX VALU OF 2THEXP(IOMELT)/TH2+OM2)
 4        COMPLEX EI,ARG
 5        EI=(0.,1.)
 6        DEN=THIN*THIN+OM*OM
 7        U2=2.*THIN*CEXP(EI*OM*ELT)/DEN
 8        RETURN
 9        END
 0 ERRORS COMPILATION COMPLETE


 1  C
 2        COMPLEX FUNCTION U3(OM,ELT,DUT)
 3  C     COMPUTES VALU OF C1 EXP(I OM ELT)(EXP(I OM DUT)+1)/(C12-0M2)
 4        COMPLEX EI,ARG
 5        DATA PI,EI,Q/3.141592654,(0.,1.),3E-3/
 6        C1=PI/DUT
 7        X=C1-OM
 8        ADEL=ABS(X)
 9        IF(ADEL.LT.Q)GO TO 20
10        ARG=EI*OM
11        U3=C1*CEXP(ARG*ELT)*(CEXP(ARG*DUT)+1.)/((C1+OM)*X)
12        GO TO 30
13     20 X=X*DUT
14        ARG=(PI/(C1+OM))*(X*(1.-X*X/12.)/2.+EI*(1.-X*X/6.))
15        U3=CEXP(EI*OM*ELT)*ARG
16     30 CONTINUE
17        RETURN
18        END
 0 ERRORS COMPILATION COMPLETE
```

Table A-2 Con't.

```
      C
            SUBROUTINE TSVAL(W,D,R,TST)
            COMMON T(5),TT(4),PA(5),PB(4),PC(4),PD(4),AA(5),AB(4)
      C     PROGRAM COMPUTES VALUES FOR CONSTANTS IN TIME SERIES
            PI=3.141592654
            Z=D+33.
            W1=W**(1./3.)
            X1=W1/Z**(5./6.)
            X2=W1/R
            TT(1)=4.34*X1
            TT(2)=3.06*X1
            TT(3)=2.48*X1
            TT(4)=2.31*X1
            T(1)=TST
            T(2)=TT(1)+T(1)
            T(3)=TT(2)+T(2)
            T(4)=TT(3)+T(3)
            T(5)=TT(4)+T(4)
      C     TT IS THE TIME INTERVAL BETWEEN PULSE PEAKS,T IS THE ELAPSED TIME
      C     TO THE PEAKS
      C     THE COMPONENT PRESURE AMPLITUDES IN EACH TIME INTERVAL ARE PA,PB,
      C     PC,AND PD
            PD(1)=8.*(Z**(2./3.))*X2
            PC(1)=.403*PD(1)
            PA(1)=2.08E4*(X2**1.13)-PC(1)
            P1=3300.*X2
            PB(1)=P1-PC(1)
      C     THE TIME CONSTANT FOR EXPONENTIAL TERMS IS AA
            AA(1)=5.8E-5*W1*X2**-.22
            P1TH1=PA(1)*AA(1)
            P1MT1=PD(1)*TT(1)
            C1=2./P1-.403
            AA(2)=(C1*P1MT1-P1TH1)/PB(1)
            AB(1)=AA(2)
            PA(2)=PB(1)
            PB(2)=.22*P1-PC(1)
            PC(2)=PC(1)
            C2=EXP(-.135*TT(2)/AA(2))
            PD(2)=2.42*(PC(2)+PA(2)*C2)
            C3=2.*PD(2)/P1-PC(2)
            AA(3)=(C3*TT(2)-PA(2)*AA(2))/PB(2)
            AB(2)=AA(3)
            PA(3)=.22*P1
            PC(3)=0.0
            PB(3)=.10*P1
            PA(4)=PB(3)
            PB(4)=.03*P1
            PA(5)=PB(4)
            PC(4)=0.0
            AA(5)=AA(3)
            AA(4)=AA(3)
            AB(3)=AA(4)
            AB(4)=AA(5)
            C1=.16*P1*P1*AA(3)
            PD(3)=C1/TT(3)
            PD(4)=0.5*C1/TT(4)
            RETURN
            END
```

Table A-3 OUTPUT OF SHOT SPECTRUM

YIELD(LBS)= 1.00
DEPTH(FT)= 60.00
RANGE(FT)= 300.00

CONSTANTS OF TIME SERIES
IN FORM PRESSURE-TIME CONSTANT FOR EACH TERM

PERIOD	PA	(THETA A)	PB	(THETA B)	PC	PD
.12083	40.94786	(.2370E-03)	13.11250	(.6933E-03)	.26834	.66586
.08519	13.11250	(.6933E-03)	2.67544	(.1222E-02)	.26834	.64939
.06905	2.94379	(.1222E-02)	1.33808	(.1222E-02)	0.00000	.11899
.06431	1.33808	(.1222E-02)	.40143	(.1222E-02)	0.00000	.06387
INFINITE	.401	(.1222E-02)				

PCLIP(PSI)= 20.997215 TCLIP= .00016132 SEC

REFL. SHOT PARAMETERS

CONSTANTS OF TIME SERIES
IN FORM PRESSURE-TIME CONSTANT FOR EACH TERM

PERIOD	PA	(THETA A)	PB	(THETA B)	PC	PD
.12083	40.94786	(.2370E-03)	13.11250	(.6933E-03)	.26834	.66586
.08519	13.11250	(.6933E-03)	2.67544	(.1222E-02)	.26834	.64939
.06905	2.94379	(.1222E-02)	1.33808	(.1222E-02)	0.00000	.11899
.06431	1.33808	(.1222E-02)	.40143	(.1222E-02)	0.00000	.06387
INFINITE	.401	(.1222E-02)				

FREQUENCY (HZ)	SPECTRUM(PSI/HZ) REAL	IMAG	ENERGY (ERG/CM2/HZ)	ENERGY LEVEL (DB RE 1.)
0.00	.1447E-02	.00( )E 01	.129275E 00	-8.88
1.00	.1430E-02	-.7673E-04	.126599E 00	-8.98
2.00	.1392E-02	-.5164E-04	.119750E 00	-9.22
3.00	.1296E-02	.1525E-04	.103686E 00	-9.84
4.00	.1034E-02	.6308E-04	.6625818-01	-11.79
5.00	.6177E-03	-.5864E-04	.237628E-01	-16.24
6.00	.8020E-04	-.4708E-03	.140793E-01	-18.51
7.00	-.3619E-03	-.1514E-02	.149532E 00	-8.25
8.00	.1595E-03	-.3117E-02	.6 103E 00	-2.21
9.00	.2064E-02	-.4083E-02	.129180E 01	1.11
10.00	.4470E-02	-.3309E-02	.190870E 01	2.81
11.00	.5796E-02	-.4818E-03	.206794E 01	3.20
12.00	.3846E-02	.2967E-02	.145617E 01	1.63
13.00	-.8548E-03	.2847E-02	.543903E 00	-2.63
14.00	-.2719E-02	-.1678E-02	.630164E 00	-2.01
15.00	.2826E-03	-.4603E-02	.131380E 01	1.19
16.00	.2717E-02	-.3532E-02	.122356E 01	.88
17.00	.2769E-02	-.2789E-02	.953163E 00	-.21
18.00	.3744E-02	-.2937E-02	.139768E 01	1.45
19.00	.4997E-02	-.1310E-02	.164754E 01	2.17
20.00	.4203E-02	.1307E-02	.113277E 01	.62
21.00	.1835E-02	.2146E-02	.492836E 00	-3.08
22.00	-.1253E-02	.1293E-02	.196877E 00	-7.06
23.00	-.3060E-02	.2300E-02	.904363E 00	-.44
24.00	-.1963E-02	.6583E-02	.274453E 01	4.38
25.00	.3965E-02	.7631E-02	.457404E 01	6.60
26.00	.7888E-02	.3870E-02	.476880E 01	6.78
27.00	.6585E-02	.1270E-02	.277918E 01	4.44
28.00	.2148E-02	.2097E-02	.536112E 00	-2.55
29.00	.8344E-03	-.2494E-03	.468112E-01	-13.30
30.00	.1132E-02	-.3070E-04	.790993E-01	-11.02
31.00	-.1528E-02	-.2345E-03	.209740E 00	-6.78
32.00	-.3201E-02	-.5756E-02	.233707E 01	3.69
33.00	.1499E-02	.9208E-02	.536295E 01	7.29
34.00	.7041E-02	.7383E-02	.642334E 01	8.08
35.00	.9148E-02	.2604E-02	.564024E 01	7.51
36.00	.7495E-02	.2561E-02	.487205E 01	5.88

A.3 The Filter Time Series and SHOTTIME

As described in Section 3 of this report, the time series must be anti-alias filtered to be processed using digital techniques. An analytic filter can be applied to an analytic time function through a multiplication of the complex spectrum of the time series by the complex filter transfer function, and transforming back to the time domain. The expressions used for this are;

$$S_o(\omega) = H(\omega)\ S_i(\omega) \tag{A.2}$$

$$p_o(t) = \frac{1}{2\pi} \int_{-\infty}^{\infty} H(\omega) S_i(\omega)\ e^{-i\omega t} d\omega \tag{A.3}$$

A four-pole Butterworth filter was chosen as the anti-alias filter because;

a) It has a flat frequency response below 0.5 x f_c (cut-off frequency), thus minizing the need for frequency response correction.

b) It is physically realizable, which eliminates the need for arbitrary decisions concerning non-causal response.

c) Its properties are analytically well known and reasonably tractable.

d) Its physical realization is readily available commercially and is frequently used in this application.

The squared magnitude of the frequency response is;

$$\left|H(\omega)\right|^2 = 1/(1 + (\frac{\omega}{\omega_c})^8)$$

The complex frequency response is;

$$H(\omega) = 1/\left[(\frac{\omega}{\omega_c})^4 + \frac{i(\omega/\omega_c)^3}{\sin(\pi/8)} - \frac{(\omega/\omega_c)^2}{2\sin^2(\pi/8)} - \frac{i(\omega/\omega_c)}{\sin(\pi/8)} + 1\right]$$

This function has four poles at the frequencies given by;

$$\omega/\omega_c = -e^{i\pi/8},\ -e^{-3\pi/8},\ -e^{-5\pi/8},\ -e^{-7\pi/8}$$

The five terms of $H(\omega)$ times the twelve non-zero terms of $S_i(\omega)$, when integrated using standard residue techniques, result in a sixty term expression for $p_o(t)$ which may be interpreted as "steady-state" response to the applied signal plus transient solutions (i.e. "ringing" at the filter poles) associated with the starting or stopping of each signal component. As a result, the significant terms in each epoch may be easily selected on causal or significance grounds.

The interactive Fortran program which was used to evaluate the numerical magnitude of each term is called SHOTTIME. A listing of the source program is given in Table A-4, while a sample output listing is given in Table A-5.

Table A-4 LISTING OF SHOT TIME

```
      C     NAME SHOTTIME 3          ********  RC=32000  ************
      C     COMPUTES VALUES OF ANALYTIC SHOT TIME SERIES AT UNIFORM TIME
      C     INCREMENTS DDT STARTING FROM T0.    THE ARRIVAL TIME OF THE SHOCK
      C     WAVE IS T1S.  MODEL IS MODIFIED WESTON (HALF SINE PLUS CONST.
      C      REPLACES NEGATIVE CONSTANT OF WESTON MODEL.)
      C     INCLUDES DELAYED AND ATTENUATED SURFACE REFLECTION WHEN NR = 1,
      C     AND TRUNCATES REFLECTION AT -CLIPC WHEN NR > 1. DELAY AND ATTEN
      C     ARE INPUT VALUES,OUTPUT ARE FILES OF 500 VALUES ON 11,FOR TABLES;
      C     FILES OF 500 VALUES + LAST VALUE REPEATED FOR PLOTS ON 12
      C           OUTPUT ON 12 IN BINARY FORMAT
      C          WHERE 26 IS USED AS DUMMY VARIABLE NUMBER
            COMMON T(5),TT(4),PA(5),PB(4),PC(4),PD(4),AA(5),AB(4)
              COMMON P1(500),T9(1)
            DIMENSION N(5),TL(20)
            PI=3.141592654
      C     INPUT SHOT DATA
        100 WRITE (3,1)
            WC=0.0
            READ(2,2)W,D,R1,NR
          1 FORMAT(37H GIVE YIELD(LBS),DEPTH(FT),RANGE(FT),
           #19H REFLECTION NUMBER /21 H SEPARATED BY COMMAS:)
          2 FORMAT(3F13.6,I2)
              IRCNT=0
            IF(NR.EQ.0) GO TO 300
            WRITE(3,3)
            READ(2,2)TDEL,ATTEN
          3 FORMAT(33H GIVE DELAY(MSEC),ATTEN RE UNITY:)
            T2S=TDEL/1000.
            IF(NR.LT.2) GO TO 300
            WRITE(3,4)
            READ(2,2)CLIPC
          4 FORMAT(44H GIVE CLIP CONSTANT(PSI) FOR NEGATIVE PHASE:)
        300 WRITE(3,5)
            READ(2,2)T0,DT,XN
          5 FORMAT(56H GIVE START TIME(MSEC),SAMPLE TIME INTERVAL(MSEC),AND NO
           #22H OF TIME SERIES VALUES/21H SEPARATED BY COMMAS:)
            WRITE(3,36)
         36 FORMAT(44H MOUNT DATA TAPE ON MT01,CURVE TAPE ON MT02.)
            NRVAL=NR
            T1=T0/1000.
            DDT=DT/1000.
            NTOT=(XN+.5)
            T1S=0.0
            JMAX=NTOT/500
            IF((JMAX*500-NTOT).NE.0)JMAX=JMAX+1
            DO 310 I=1,JMAX
        310 TL(I)=FLOAT((I-1)*500)*DDT+T1
            PAUSE 11
            DO 1000 JT=1,JMAX
            AMP=1.
            NR=NRVAL
            T1=TL(JT)
            DO 350 I=1,500
            P1(I)=0.
        350 T9(I)=0.
            NTOT1=500
            IF(JT.EQ.JMAX)NTOT1=NTOT-(JMAX-1)*500
            CALL TSVAL(W,D,R1,T1S)
```

```
      CALL PTS(T1,DDT,NTOT1,AMP,WC)
C       OUTPUT HEADING
        WRITE(3,25)NTOT1
      IF(JT.GT.1)GO TO 700
      WRITE(11,6)
      WRITE(11,7)W,D,R1
      FC=WC/(2.*PI)
      WRITE(11,8)T0,DT,XN,FC
      WRITE(11,21)
  500 CONTINUE
      WRITE(11,22)
      DO 600 I=1,4
      L=I+1
      WRITE(11,9)(T(I),PA(I),AA(I),PB(I),T(L),AB(I),PC(I),PD(I),TT(I))
  600 CONTINUE
      WRITE(11,10)T(5),PA(5),AA(5)
  700 IF(NR.GT.0) GO TO 800
      IF(JT.GT.1)GO TO 900
      WRITE(11,11)
      ENDFILE 11
    6 FORMAT(1H1,25H TIME SERIES OF SHOT DATA)
    7 FORMAT(//12H YIELD(LBS)=,F8.2/11H DEPTH(FT)=,F9.2/11HRANGE(FT)=,
     #F9.2)
    8 FORMAT(//37H START TIME(RE SHOCK DIRECT ARRIVAL)=,F9.5,6H(MSEC)/
     #17H SAMPLE INTERVAL=,F9.5,6H(MSEC)//15H NO OF SAMPLES=,F9.0,
     #10X,15H FILTER CUTOFF=,F13.4,4H HZ.)
   21 FORMAT(//51H CONSTANTS OF TIME SERIES. TIME SERIES GENERAL FORM/
     #62H P(T1)=PA*EXP((T-T1)/AA)+PB*EXP((T1-T1)/AB+PC-PD*SIN(T1-T)/TT))
   22 FORMAT(//5X,6HT(SEC),5X,7HPA(PSI),5X,7HAA(SEC),5X,7HPB(PSI),5X,
     #7HT1(SEC),5X,7HAB(SEC),5X,7HPC(PSI),5X,7HPD(PSI),5X,7HTT(SEC))
    9 FORMAT(F12.8,F12.6,F12.10,F12.6,F12.8,F12.10,2F12.6,F12.8)
   10 FORMAT(F12.8,F12.6,F12.10,4X,3H0.0,6X,8H1PF1N1TE,3X,3H0.0,13X,
     #3H0.0,9X,3H0.0,7X,3H0.0////)
   11 FORMAT(1H1,//50X,18HTIME SERIES VALUES//
     #5H NO. ,5(20HTIME(MSEC) PRES(PSI),3X)//)
  900 CONTINUE
C     OUTPUT TIME SERIES VALUES IN PAGES OF 100 LINES WITH
C     5 SETS OF VALUES PER LINE, FOR HARD COPY
C     FOR PLOT, 500 VALUES FOR 1ST PAGE, 501 OR LESS FOR CONTINUING
C       PAGES WITH LAST VALUE REPEATED AT TOP OF NEW PAGE, IN BINARY
C     OUTPUT DATA FILES
      NC=(JT-1)*500
      DO 920 K=1,NTOT1,5
      N1 = K+NC
      N2 = K+4
      DO 910 I=K,N2
  910 T9(I)=1000.*T9(I)
      WRITE(11,25) N1,(T9(I),P1(I),I=K,N2)
  920 CONTINUE
   25 FORMAT(I5,5(F10.4,F10.6,3X))
      GO TO 1000
C
C     BRANCH TO HERE FOR NR.GT.0. COMPUTE AND ADD IN EFFECT OF
C     SURFACE REFLECTION IF NR=1. TRUNCATES VALUES AT -CLIPC WHEN NR.>1
C     COMPUTE NEW TSVAL AND PRESSURE TIME SERIES. TS VALUES ARE
C     SUBTRACTED FROM P9.
  800   RR=R1/ATTEN
        CALL TSVAL(W,D,RR,T2S)
```

Table A-4 Con't.

```
117           IF(CLIPC.GT.PA(1))NR=1
118           IF(NR.LT.2)GO TO 801
119           AMP=-CLIPC
120           GO TO 802
121    801    AMP=-2.0*PA(1)
122    802    CALL PTS(T1,DDT,NTOT1,AMP,WC)
123           WRITE(3,755)
124    755    FORMAT(11H OK  AT # 5)
125           IF(JT.GT.1)GO TO 900
126           IF(NR.LT.2)GO TO 840
127           WRITE(11,31)AMP
128      31 FORMAT(54H THE NEGATIVE PHASE OF THE DELAYED PLUS REFLECT WAVE ,
129         #18HHAS BEEN TRUNCATED/13H TO THE VALUE,F11.6,5H(PSI)///)
130     840 CONTINUE
131         IF(JT.GT.1)GO TO 900
132         ATDB=20.*ALOG10(ATTEN)
133         SATDB=1.13*ATDB
134         WRITE(11,32)RR,TDEL,ATTEN,ATDB,SATDB
135      32 FORMAT(56H THE SURFACE REFLECTED WAVE AMPLITUDES WERE COMPUTED FRO
136         #24HM A NEW SET OF CONSTANTS/
137         #57H THE CONSTANTS ARE BASED ON A RANGE FOR THE REFLECTION OF,F10.2
138         #,4H(FT)/15H AND A DELAY OF,F10.6,6H(MSEC)//
139         #38H THIS CORRESPONDS TO AN ATTENUATION OF,F9.7,1H(,F6.2,4H DB,/
140         #51H    EXCEPT FOR THE SHOCK WAVE WHICH IS ATTENUATED BY,F6.2,4H DB)
141         #//58H THE NEW TIME SERIES CONSTANTS FOR THE REFLECTED WAVE ARE://)
142         NR=0
143         GO TO 500
144    C    RETURNED TO PRINT TIME CONSTANTS AND TIME SERIES VALUES
145     1000 CONTINUE
146          ENDFILE 11
147          ENDFILE 26
148          WRITE(3,1001)
149     1001 FORMAT(21H NEW RUN?1,=YES;0,=NO)
150           READ(2,25)I
151          IF(I.EQ.1)GO TO 100
152          STOP
153          END
  0 ERRORS COMPILATION COMPLETE
```

Table A-4 Con't.

```
      SUBROUTINE TSVAL(W,D,R,TST)
      COMMON T(5),TT(4),PA(5),PB(4),PC(4),PD(4),AA(5),AB(4)
C     PROGRAM COMPUTES VALUES FOR CONSTANTS IN TIME SERIES
      PI=3.141592654
      Z=D+33.
      W1=W**(1./3.)
      X1=W1/Z**(5./6.)
      X2=W1/R
      TT(1)=4.34*X1
      TT(2)=3.06*X1
      TT(3)=2.48*X1
      TT(4)=2.31*X1
      T(1)=TST
      T(2)=TT(1)+T(1)
      T(3)=TT(2)+T(2)
      T(4)=TT(3)+T(3)
      T(5)=TT(4)+T(4)
C     TT IS THE TIME INTERVAL BETWEEN PULSE PEAKS,T IS THE ELAPSED TIME
C     TO THE PEAKS
C     THE COMPONENT PRESURE AMPLITUDES IN EACH TIME INTERVAL ARE PA,PB,
C     PC,AND PD
      PD(1)=8.*(Z**(2./3.))*X2
      PC(1)=.403*PD(1)
      PA(1)=2.08E4*(X2**1.13)-PC(1)
      P1=3300.*X2
      PB(1)=P1-PC(1)
C     THE TIME CONSTANT FOR EXPONENTIAL TERMS IS AA
      AA(1)=5.8E-5*W1*X2**-.22
      P1TH1=PA(1)*AA(1)
      P1MT1=PD(1)*TT(1)
      C1=2./PI-.403
      AA(2)=(C1*P1MT1-P1TH1)/PB(1)
      AB(1)=AA(2)
      PA(2)=PB(1)
      PB(2)=.22*P1-PC(1)
      PC(2)=PC(1)
      C2=EXP(-.135*TT(2)/AA(2))
      PD(2)=2.42*(PC(2)+PA(2)*C2)
      C3=2.*PD(2)/P1-PC(2)
      AA(3)=(C3*TT(2)-PA(2)*AA(2))/PB(2)
      AB(2)=AA(3)
      PA(3)=.22*P1
      PC(3)=0.0
      PB(3)=.10*P1
      PA(4)=PB(3)
      PB(4)=.03*P1
      PA(5)=PB(4)
      PC(4)=0.0
      AA(5)=AA(3)
      AA(4)=AA(3)
      AB(3)=AA(4)
      AB(4)=AA(5)
      C1=.16*P1*P1*AA(3)
      PD(3)=C1/TT(3)
      PD(4)=0.5*C1/TT(4)
      RETURN
      END
 0 ERRORS COMPILATION COMPLETE
```

Table A-4 Con't.

```
      SUBROUTINE PTS(T0,DDT,NTOT,AMP,WC)
      COMMON T(5),TT(4),PA(5),PB(4),PC(4),PD(4),AA(5),AB(4),P1(500)
      COMMON T9(1)
C     COMPUTES PRESSURE TIME SERIES VALUES FROM T0 IN STEPS DDT FOR NTOT
C     STEPS. TIME AND PRESSURE VALUES RETURNED IN T9 AND P1
C     VERSION 2- SIGNAL LOW PASS FILTERED THROUGH A 4POLE BUTTERWORTH
C     (48DB/OCTAVE SLOPE) AND -3DB POINT AT WC FILTER IS IMPLEMENTED
C     ANALYTICALLY ON THE ORIGINAL ANALYTIC TIME SERIES EXPRESSION
      COMPLEX OM(2),HR(5,2),E1,A1,A2,HRN(2),ARG,CP,B1,B2,H1,H2,H3
      COMPLEX EX,H,PIM,WR(2),CPP
      DIMENSION R(4),A(4)
      DATA E1,A1,A2/(0.,1.),(.9238795,.38268343),(.38268343,.9238795)/
      DATA B1,B2/(-.191341,-.4619397),(1.115221,.4619398)/,P1/3.141593/
      Q=1.0E-8
      IF(WC.NE.0.) GO TO 8
      WRITE(3,2)
    2 FORMAT(35H GIVE FILTER CUTOFF FREQ.(HZ,F12.4))
      READ(2,3)WC
    3 FORMAT(F12.4)
      WC=2.*P1*WC
C       FIND CLIPPING PARAMETERS
    8  IF(AMP.GT.0.)GO TO 9
       PCLIP=-AMP
       IF(PCLIP.GT.PA(1))GO TO 6
       TCC=-AA(1)*ALOG((PCLIP-PC(1))/PA(1))
       PCLIP=PA(1)*EXP(-TCC/AA(1))+PC(1)-PD(1)*SIN(P1*TCC/TT(1))
       TC=TCC+T(1)
    6  AMP=-1
    9 OM(1)=WC*-1.*A1
      OM(2)=WC*-1.*A2
      HRN(1)=WC*B1
      HRN(2)=WC*B2
      DO 10 I=1,4
      J=I+1
      R(I)=P1/TT(I)
      A(I)=1./AA(J)
   10 CONTINUE
      DO 20 N=1,2
      HR(1,N)=HRN(N)*(PA(1)/(OM(N)+E1/AA(1))
     *+PC(1)/OM(N)-E1*PIM(PD(1),OM(N),R(1)))
      HR(2,N)=HRN(N)*E1*-1.*(PIM(PD(1),OM(N),R(1))
     *+PIM(PD(2),OM(N),R(2))+2.*PA(2)*A(1)/(OM(N)*OM(N)+A(1)*A(1)))
      HR(3,N)=HRN(N)*(PIM(PD(2),OM(N),R(2))
     *+PIM(PD(3),OM(N),R(3))+2.*PB(2)*A(2)/(OM(N)*OM(N)+A(2)*A(2))
     *+E1*PC(2)/(OM(N)+E1/AA(3)))*E1*-1.
      HR(4,N)=HRN(N)*E1*-1.*(PIM(PD(3),OM(N),R(3))
     *+PIM(PD(4),OM(N),R(4))+2.*PA(4)*A(3)/(OM(N)*OM(N)+A(3)*A(3)))
      HR(5,N)=HRN(N)*(PIM(PD(4),OM(N),R(4))
     *+2.*PA(5)*A(4)/(OM(N)*OM(N)+A(4)*A(4)))*E1*-1.
   20 CONTINUE
      DO 30 I=1,5
      DO 30 N=1,2
      HR(I,N)=2.*(HR(I,N))
   30 CONTINUE
      OM(1)=E1*OM(1)
      OM(2)=E1*OM(2)
    4 FORMAT(4F12.4)
C     TEST LOOP PARAMETER
```

Table A-4 Con't.

```
      IF(DDT.GT.0.)GO TO 50
      WRITE(3,1)
    1 FORMAT(51H FATAL INCREMENT ERROR IN SUB PTS,ABORT RUN AND FIX)
  751  FORMAT(11H  OK AT # 1)
  752  FORMAT (11H  OK AT # 2)
  753  FORMAT(11H  OK AT # 3)
  754  FORMAT(11H  OK AT # 4)
      GO TO 1000
C     INITIALIZE VALUES
   50 J=1
      I=1
      T1=T0
      IF(T1.GE.T(5))J=5
      TM1=T(1)
      TMAXM=FLOAT(NTOT)*DDT+T0
   90 L=J+1
      IF(L.EQ.6)GO TO 400
      TMAX=T(L)
      IF(TMAX.GT.TMAXM)TMAX=TMAXM
      IF(T1.LE.TMAX)GO TO 100
      J=J+1
      GO TO 90
  100 CONTINUE
C     CHECK FUNCTION IN RANGE OR COMPUTE SPECIAL VALUES
      IF(T1.GE.TM1)GO TO 200
      P1(I)=0.+P1(I)
      T9(I)=T1
      T1=DDT*FLOAT(I)+T0
      I=I+1
      GO TO 100
  200 IF(T1.GE.T(5))GO TO 400
C     COMPUTE FUNCTION VALUES
  250 ARG=E1*-1./AA(J)
      H1=H(ARG,WC)
      ARG=E1/AA(L)
      H2=H(ARG,WC)
      ARG=P1/TT(J)
      H3=H(ARG,WC)
      ARG=(P1/TT(J))*E1
  300 V=(T(J)-T1)/AA(J)
      V=EXP(V)*PA(J)
      B=(T1-T(L))/AA(L)
      B=EXP(B)*PB(J)
  301   IF(T1.GT.T(2))GO TO 320
        IF(AMP.GT.0.)GO TO 320
         IF(PCL1P.GT.PA(1))GO TO 320
       WR(1)=-A1*WC
      WR(2)=-A2*WC
      IF(T1.GT.TC) GO TO 310
      CP=HRN(1)*CEXP(E1*(T(1)-T1)*WR(1))/WR(1)
      CP=HRN(2)*CEXP(E1*(T(1)-T1)*WR(2))/WR(2)+CP
      P1(I)=PCL1P*(1.+2.0*REAL(CP))*AMP+P1(I)
      GO TO 340
  310 AARG=P1*TCC/TT(1)
      CP=V*H1+B*H2+PD(J)*AIMAG(H3*CEXP((T(J)-T1)*ARG))+PC(1)
      DO 311 IJ=1,2
      CPP=CEXP(E1*WR(IJ)*(T(1)-T1))*HRN(IJ)*2.0
      CP=CP+CPP*(PA(1)/(WR(IJ)+E1/AA(1))+PC(1)*CEXP(E1*TCC*WR(IJ))/
```

Table A-4 Con't.

```
      *WR(IJ))
       CPP=CPP*CEXP(EI*WR(IJ)*TCC)/(WR(IJ)**2-(PI/TT(I))**2)*PD(I)
       CP=CP-CPP*(EI*PI*COS(AARG)/TT(I)+WR(IJ)*SIN(AARG))
  311  CONTINUE
  312  P1(I)=P1(I)+AMP*REAL(CP)
       GO TO 340
  320  CP=V*H1+B*H2+PD(J)*AIMAG(H3*CEXP((T(J)-T1)*ARG))
      *+REAL(EX(T1,OM(1),T(J))*HR(J,1)+EX(T1,OM(2),T(J))*HR(J,2))
       P1(I)=(REAL(CP)+PC(J))*AMP+P1(I)
  340  T9(I)=T1
       T1=DDT*FLOAT(I)+T0
       I=I+1
       IF(T1.LT.TMAX)GO TO 300
       IF(I.GT.NTOT)GO TO 1000
       J=J+1
       L=J+1
       TMAX=T(L)
       IF(TMAX.GT.TMAXM)TMAX=TMAXM
       IF(J.LT.5)GO TO 250
  400  IF(I.GT.NTOT)GO TO 1000
       ARG=EI*-1./AA(5)
       H1=PA(5)*H(ARG,WC)
  450  DIF=T(5)-T1
       CP=H1*EXP(DIF*A(4))+REAL(CEXP(DIF*OM(1))*HR(5,1)
      S+CEXP(DIF*OM(2))*HR(5,2))
       P1(I)=REAL(CP)*AMP+P1(I)
       T9(I)=T1
       T1=DDT*FLOAT(I)+T0
       I=I+1
  500  IF(I.GT.NTOT) GO TO 1000
       IF(ABS(REAL(CP)).GT.0) GO TO 450
       N1=I
       DO 600 I=N1,NTOT
       P1(I)=0.+P1(I)
       T9(I)=DDT*FLOAT(I)+T0
  600  CONTINUE
 1000  IF(AMP.LT.0.)AMP=-PCLIP
         RETURN
       END
    0 ERRORS COMPILATION COMPLETE
```

Table A-4 Con't.

```
1          COMPLEX FUNCTION H(A,W)
2          COMPLEX EI,A,C
3          EI=(0.,1.)
4          C=A/W
5          D=SIN(3.141593/8.)
6          H=1./(C*C*C*C*C-C*C/(2.*D*D)+1.+EI*(C*(C*C-1.))/D)
7          RETURN
8          END
0 ERRORS COMPILATION COMPLETE
```

```
1          COMPLEX FUNCTION PIM(P,O,T)
2          COMPLEX O
3          PIM=P*T/(O*O-T*T)
4          RETURN
5          END
0 ERRORS COMPILATION COMPLETE
```

```
1          COMPLEX FUNCTION EX(T,O,A)
2          COMPLEX O
3          EX=CEXP((A-T)*O)
4          RETURN
5          END
0 ERRORS COMPILATION COMPLETE
```

Table A-5 OUTPUT OF SHOT TIME

1 TIME SERIES OF SHOT DATA

YIELD(LBS)= 1.00
DEPTH(FT)= 60.00
RANGE(FT)= 300.00

START TIME(RE SHOCK DIRECT ARRIVAL)= -.03052(MSEC)
SAMPLE INTERVAL= .24414(MSEC)

NO OF SAMPLES= 4096. FILTER CUTOFF= 1024.0000 HZ.

CONSTANTS OF TIME SERIES. TIME SERIES GENERAL FORM
P(T)=PA*EXP((T-T1)/AA)+PB*EXP((T1-T1)/AB+PC-PD*SIN(T1-T)/TT)

T(SEC)	PA(PSI)	AA(SEC)	PB(PSI)	T1(SEC)	AB(SEC)	PC(PSI)	PD(PSI)	TT(SEC)
0.00000000	48.947561	.0002370894	13.112503	.12083101	.0006933203	.268341	.565858	.12083101
.12083101	13.112503	.0006933203	2.675445	.20602524	.0012215166	.268341	.649387	.08519423
.20602524	2.943786	.0012215166	1.338084	.27597150	.0012215166	0.000000	.118991	.06904629
.27597150	1.338084	.0012215166	.401425	.33938479	.0012215166	0.000000	.063874	.06431329
.33938479	.401425	.0012215166	0.0	INFINITE	0.0	0.0	0.0	0.0

TIME SERIES VALUES

NO.	TIME(MSEC)	PRES(PSI)	TIME(MSEC)	PRES(PSI)	TIME(MSEC)	PRES(PSI)	TIME(MSEC)	PRES(PSI)	TIME(MSEC)	PRES(PSI)
# REQUESTED 100, # PROCESSED 36										
1	-.0305	0.000000	.2136	2.355864	.4578	13.964046	.7019	16.556503	.9460	7.276167
6	1.1902	.312582	1.4343	-.289458	1.6785	.716968	1.9226	.659263	2.1667	.217579
11	2.4109	.128794	2.6550	.229984	2.8992	.259706	3.1433	.226382	3.3874	.207491
16	3.6316	.209867	3.8757	.210642	4.1199	.205302	4.3640	.199352	4.6081	.195318
21	4.8523	.191663	5.0964	.187486	5.3406	.183131	5.5847	.178914	5.8288	.174772
26	6.0730	.170603	6.3171	.166413	6.5613	.162232	6.8054	.158065	7.0495	.153901
31	7.2937	.149739	7.5378	.145581	7.7820	.141430	8.0261	.137284	8.2702	.133142
36	8.5144	.129007	8.7585	.124876	9.0027	.120752	9.2468	.116633	9.4909	.112521
41	9.7351	.108615	9.9792	.104515	10.2234	.100222	10.4675	.096136	10.7116	.092057
46	10.9558	.087985	11.1999	.083920	11.4441	.079862	11.6882	.075812	11.9323	.071770
51	12.1765	.067736	12.4206	.063709	12.6648	.059692	12.9089	.055682	13.1530	.051681
56	13.3972	.047689	13.6413	.043706	13.8855	.039731	14.1296	.035766	14.3737	.031811
61	14.6179	.027864	14.8620	.023928	15.1062	.020001	15.3503	.016085	15.5944	.012178
66	15.8386	.008282	16.0827	.004397	16.3269	.000521	16.5710	-.003343	16.8151	-.007196
71	17.0593	-.011638	17.3034	-.014569	17.5476	-.018689	17.7917	-.022497	18.0358	-.026293
76	18.2800	-.030077	18.5241	-.033849	18.7683	-.037610	19.0124	-.041358	19.2565	-.045093
81	19.7007	-.048816	19.7448	-.052526	19.9890	-.056223	20.2331	-.059907	20.4772	-.063577
86	20.7214	-.067235	20.9655	-.070879	21.2097	-.074508	21.4538	-.078125	21.6979	-.081727
91	21.9421	-.085316	22.1862	-.088890	22.4304	-.092449	22.6745	-.095994	22.9186	-.099525

APPENDIX B

ERRORS ASSOCIATED WITH REALIZABLE ANTI-ALIASING FILTERS

APPENDIX B

Errors Associated with Realizable Anti-aliasing Filters

Equations 3.1 and 3.3 provide a basis for estimating the error due to small amounts of aliasing for several important cases that will be discussed here. We will consider two cases, that where the energy density spectrum is constant vs frequency (corresponding to that of an impulse of infinitesmal duration), and that where the spectrum rolls off smoothly at 6 dB/octave above some frequency (corresponding to an impulse with an exponential decay). For both cases we will employ an ideal n-pole Butterworth anti-aliasing filter as representative of a realizable filter. The first case represents a conservative approach, which is applicable for an arbitrary shot spectrum, while the second case may be used when more information is available about the spectrum.

For the case of weak aliasing, we can treat the effect of aliasing as noise that contributes to the computed spectrum, and compute an equivalent signal to noise ratio.

From Equation 3.2 we have in terms of energy,

$$E'(f) = \sum_{q=-\infty}^{\infty} 2P^2(f - 2qf_m)$$

where $f_m = 1/\Delta t$

For an n-pole Butterworth filter with cutoff frequency f_c,

we have

$$H^2(f) = \frac{1}{1 + (f/f_c)^{2n}}$$

Thus, for Case 1 (noting that the energy is the sum of equal contributions from $P^2(f)$ and $P^2(-f)$),

$$E_1(f) = 2P_1^2(f) = \frac{2C}{1 + (f/f_c)^{2n}}, \quad f > 0 \qquad \text{(B.1)}$$

and for Case 2 (with roll off at f_r)

$$E_2(f) = 2P_2^2(f) = \frac{2C}{(1 + (f/f_r)^2)(1 + (f/f_c)^{2n})}, f > 0 \qquad \text{(B.2)}$$

(B.2)

CASE 1 - FLAT SPECTRUM

Substituting B.1 in 3.4 and simplifying yields:

$$E_1'(f) = E_1(f) + 2C \sum_{q=1}^{\infty} \left[\frac{1}{1 + \left(\frac{f + 2qf_N}{f_c} \right)^{2n}} + \frac{1}{1 + \left(\frac{f - 2qf_N}{f_c} \right)^{2n}} \right]$$

We note that $f \leq f_N$ and make the reasonable assumption that $f_c \leq f_N$. Ignoring 1 in the denominator of each series (since the terms in parenthesis are greater than 1), we have:

$$E_1''(f) = E_1(f) + \frac{2C}{\left(\frac{2f_N}{f_c}\right)^{2n}} > E_1'$$

$$\times \sum_{q=1}^{\infty} \frac{1}{(a+q)^{2n}} + \frac{1}{(a-q)^{2n}}$$

where $a = \frac{f}{2f_N}$.

By our assumptions, $0 < a \leq \frac{1}{2}$, so we can replace the series by the following upper bounds:

$$\sum_{q=1}^{\infty} \frac{1}{(a+q)^{2n}} \leq \sum_{q=1}^{\infty} \frac{1}{q^{2n}} = \xi(2n)$$

$$\sum_{q=1}^{\infty} \frac{1}{(a-q)^{2n}} \leq \sum_{q=1}^{\infty} \frac{1}{(q-\frac{1}{2})^{2n}}$$

$$= \frac{1}{(\frac{1}{2})^{2n}} + \sum_{q=2}^{\infty} \frac{1}{(q-\frac{1}{2})^{2n}} < \frac{1}{(\frac{1}{2})^{2n}}$$

$$+ \sum_{q=1}^{\infty} \frac{1}{q^{2n}} = 2^{2n} + \xi(2n)$$

where $\xi(n)$ is the Rieman Zeta Function,[12] for integer n. Some values of this function are given in Table B-1.

The upper bound estimate for the energy spectrum with aliasing is,

$$E_1'''(f) = E_1(f) + \frac{2C}{\left(\frac{2f_n}{f_c}\right)^{2n}} \cdot (2^{2n} + 2\xi(2n)) > E_1'' > E_1'$$

The signal to alias-noise ratio is,

$$SN_1(n,f) \leq \frac{E_1(f)}{E_1'''(f) - E_1(f)} = \left(\frac{2f_N}{f_c}\right)^{2n} / ((2^{2n}+2\xi(2n))(1+(f/f_c)^{2n})$$

---

[12] M. Abramowitz and I. A. Stegun, Handbook of Mathematical Functions, National Bureau of Standards, Applied Mathematical Series, Chapter 23.2 and Table 23.3 (June 1964)

Table B-1

Values of Riemann Zeta Function

n	$\xi(n)$
2	1.64493
4	1.08232
6	1.01734
8	1.00407
10	1.00099
12	1.00024

$$SN_1(nf) \leq (f_N/f_c)^{2n/2} \qquad (B.3)$$

for $f, f_c \leq f_m$

Equation B.3 may be converted to decibels by taking 10 $\log_{10}$ of the right hand side. Table B-2 provides an evaluation of Equation B.3 for various values of f_c/f_m at the frequency $f = f_c$.

CASE 2 SPECTRUM ROLLOFF AT f_r. For this case:

$$E_2'(f) = E_2(f) + 2C \sum_{q=1}^{\infty} \frac{1}{(1+((f+2qf_N)/f_r)^2)(1+((f+2qf_N)/f_c)^{2n})}$$

$$+ \frac{1}{(1+((f+2qf_N)/f_r)^2)(1+((f-2qf_N)/f_c)^{2n})}$$

with the assumption that $f_r \leq 2f_N$, in addition to the assumptions of Case 1. We can ultimately reach the simplified expression for an upper bound to the aliased energy spectrum of:

$$E_2'''(f) = E_2(f) + \frac{2C}{(\frac{2f_N}{f_r})^2 (\frac{2f_N}{f_c})^{2n}} (2^{2n+2} + 2\xi(2n+2))$$

with signal to noise ratio,

$$SN_2 = (\frac{2f_N}{f_r})^2 (\frac{2f_N}{f_c})^2 / (2^{2n+2} + 2\xi(2n+2)(1+f/f_r)^2)(1+f/f_c)^{2n})$$

$$\geq (\frac{f_N}{f_r})^2 (\frac{f_N}{f_c})^{2n} / 4$$

Study of this expression indicates that the presence of roll off of 6 dB/octave commencing at a frequency f_r is roughly

Table B-2

SIGNAL TO NOISE RATIO FOR CASE 1

Signal to noise ratio for various values of cutoff frequency and anti-aliasing filter order evaluated at the Nyquist frequency (f_N) for a flat input spectrum.

		Signal to Alias Noise Ratios(dB)		
Filter Order		2 (12dB/oct)	4 (24dB/oct)	6 (36dB/oct)
Cutoff Frequency (f_c) / Nyquist Frequency (f_N)	.5	8.4	21.0	33.1
	.4	12.3	28.8	44.7
	.315	16.4	36.8	56.8
	.25	20.5	45.1	69.2
	.20	24.4	52.9	80.8
	.16	28.4	60.9	92.9
	.125	32.6	69.2	105.4

equivalent (as might be expected) to adding another pole to the antialiasing filter, at frequencies below the start of roll off. However, above the frequency where roll off occurs, the improvement decreases because the level of the signal is decreasing; i.e.,

$$\frac{SN_2(n,f)}{SN_1(n,f)} \approx \left(\frac{f_N}{f_r}\right)^2 / (1+(f/f_r)^2) \qquad (B.4)$$

Thus if $f_r << f_N$ the signal to noise ratio at $f = f_N$ will be the same as in the case of the flat spectrum! If f_c is chosen as significantly less than f_N, then at f_c the signal to noise ratio is improved by 20 log (f_N/f_c).

Thus we conclude that the effect of a small amount of aliasing is to introduce a frequency-dependent signal to noise ratio that depends to some extent on the shape of the spectrum. For a flat or falling spectrum, the worst-case signal to noise ratio occurs at the maximum frequency of interest. As is expected the aliasing noise error can be reduced to an arbitrarily small amount by choosing an anti-aliasing filter with sufficiently steep attenuation characteristics, and setting the cutoff frequency sufficiently far below the Nyquist frequency.

APPENDIX C

EXPERIMENT PLAN
SUS MINI-EXPERIMENT

APPENDIX C

EXPERIMENT PLAN - SUS MINI-EXPERIMENT

C.1. SITUATION

Signal, Underwater Sound (SUS) are widely used as sources for experimental evaluation of long range propagation. Recent studies have indicated the desirability for improving upon the accuracy of calibration of these sources. As part of an analysis of the feasibility of performing a large scale experiment, it is necessary to identify the inherent variability of the source in terms of fundamental parameters.

C.2. TECHNICAL OBJECTIVES

The technical objectives of the program are:

- Identify the yield and depth variability inherent in SUS charge firings using a statistically significant data sample.
- To the extent possible, identify the variability of the frequency spectrum of the surface-reflected wave within the frequency range of observation.
- Accumulate a data base from which additional information could be derived from additional signal processing.

The concept of the experiment that will satisfy these objectives is to set off a long series of SUS shots at the several depths of interest, and record the resulting acoustic signals using appropriately positioned and calibrated signal acquisition systems so that the depth of the shot can be determined to acceptable accuracy from the relative time of arrival of direct and surface-reflected signals only. This data plus the bubble pulse frequency of the shot permits estimation of shot yield independent of the magnitude of the acoustic signal received. The variability of the surface reflection may be identified by direct comparison of the spectra of the direct and reflected signals when they can be separated in time, or more sophisticated signal processing when they cannot be separated.

C.3. TECHNICAL PLAN

C.3.1 General

The plan by which data will be acquired to fulfill the technical objectives is described below.

C.3.1.1 Overview

The acquisition of data during this exercise is expected to be completed within a time period of about five hours plus time for deployment and recovery of data acquisition systems. The planned deployment of instrumentation is shown schematically in Figure C-1, while a plan view of the experimental configuration and shot region are shown in Figure C-2. As shown in Figure C-2, the shots are fired in an annular region of inner radius 500 m and an outer radius of 1000 m. The signal acquisition systems planned for use in this exercise are the PAR system (Programmable Acoustic Recorder). PAR 1, as deployed, is defined as the center of the shot circle. It has deep hydrophones placed at nominally 2750 m and 3050 m depths, which are used to identify the angle from vertical, and depth of the shot. The signals will then be used to study the variation of surface-reflections at near-vertical incidence. PAR 2 is placed at 3000 m horizontal range from PAR 1. It has shallow hydrophones at 500 m and 800 m depths, which will be used as backups for

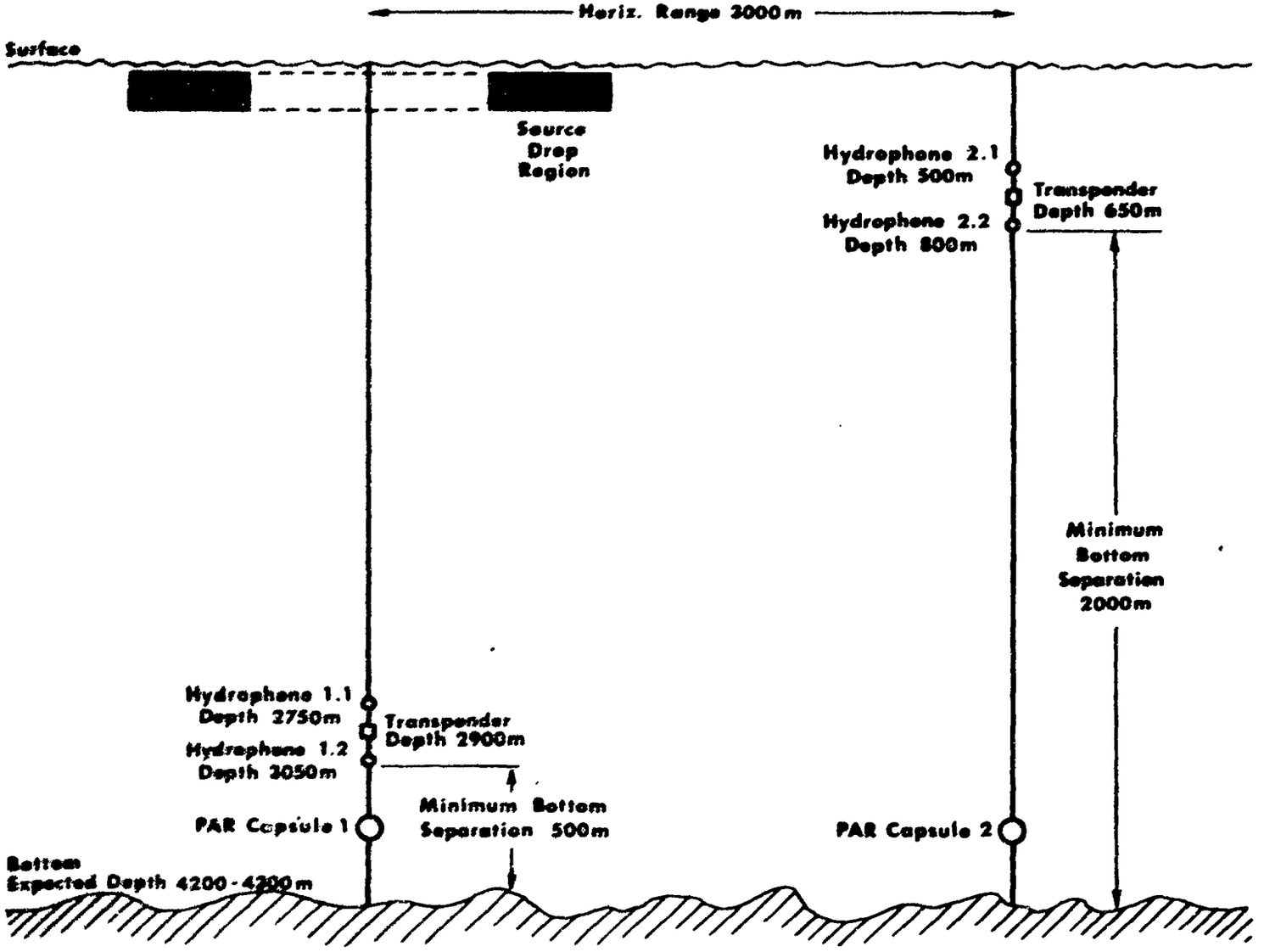

Figure C-1 Instrumentation Deployment

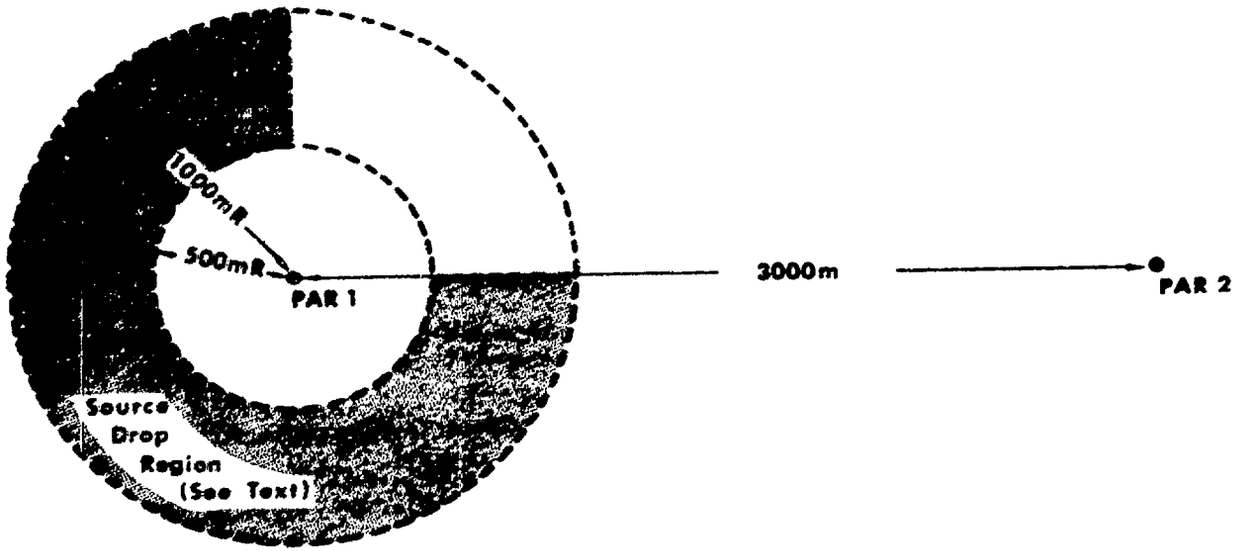

Figure C-2 Plan view of experiment area

depth determination and to study surface reflection effects at near-grazing incidence. Both hydrophone arrays will be provided with transponders that will be used to identify ship position relative to the array, as well as relative positions of the arrays. The SUS are dropped in the annular region so as to produce a nominally constant orientation to PAR 1, while providing a nominal 2/1 range variation to PAR 2. A total of 100 shots are to be fired at each of three depths (18 m, 91 m and 274 m respectively). A circular transit of the source area at a nominal speed of 6 knots, using a radius that places the ship near the outer perimeter of the source area , will require approximately 30 minutes. The source area layout and experiment timing are based on the assumption that the ship will transit the area in 30 minutes (corresponding to a turn rate of 0.2°/sec, for 6.0 kts ship speed and a circle radius of 870 m). During each circle maneuver, 33 shots will be fired, requiring a total of nine circle maneuvers to be performed. The same depth shot will be used for all shots on each circle, but depths will be changed between circles (i.e., 33 18 m, followed by 33 91 m, followed by 33 274 m). Use of approximately 90° of the annular sector is not desirable because the presence of the ship will distort the surface-reflection to PAR 2 and use of the transponder will interfere with data acquisition. Therefore each of the 33 shots will be fired at intervals of 40 $\pm$5 seconds so that the total shot firing time per circle is

22 ±0.5 minutes. The angular sector not used depends upon where the firing mechanism is located on the ship and the ship path. The sector indicated in Figure 2 (i.e. 270° to 360° from the line between PAR 1 and 2) is appropriate for launching of SUS from the ship stern at a bearing of 135° to 180° from ship centerline, and ship circling to the right. The last 90° of the circle is to be used to verify ship tracking relative to PAR 1, and time of crossing the axis of PAR 1 - PAR 2, as determined from the signals received from the transponders. During this time interval, the PAR units will also be performing internal calibration programs, on alternate circles.

C.3.1.2 Schedule

C.3.1.2.1 Ship Schedule

Time from first SUS	
-1200 - 0000	Deck calibration and deploy PAR 1 and PAR 2. PAR in-water pre-cal. Determine PAR 1 and PAR 2 positions, and array depths. Deploy deep XBT.
0000 - 0023	Start first circle. Drop 33 19 m SUS
0023 - 0030	Complete first circle, check position re PAR 1 and axis crossing re PAR 2.
0030 - 0053	Start second circle. Drop 33 91 m SUS
0053 - 0100	Complete second circle, check position re PAR 1 and axis crossing re PAR 2. Deploy XBT.

0057 - 0058 PAR internal calibration cycle

0100 - 0430 Repeat above for total of 9 circles.

0445 - 0500 PAR internal calibration.

C.3.1.2.2 PAR Calibration Schedule

Time Relative to first shot

-0030 - 0014 In-water Pre-cal

22 - 30 second duration sine wave calibrations (see frequency table, Table C-1) (11 min)

6 - 30 second duration square wave calibrations, 6 Hz, 11 Hz, 17 Hz, 21 Hz, 34 Hz, 41 Hz (3 min)

1 - 1 minute 3.33 Hz rectangular wave calibration (1 min)

1 - 1 minute preamplifier calibration (1 min)

0057 - 0058
0157 - 0158
0257 - 0258
0357 - 0358
0457 - 0458

1 minute, 10 Hz square wave cal at preamps to all hydrophones.

0530 - 0546 In-Water Post-Cal; repeat above Pre-Cal

TABLE C-1

PAR Frequency Calibration Table
Use Two Synthesizers Sine-Sine

	Frequency Table -- Hz	
Cal. Number	Synthesizer 1	Synthesizer 2
1	14	157
2	20	163
3	27	170
4	34	177
5	41	184
6	48	191
7	54	197
8	61	204
9	68	211
10	75	218
11	82	225
12	88	231
13	95	238
14	102	245
15	109	252
16	116	259
17	123	266
18	129	272
19	136	279
20	143	286
21	150	293
22	157	300

NOTE: Frequency for synthesizer 2 is frequency for synthesizer 1 plus 143 Hz. Frequencies may be reordered, or traded to reduce programming size.

C.3.2 Experimental Operations

C.3.2.1 Signal Measurements

Signal will be acquired on two PAR units of two hydrophones each, with data from each hydrophone to be recorded on four (4) tape recorder channels. The channel gains are to be set with the anticipation of a nominal peak pressure in the water of 199 dB re 1μPa. The nominal peak pressure expected in the DC-300 Hz band is 188 dB re 1μPa. The four tape recorder channels are to be set with nominal peak record sensitivities in the 0 - 300 Hz passband region as follows (dB re 1μPa):

a) 196 dB

b) 190 dB

c) 184 dB

d) 178 dB

These record channels should all be set for 300 Hz low-pass filter and phase reference marker on.

The calibration schedule for the PAR micro-processor should be programmed according to Section 3.1.2.2. Calibration peak signal amplitudes for sine and square waves should be set to correspond to 2 dB below nominal full scale on the tape recorder (i.e., for 1.414 V full scale recorder response (1% harmonic distortion), set peak sine and square wave voltages to 1.12 V).

C.3.2.2 Environmental Measurements

The required environmental and test geometry measurements include:

a. Depth of hydrophone transponders determined to within ± 3 m.

b. Horizontal range between PAR 1 and PAR 2 to ± 15 m.

c. XBT recordings of velocity profile to depth of deep array twice (before and after experiment) and four shallow XBT (hourly) during the data acquisition.

d. Vertical separation between hydrophones on each array shall be determined to ± 0.3 m.

e. Determination of the fall time of each shot shall be determined on board to ± 0.01 min or ± 0.5 sec.

f. Ship horizontal range to PAR 1 should be determined to a specific radius to within ± 100 m. Radius to be identified on board.

g. Charts showing nominal location of each shot (bearing $\pm 5^{\circ}$, range ± 100 m relative to PAR 1) shall be maintained.

h. Meteorological conditions and sea state shall be logged hourly, and significant changes noted when they occur.

C.3.2.3 Ship Operations

As noted in the above sections the required ship operations are as follows:

- Deploy PAR units
- Deploy deep XBT
- Maneuver to identify PAR array depths and horizontal separation using installed transponder.
- Perform nine 30-minute circling maneuvers around PAR 1, deploying 33 SUS shots per circle, and shallow XBT on every alternate circle.

C.4 DATA ANALYSIS

C.4.1 Discussion

The objectives of the SUS mini-experiment are to provide data on; a) the variability of yield and depth and b) the variability of surface-reflected rays from SUS explosions. The data analysis deals separately with these two objectives.

The experiment is designed so that yield and depth can be determined from time domain measurements only. These specific measurements include; a) difference in time of arrival of the direct signal at two different vertical hydrophones; and for each hydrophone, b) difference in time of arrival between direct and surface-reflected signal, and c) time between shock and bubble pulse peak (bubble pulse period). Data analysis will consist of reviewing the multi-rack recordings of the signals from four hydrophones of 300 shots, and identifying the above time parameters. These parameters will then be used as inputs to provide estimates of depth and yield for each shot. Statistical analysis of depth and yield estimates will then provide parameters that describe shot variability. Representative spectra of selected shots will be compared to identify the significance of the yield and depth variations on the resulting source level.

The second experiment objective, to study surface-reflection variability, is accomplished by comparison of spectra of isolated direct and surface-reflected signals from individual shots. The

proposed form of this comparison is the difference between energy spectra of direct and surface-reflected signals. The average value of this difference over all similar shots represents a measure of the surface-reflection loss. The standard deviation (i.e. rms value) of this difference is a measure of the surface-reflection variability. This approach is sufficient when the signals are separated in time, but is not applicable for shallow (18 m) shots where significant overlap occurs. In this case advanced signal processing techniques to deconvolve the direct and surface-reflected signals are required to separate them for the above analysis. The principal approach for attacking this problem is expected to involve correlation analysis to identify portions of the signal that are unique to the direct and surface-reflected components.

C.4.2 Task Statements

1. Analyze recordings of 300 shots from SUS mini-experiment to determine yield and depth variability and statistical measures of the variation. Identify the impact of this variation on the acoustic signal.

2. Analyze recordings to identify variations in surface-reflected signals. Such an analysis is to include identification of mean and variation of the difference in direct- and surface-reflected energy spectra.

DEPARTMENT OF THE NAVY
OFFICE OF NAVAL RESEARCH
875 NORTH RANDOLPH STREET
SUITE 1425
ARLINGTON VA 22203-1995

IN REPLY REFER TO:

5510/1
Ser 321OA/011/06
31 Jan 06

MEMORANDUM FOR DISTRIBUTION LIST

Subj: DECLASSIFICATION OF LONG RANGE ACOUSTIC PROPAGATION PROJECT (LRAPP) DOCUMENTS

Ref: (a) SECNAVINST 5510.36

Encl: (1) List of DECLASSIFIED LRAPP Documents

1. In accordance with reference (a), a declassification review has been conducted on a number of classified LRAPP documents.

2. The LRAPP documents listed in enclosure (1) have been downgraded to UNCLASSIFIED and have been approved for public release. These documents should be remarked as follows:

   Classification changed to UNCLASSIFIED by authority of the Chief of Naval Operations (N772) letter N772A/6U875630, 20 January 2006.

   DISTRIBUTION STATEMENT A: Approved for Public Release; Distribution is unlimited.

3. Questions may be directed to the undersigned on (703) 696-4619, DSN 426-4619.

BRIAN LINK
By direction

Subj: DECLASSIFICATION OF LONG RANGE ACOUSTIC PROPAGATION PROJECT (LRAPP) DOCUMENTS

DISTRIBUTION LIST:

NAVOCEANO (Code N121LC – Jaime Ratliff)
NRL Washington (Code 5596.3 – Mary Templeman)
PEO LMW Det San Diego (PMS 181)
DTIC-OCQ (Larry Downing)
ARL, U of Texas
Blue Sea Corporation (Dr.Roy Gaul)
ONR 32B (CAPT Paul Stewart)
ONR 321OA (Dr. Ellen Livingston)
APL, U of Washington
APL, Johns Hopkins University
ARL, Penn State University
MPL of Scripps Institution of Oceanography
WHOI
NAVSEA
NAVAIR
NUWC
SAIC

Declassified LRAPP Documents

Report Number	Personal Author	Title	Publication Source (Originator)	Pub. Date	Current Availability	Class.
DASC 012-C-77	Unavailable	LRAPP PACIFIC DYNAMIC ARCHIVE (U) SEPTEMBER 1976	Daniel Analytical Services Corporation	770201	NS; ND	U
SAI-78-527-WA	Spofford, C. W.	NELANT DATA ASSESSMENT APPENDIX III-MODELING REPORT	Science Applications, Inc.	770225	ND AVA047680	U
PSI TR 036049	Barnes, A. E., et al.	OCEAN ROUTE ENVELOPES	Planning Systems Inc.	770419	ND	U
Unavailable	Unavailable	TAP II BEAMFORMING SYSTEM SOFTWARE FINAL REPORT	Bunker-Ramo Corp. Electronic Systems Division	770501	ADC011789	U
S01037C8	Unavailable	TAP 2 PROCESSING SYSTEM FINAL REPORT HARDWARE DOCUMENTATION (U)	Bunker-Ramo Corp. Electronic Systems Division	770501	ADC011790; NS; ND	U
Unavailable	Weinberg, H.	GENERIC FACT	Naval Underwater Systems Center	770601	ADB019907	U
Unavailable	Unavailable	TASSRAP II OB SYSTEM TEST	Analysis and Technology, Inc.	770614	ADA955352	U
Unavailable	Unavailable	LRAPP TECHNICAL SUPPORT	Texas Instruments, Inc.	770624	ND	U
Unavailable	Bessette, R. J., et al.	TASSRAP INPUT MODULE	Analysis and Technology, Inc.	770729	ADA955340	U
Unavailable	Unavailable	TAP-II PHASE II FINAL REPORT	Bunker-Ramo Corp. Electronic Systems Division	770901	ADC011791	U
Unavailable	Unavailable	LONG RANGE ACOUSTIC PROPAGATION PROJECT (LRAPP)	Xonics, Inc.	770930	ADA076269	U
SAI78696WA	Unavailable	REVIEW OF MODELS OF BEAM-NOISE STATISTICS (U)	Science Applications Inc.	771101	NS; ND	U
TRACORT77RV109 C	Unavailable	FINAL REPORT FOR CONTRACT N00014-76-C-0066 (U)	Tracor Sciences and Systems	771130	ADC012607; NS; ND	U
Unavailable	Unavailable	LONG RANGE ACOUSTIC PROPAGATION PROJECT (LRAPP)	Xonics, Inc.	771231	ADB041703	U
Unavailable	Homer, C. I.	SUS SOURCE LEVEL ERROR ANALYSIS ADA055600	Underwater Systems, Inc.	780120	ND	U
Unavailable	Fitzgerald, R. M.	LOW-FREQUENCY LIMITATION OF FACT	Naval Research Laboratory	780131	ADA054371	U
Unavailable	Unavailable	MIDWATER ACOUSTIC MEASUREMENT SYSTEM - PAR AND ACODAC	Texas Instruments, Inc.	780228	ADB039924	U
ORI TR 1245	Moses, E. J.	OPTIONS, REQUIREMENTS, AND RECOMMENDATIONS FOR AN LRAPP ACOUSTIC ARRAY PERFORMANCE MODEL	ORI, Inc.	780331	ND	U
Unavailable	Hosmer, R. F., et al.	COMBINED ACOUSTIC PROPAGATION IN EASTPAC REGION (EXERCISE CAPER): INITIAL ACOUSTIC ANALYSIS	Naval Ocean Systems Center	780601	ADB032496	U
LRAPPRC78023	Watrous, B. A.	LRAPP EXERCISE ENVIRONMENTAL DATA INVENTORY, JUNE 1978 (U)	Naval Ocean R&D Activity	780601	NS; ND	U
TR052085	Solomon, L. P., et al.	HISTORICAL TEMPORAL SHIPPING (U)	Planning Systems Inc.	780628	NS; ND	U